

DUKE POWER COMPANY
P.O. BOX 33189
CHARLOTTE, N.C. 28242

HAL B. TUCKER
VICE PRESIDENT
NUCLEAR PRODUCTION

TELEPHONE
(704) 373-4531

July 28, 1988

U. S. Nuclear Regulatory Commission
Attention: Document Control Desk
Washington, D. C. 20555

Subject: Catawba Nuclear Station
Docket Nos. 50-413 and 50-414
McGuire Nuclear Station
Docket Nos. 50-369 and 50-370

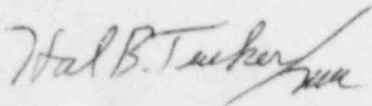
Dear Sir:

On May 13, 1988, a telecon was held between representatives from Duke Power Company (Duke) and the NRC Staff to discuss the resolution of issues concerning equipment survivability during deliberate ignition of hydrogen in containment. From this meeting, we committed to provide hydrogen and steam release histories into containment for an appropriate selection of degraded core accident sequences using similar methodology to the Mark III Containment, Hydrogen Control Owners Group (HCOG).

We were unable to calculate release histories via mechanistic methodologies while complying with the 75 percent metal-water reactor (MWR) requirements of 10 CFR 50.44. Therefore, release histories, which were comprised of a mechanistic portion, and a non-mechanistic portion for extrapolation to 75 percent clad oxidation, were developed. The attached document provides hydrogen and steam release histories to containment for a spectrum of accident sequences using MAAP, Version 3.0B, for the mechanistic portion of the calculation, and the HCOG methodology for the non-mechanistic extrapolation to 75 percent clad oxidation.

In order to facilitate the review process, the format of the attached information resembles the HCOG licensing submittals HGN-034 (May 17, 1985), HGN-052 (August 1, 1985), and HGN-096 (July 30, 1986). The attached results will form the basis for analyzing the response of containment and its associated systems to the accident sequences pending NRC approval.

Very truly yours,



Hal B. Tucker

PGL/35/sbn

Attachments

8808110063 880728
PDR ADOCK 05000369
P PNU

G008
11

U. S. Nuclear Regulatory Commission
July 28, 1988
Page Two

xc: Dr. J. Nelson Grace, Regional Administrator
U. S. Nuclear Regulatory Commission
Region II
101 Marietta Street, NW, Suite 2900
Atlanta, Georgia 30323

Mr. P. K. Van Doorn
NRC Resident Inspector
Catawba Nuclear Station

U. S. Nuclear Regulatory Commission

July 28, 1988

Page Three

bxc: (w/o attachments)

H. D. Brewes

L. T. Burba

B. J. Dolan

R. L. Gill

C. D. Ingram

R. W. Ouellette

N. A. Rutherford

J. G. Torre

File: CN-801.01

R.M. Glover

R. O. Sharpe

DUKE POWER COMPANY

Catawba Nuclear Station

Phase I Submittal for the Plan to Resolve Issues Concerning
Control of Combustible Gases in Containment as Outlined by
10CFR50.44.

The first phase in the plan to resolve issues concerning equipment survivability during deliberate ignition of hydrogen in containment is the selection of specific accident sequences to be analyzed. A spectrum of accident sequences that envelope the range of hydrogen and steam release rates have been studied. Since steam flow through the core is the limiting factor for clad oxidation, primary system pressure is the parameter of importance due to its effect on steam availability. Therefore, the following sequences were analyzed:

- S₁D (low primary system pressure)
- S₂D (intermediate primary system pressure)
- TMLU (high primary system pressure)

As a result of NRC Staff interest over sequences involving ECCS failure in the recirculation mode, S₂H will also be investigated. These accident sequences envelope the possible primary system pressure conditions under which hydrogen could be developed in the primary system, the release rates of that hydrogen to containment, and conditions in containment at the time of hydrogen release. For each sequence, ECCS was not recovered until hydrogen production had reached its peak value for the case of simply boiling away the remaining water inventory in the core region (an unmitigated case), consistent with the HCOG methodology. Primary system breaks were assumed to occur in the hot leg in order to allow minimum holdup time of hydrogen as it's produced in the core. It was assumed that oxidation could take place on both sides of the Zircaloy fuel cladding to account for steam ingress after clad rupture.

MAAP, Version 3.0B, was used to analyze the four degraded core sequences. MAAP is a computer code developed by the Industry Degraded Core Rulemaking (IDCOR) Program. It is designed to provide realistic thermal-hydraulic assessments for severe core damage accident sequences.

The model divides the primary system into fifteen nodes as shown in Figure 1. Nodes exist for the core region, upper plenum, reactor "dome" (upper head), downcomer and lower head, pressurizer, and five nodes in each modeled coolant loop. Two coolant loops are represented and are denoted the "broken" and "unbroken" loops. The unbroken loop consists of all the coolant loops except one. This primary system nodalization permits a detailed accounting of the water/steam which is available for cooling the core and for reacting with the Zircaloy fuel cladding. In addition, this arrangement allows the user to track hydrogen through the primary system and thereby calculate release rates to the containment. The core is further divided into a user selected number of subnodes; a 4 radial X 17 axial nodalization is used for the Catawba analysis.

The safety systems considered in this analysis include the charging pumps (NV), safety injection pumps (NI), low pressure injection pumps (ND), cold leg accumulators, auxiliary feedwater, and containment sprays. These are shown in Figure 2 along with other systems important to accident progression, such as the pressurizer and steam generator safety and power operated relief valves. In order to model individual accident sequences, all of these systems can be enabled or disabled by the user through the use of MAAP "event codes." For a complete description of the relevant MAAP models used in this calculation refer to Appendix 5.

The four sequences analyzed are discussed below:

S₁D SEQUENCE

The S₁D sequence was modeled as a 6-inch diameter break on the hot leg, followed by failure of the emergency core cooling system (ECCS). The auxiliary feedwater system was assumed to function properly and provided secondary side heat removal. Within 6 minutes the primary system pressure had dropped below the cold leg accumulator(s) initial discharge setpoint (646 psia), resulting in rapid depletion of accumulator(s) inventory. The loss of primary system inventory through the 6-inch diameter break on the hot leg eventually led to core uncover and a loss of decay heat removal (0.51 hrs.).

The core continued to heat up, and subsequent oxidation of the Zircaloy cladding began at 0.64 hours. By 0.73 hours the hottest core node had reached the UO₂-Zr-ZrO₂ eutectic melting temperature of 2500 °K. ECCS was recovered at 1.22 hours with all NI and NV pumps available. The majority of the hydrogen gas was expelled through the break by 1.92 hours.

The total fraction of the clad oxidized was 25.5%. Appendix 1 contains relevant plots for the S₁D sequence, which consists of the following parameters as a function of time:

FIGURE NUMBER	DESCRIPTION
1.01	H ₂ Flow Out of Hot Leg Break (kg/s)
1.02	Water/Steam Flow Out of Hot Leg Break (kg/s)
1.03	Integrated Mass of H ₂ Generated in the Core (lb)
1.04	Mass of H ₂ in the Primary System (lb)
1.05	Mass of H ₂ in the Pressurizer (lb)
1.06	Water Temperature in the Core (°F)
1.07	Primary System Pressure (psia)
1.08	ECCS Flow to Cold Legs (lb/hr)
1.09	Accumulator(s) Flow to Cold Legs (lb/hr)
1.10	Reactor Vessel Water Level (ft)
1.11	Accumulator(s) Pressure (psia)

As previously stated, the core is divided into 4 radial X 17 axial nodes. Rather than submit core node temperatures for all 68 nodes, 3 representative axial cross-sections will be presented as follows:

1.12	Top of Active Fuel Axial Node X 4 Top Radial Nodes (°F)
1.13	Middle of Active Fuel Axial Node X 4 Middle Radial Nodes (°F)
1.14	Bottom of Active Fuel Axial Node X 4 Bottom Radial Nodes (°F)

S₂D SEQUENCE

The S₂D sequence was modeled as a 2-inch diameter break on the hot leg, followed by failure of ECCS injection. Auxiliary feedwater was assumed to operate during this sequence. The core uncovered at 0.61 hours, and subsequent oxidation of the Zircaloy cladding began at 0.72 hours. By 0.90 hours the hottest core node had reached the UO₂-Zr-ZrO₂ eutectic melting temperature. The primary system pressure dropped below the cold leg accumulator(s) initial discharge setpoint at 1.03 hours, thereby introducing a discontinuous reflood source to the reactor vessel. ECCS was recovered at 1.20 hours with all NI and NV pumps available. The majority of the hydrogen gas was expelled through the break by 2.08 hours.

The total fraction of the clad oxidized was 23.1%. Appendix 2 contains relevant plots for the S₂D sequence, which consists of the following parameters as a function of time:

FIGURE NUMBER	DESCRIPTION
2.01	H ₂ Flow Out of Hot Leg Break (kg/s)
2.02	Water/Steam Flow Out of Hot Leg Break (kg/s)
2.03	Integrated Mass of H ₂ Generated in the Core (lb)
2.04	Mass of H ₂ in the Primary System (lb)
2.05	Mass of H ₂ in the Pressurizer (lb)
2.06	Water Temperature in the Core (°F)
2.07	Primary System Pressure (psia)
2.08	ECCS Flow to Cold Legs (lb/hr)
2.09	Accumulator(s) Flow to Cold Legs (lb/hr)
2.10	Reactor Vessel Water Level (ft)
2.11	Accumulator(s) Pressure (psia)
2.12	Top of Active Fuel Axial Node X 4 Top Radial Nodes (°F)
2.13	Middle of Active Fuel Axial Node X 4 Middle Radial Nodes (°F)
2.14	Bottom of Active Fuel Axial Node X 4 Bottom Radial Nodes (°F)

TMLU SEQUENCE

The TMLU sequence was modeled as a station blackout. As a result of loss of power, main feedwater failed, ECCS failed, and the MSIVs closed. It was also assumed that the auxiliary feedwater system failed and the pressurizer PORVs failed to open.

Initially, the decay heat from the core was removed by boiling the water remaining in the steam generators. However, as the secondary side inventory was depleted, heat transfer from the primary system to the secondary system decreased, and at 0.98 hours the pressurizer safety valves lifted relieving pressure to the Pressurizer Relief Tank (PRT). At 1.42 hours the PRT rupture disk blew out and began the release of steam to containment. By 1.45 hours the steam generators had boiled completely dry.

At approximately 1.88 hours, the core began to uncover, and at 2.41 hours the hottest core node had reached the UO_2 -Zr-ZrO₂ eutectic melting temperature. At 2.80 hours the ECCS was restored with the NV pumps providing cooling water by pumping against the high primary system pressure. Because primary system pressure remains elevated, the cold leg accumulator(s) never discharge during this sequence. The release of hydrogen gas was controlled by the pressurizer safety valves and the pressurizer PORVs (after power restoration) by relieving pressure to the PRT and, therefore, the majority of hydrogen gas escaped slowly from the primary system over a five hour period. Auxiliary feedwater was not restored when power became available in order to expedite the discharge of hydrogen gas from the primary system to containment.

The total fraction of the clad oxidized was 31.6%. Appendix 3 contains relevant plots for the TMLU sequence, which consists of the following parameters as a function of time:

FIGURE NUMBER	DESCRIPTION
3.01	H ₂ Flow Out of the PRT (kg/s)
3.02	Water/Steam Flow Out of the PRT (kg/s)
3.03	Integrated Mass of H ₂ Generated in the Core (lb)
3.04	Mass of H ₂ in the Primary System (lb)
3.05	Mass of H ₂ in the Pressurizer (lb)
3.06	Water Temperature in the Core (°F)
3.07	Primary System Pressure (psia)
3.08	ECCS Flow to Cold Legs (lb/hr)
3.09	Downcomer Water Level in the Steam Generator(s) (ft)
3.10	Reactor Vessel Water Level (ft)
3.11	Top of Active Fuel Axial Node X 4 Top Radial Nodes (°F)
3.12	Middle of Active Fuel Axial Node X 4 Middle Radial Nodes (°F)
3.13	Bottom of Active Fuel Axial Node X 4 Bottom Radial Nodes (°F)

S₂H SEQUENCE

The S₂H sequence was modeled as a 2-inch diameter break on the hot leg with successful ECCS injection but failure of ECCS to operate in the recirculation mode.

The sequence began with a 2-inch diameter break on the hot leg. By 64.3 seconds the primary system pressure had dropped to the ECCS set point of 1860 psia, and all high head pumps began injection of cooling water into the primary system. Containment sprays were initiated automatically at 85.0 seconds causing rapid depletion of Fueling Water Storage Tank (FWST) inventory. At 0.67 hours the FWST was empty, and ECCS failed to switch over to the recirculation mode of core cooling.

The loss of primary inventory resulted in the core being uncovered at 1.10 hours. Hydrogen production from Zircaloy oxidation began at 1.22 hours. By 1.43 hours the hottest core node had reached the UO_2 -Zr-ZrO₂ eutectic melting temperature. The primary system pressure dropped below the cold leg

accumulator(s) initial discharge setpoint at 1.51 hours, thereby introducing a discontinuous reflood source to the reactor vessel. ECCS was restored at 1.79 hours with all NI and NV pumps operating in the recirculation mode. The majority of the hydrogen gas was expelled through the break by 2.80 hours.

The total fraction of the clad oxidized was 25.2%. Appendix 4 contains relevant plots for the S₂H sequence, which consists of the following parameters as a function of time:

FIGURE NUMBER	DESCRIPTION
4.01	H ₂ Flow Out of Hot Leg Break (kg/s)
4.02	Water/Steam Flow Out of Hot Leg Break (kg/s)
4.03	Integrated Mass of H ₂ Generated in the Core (lb)
4.04	Mass of H ₂ in the Primary System (lb)
4.05	Mass of H ₂ in the Pressurizer (lb)
4.06	Water Temperature in the Core (°F)
4.07	Primary System Pressure (psia)
4.08	ECCS Flow to Cold Legs (lb/hr)
4.09	Accumulator(s) Flow to Cold Legs (lb/hr)
4.10	Reactor Vessel Water Level (ft)
4.11	FWST Water Level (ft)
4.12	Accumulator(s) Pressure (psia)
4.13	Top of Active Fuel Axial Node X 4 Top Radial Nodes (°F)
4.14	Middle of Active Fuel Axial Node X 4 Middle Radial Nodes (°F)
4.15	Bottom of Active Fuel Axial Node X 4 Bottom Radial Nodes (°F)

Although injection of ECCS into the vessel should rapidly quench the core and terminate hydrogen production, the improbable case which results in continued oxidation equivalent to 75% MWR has been considered. Since a completely mechanistic model is not capable of predicting hydrogen production equivalent to the amount mandated by 10CFR50.44, a non-mechanistic model similar to the HCOG methodology has been utilized.

The non-mechanistic model that is being used to predict hydrogen production is based upon an energy balance in a severely damaged core which no longer retains an intact geometry. The core is assumed to have deformed into a debris bed which is postulated to form following injection of ECCS into a severely overheated core. To assure that the damaged core is coolable it is necessary that energy losses from the damaged core are at least adequate to remove decay energy in the core; plus energy produced by continued oxidation of Zircaloy in the core; plus excess stored energy in the core. It is additionally assumed that termination of the Zircaloy oxidation at 75% MWR requires a quenched core at that time.

This can be presented in equation form as:

$$(1) \quad Q_{\text{loss}} \geq Q_{\text{dh}} + Q_{\text{ox}} + Q_{\text{s}}$$

where:

- Q_{loss} = Energy loss rate from the damaged core to surrounding water;
 Q_{dh} = Rate of core decay heat;
 Q_{ox} = Rate of exothermic energy produced by oxidation of Zircaloy in the damaged core;
 Q_s = Release of excess energy stored in the damaged core =
 $E_{core}(T) - E_{core}(T_{sat})$ over some time period;
 E_{core} = Energy stored in the core and associated structures as a function of temperature.

If the losses from the debris bed do not exceed the sum of the decay heat, the oxidation energy and the excess stored energy, then the debris will continue to overheat and will eventually challenge the integrity of the lower vessel head. The limiting case would, therefore, be a severely deformed core in which the long-term sum of the decay energy, the oxidation energy, and the excess stored energy approaches the maximum heat loss from the debris bed.

Hydrogen production would occur over the extended period of time:

$$t_{12} = t_2 - t_1$$

where:

t_2 = time when 75% MWR is achieved and the core is quenched;

t_1 = time when the mechanistically produced hydrogen has been released to containment.

(The sequence dependent parameters referenced in the following discussion apply to the S₁D sequence.)

The decay heat can be expressed as:

$$(2) \quad Q_{dh} = 349.6 t^{-0.253} \text{ (MW)},$$

which is a curve fit to the decay heat history for Catawba reload cycles of 390 days, using 3.8 w/o enrichment Westinghouse Optimized Fuel Assemblies (See Attachment 6). This curve fit is accurate to +1.6%, -2.8% over the required time span (approximately 6912 to 16068 seconds following scram).

The total amount of energy of each term in Equation (1) can be determined for the problem time span (t_{12}). Equation (2) can be integrated to find the total decay heat:

$$(3) \quad Q_{dh12} = \int_{t_1}^{t_2} Q_{dh}(t) dt$$

or

$$(4) \quad Q_{dh12} = 468.0 \left[t_2^{0.747} - t_1^{0.747} \right] \text{ (MW-sec)}.$$

For the Zircaloy oxidation energy term, Q_{ox12} , we know that 75% MWR = 1496.6 lbs. of hydrogen, and that the ECCS reflood case produced 508 lbs. (25.5% MWR) of hydrogen. Therefore, the remaining mass of hydrogen to be generated, M_{H12} , is:

$$(5) \quad M_{H12} = 1496.6 - 508 = 988.6 \text{ lbs. of } H_2$$

From the NRC-sponsored thermal properties package MATPRO-11, we have:

$$(6) \quad Q_{ox} = 66.68 \text{ MW-sec/lb of } H_2 \text{ produced.}$$

Combining Equations (5) and (6) yields:

$$(7) \quad Q_{ox12} = 6.59 \times 10^4 \text{ MW-sec.}$$

The energy storage term can be stated as:

$$(8) \quad Q_{s12} = \int_{T_{sat}}^{T_1} Q_s(T) dT$$

When the average temperature of the debris bed exceeds 2173 °K, the Zircaloy in the debris bed will exceed the Zircaloy melting temperature, and the existence of a debris bed is no longer assured. The energy stored in the core will be maximized if the average debris bed temperature is assumed to equal 2173 °K. For the S₁D sequence, the equilibrium primary system pressure is approximately 60 psia after core recovery. Assuming that the core will quench to approximately T_{sat} for 60 psia system pressure (≈ 418 °K) we have the following equation for the energy storage term:

$$(9) \quad Q_{s12} = \int_{418}^{2173} Q_s(T) dT$$

The energy storage term in the fuel, cladding, baffles, and formers can be readily calculated based upon known masses of the core components, and their corresponding specific heats as a function of temperature. The total stored energy which must be removed in t_{12} as the core cools from 2173 °K to 418 °K is:

$$(10) \quad Q_{s12} = 7.03 \times 10^4 \text{ MW-sec}$$

The maximum heat loss which can occur from the severely deformed core is controlled by the size of the assumed debris bed, and the heat transfer assumed to occur. The model which has been used assumes that the deformed core occupies the entire core region of the inside of the core barrel. The model conservatively evaluates heat losses from the top, bottom and sides of the debris bed. Heat loss from the top of the bed is assumed to be limited by the pool boiling critical heat flux which is calculated to be 2.13 MW/m² for the S₁D sequence. Heat loss from the bottom surface of the core is conservatively assumed to be controlled by horizontal upward plate film boiling. This represents a conservative maximized treatment of heat transfer from the lower surface, since downward heat transfer into a pool of water is likely to be much smaller than the maximum heat transfer which would occur due to film boiling. The downward heat transfer for the S₁D sequence is calculated to be 0.223 MW/m².

Heat transfer through the side of the debris bed is assumed to be controlled by conduction through the stainless steel core barrel. For the S₁D sequence, heat transfer through the sides of the core is calculated to be 0.507 MW/m². The total amount of heat which can be removed from the core is:

$$(11) \quad Q_{\text{loss}} = Q_{\text{top}} + Q_{\text{bottom}} + Q_{\text{sides}}$$

Based upon the assumed size of the debris bed (i.e., the entire core region area inside the core barrel), the maximum heat loss from the severely deformed core is calculated to be:

$$(12) \quad Q_{\text{loss}} = 48.0 \text{ MW}$$

The full energy balance will now be expressed as an equality by incorporating the production time span, t_{12} , into Equation (1) and substituting Equations (4), (7), (10) and (12) into the resulting equation:

$$(13) \quad Q_{\text{loss}} t_{12} = Q_{\text{dh}12} + Q_{\text{ox}12} + Q_{\text{s}12}$$

or

$$(14) \quad 48.0 (t_2 - t_1) \text{ MW-sec} = 468.0 \left[t_2^{0.747} - t_1^{0.747} \right] \text{ MW-sec} \\ + 6.59 \times 10^4 \text{ MW-sec} + 7.03 \times 10^4 \text{ MW-sec}$$

Combining like terms, and since t_1 occurs when the majority of the hydrogen gas was expelled through the break (1.92 hours (6912 seconds) for the S₁D sequence) gives the following equation:

$$(15) \quad 0.102564 t_2 = t_2^{0.747} + 261.7$$

which, when solved iteratively, yields:

$$t_2 = 16068 \text{ seconds}$$

Therefore, for the S₁D sequence, the average rate of hydrogen production over the time span of t_{12} to reach a total hydrogen production equal to 75% MWR is:

$$\dot{M}_{\text{H}12} = \frac{M_{\text{H}12}}{t_{12}} = \frac{988.6 \text{ lbs}}{16068-6912 \text{ secs}}$$

or

$$\dot{M}_{\text{H}12} = 0.108 \text{ lbm/sec}$$

for a period of 16068-6912 secs = 9156 secs (2.54 hrs.)

Since the non-mechanistic model description given for the S₁D sequence also applies to the S₂D, TMLU, and S₂H sequences, the results for the remaining three sequences will be presented in an abbreviated format.

S₂D Sequence

$$(1) \quad Q_{\text{loss}} \geq Q_{\text{dh}} + Q_{\text{ox}} + Q_{\text{s}}$$

$$(2) \quad Q_{\text{dh}} = 349.6 t^{-0.253} \text{ (MW)}$$

This curve fit is accurate to +1.6%, -2.8% over the required time span (approximately 7488 to 13192 seconds following scram).

$$(3) \quad Q_{\text{dh12}} = \int_{t_1}^{t_2} Q_{\text{dh}}(t) dt$$

$$(4) \quad Q_{\text{dh12}} = 468.0 \left[t_2^{0.747} - t_1^{0.747} \right] \text{ (MW-sec).}$$

$$(5) \quad M_{\text{H12}} = 1496.6 - 460 = 1036.6 \text{ lbs. of H}_2$$

$$(6) \quad Q_{\text{ox}} = 66.68 \text{ MW-sec/lb of H}_2 \text{ produced.}$$

$$(7) \quad Q_{\text{ox12}} = 6.91 \times 10^4 \text{ MW-sec.}$$

$$(8) \quad Q_{\text{s12}} = \int_{T_{\text{sat}}}^{T_1} Q_{\text{s}}(T) dT$$

For the S₂D sequence, the equilibrium primary system pressure is approximately 210 psia after core recovery. Assuming that the core will quench to approximately T_{sat} for 210 psia system pressure (≈ 470 °K) we have the following equation for the energy storage term:

$$(9) \quad Q_{\text{s12}} = \int_{470}^{2173} Q_{\text{s}}(T) dT$$

$$(10) \quad Q_{\text{s12}} = 6.86 \times 10^4 \text{ MW-sec}$$

$$(11) \quad Q_{\text{loss}} = Q_{\text{top}} + Q_{\text{bottom}} + Q_{\text{sides}}$$

$$\begin{aligned} \text{Upward heat loss} &= 3.02 \text{ MW/m}^2 \\ \text{Downward heat loss} &= 0.314 \text{ MW/m}^2 \\ \text{Side heat loss} &= 0.487 \text{ MW/m}^2 \end{aligned}$$

$$(12) \quad Q_{\text{loss}} = 58.1 \text{ MW}$$

$$(13) \quad Q_{\text{loss}} t_{12} = Q_{\text{dh12}} + Q_{\text{ox12}} + Q_{\text{s12}}$$

$$(14) \quad 58.1 (t_2 - t_1) \text{ MW-sec} = 468.0 \left[t_2^{0.747} - t_1^{0.747} \right] \text{ MW-sec} + \\ 6.91 \times 10^4 \text{ MW-sec} + 6.86 \times 10^4 \text{ MW-sec}$$

t₁ occurs at 2.08 hours (7488 seconds)

$$(15) \quad 0.124145 t_2 = t_2^{0.747} + 440.1$$

which, when solved iteratively, yields:

$$t_2 = 13171 \text{ seconds}$$

Therefore, for the S₂D sequence, the average rate of hydrogen production over the time span of t_{12} to reach a total hydrogen production equal to 75% MWR is:

$$\dot{M}_{H12} = \frac{M_{H12}}{t_{12}} = \frac{1036.6 \text{ lbs}}{13171-7488 \text{ secs}}$$

or

$$\dot{M}_{H12} = 0.182 \text{ lbm/sec}$$

for a period of 13171-7488 secs = 5683 secs (1.58 hrs.)

TMLU Sequence

$$(1) \quad Q_{\text{loss}} \geq Q_{\text{dh}} + Q_{\text{cx}} + Q_{\text{s}}$$

$$(2) \quad Q_{\text{dh}} = 366.1 t^{-0.257} \text{ (MW)}$$

This curve fit is accurate to +0.005% over the required time span (approximately 24480 to 28501 seconds following scram).

$$(3) \quad Q_{\text{dh}12} = \int_{t_1}^{t_2} Q_{\text{dh}}(t) dt$$

$$(4) \quad Q_{\text{dh}12} = 492.7 \left[t_2^{0.743} - t_1^{0.743} \right] \text{ (MW-sec).}$$

$$(5) \quad M_{H12} = 1496.6 - 630 = 866.6 \text{ lbs. of } H_2$$

$$(6) \quad Q_{\text{ox}} = 66.68 \text{ MW-sec/lb of } H_2 \text{ produced.}$$

$$(7) \quad Q_{\text{ox}12} = 5.78 \times 10^4 \text{ MW-sec}$$

$$(8) \quad Q_{\text{s}12} = \int_{T_{\text{sat}}}^{T_1} Q_{\text{s}}(T) dT$$

For the TMLU sequence, the equilibrium primary system pressure is approximately 2335 psia after core recovery. Assuming that the core will quench to approximately T_{sat} for 2335 psia system pressure ($\approx 621^\circ\text{K}$) we have the following equation for the energy storage term:

$$(9) \quad Q_{\text{s}12} = \int_{621}^{2173} Q_{\text{s}}(T) dT$$

$$(10) \quad Q_{s12} = 6.35 \times 10^4 \text{ MW-sec}$$

$$(11) \quad Q_{\text{loss}} = Q_{\text{top}} + Q_{\text{bottom}} + Q_{\text{sides}}$$

Upward heat loss = 2.95 MW/m^2
 Downward heat loss = 0.504 MW/m^2
 Side heat loss = 0.429 MW/m^2

$$(12) \quad Q_{\text{loss}} = 56.9 \text{ MW}$$

$$(13) \quad Q_{\text{loss}} t_{12} = Q_{\text{dh}12} + Q_{\text{ox}12} + Q_{\text{s}12}$$

$$(14) \quad 56.9 (t_2 - t_1) \text{ MW-sec} = 492.7 \left[t_2^{0.743} - t_1^{0.743} \right] \text{ MW-sec} + 5.78 \times 10^4 \text{ MW-sec} + 6.35 \times 10^4 \text{ MW-sec}$$

t_1 occurs at 6.8 hours or 24480 seconds

$$(15) \quad 0.115486 t_2 = t_2^{0.743} + 1249.9$$

which, when solved iteratively, yields:

$$t_2 = 28501 \text{ seconds}$$

Therefore, for the TMLU sequence, the average rate of hydrogen production over the time span of t_{12} to reach a total hydrogen production equal to 75% MWR is:

$$\dot{M}_{\text{H}12} = \frac{M_{\text{H}12}}{t_{12}} = \frac{866.6 \text{ lbs}}{28501-24480 \text{ secs}}$$

or

$$\dot{M}_{\text{H}12} = 0.216 \text{ lbm/sec}$$

for a period of 28501-24480 secs = 4021 secs (1.12 hrs.)

S₂H Sequence

$$(1) \quad Q_{\text{loss}} \geq Q_{\text{dh}} + Q_{\text{ox}} + Q_{\text{s}}$$

$$(2) \quad Q_{\text{dh}} = 224.0 t^{-0.206} \text{ (MW)}$$

This curve fit is accurate to +2.1%, -1.1% over the required time span (approximately 10080 to 15339 seconds following scram).

$$(3) \quad Q_{\text{dh}12} = \int_{t_1}^{t_2} Q_{\text{dh}}(t) dt$$

$$(4) \quad Q_{\text{dh}12} = 282.1 \left[t_2^{0.794} - t_1^{0.794} \right] \text{ (MW-sec).}$$

$$(5) \quad M_{H12} = 1496.6 - 502 = 994.6 \text{ lbs. of } H_2$$

$$(6) \quad Q_{ox} = 66.68 \text{ MW-sec/lb of } H_2 \text{ produced.}$$

$$(7) \quad Q_{ox12} = 6.63 \times 10^4 \text{ MW-sec}$$

$$(8) \quad Q_{s12} = \int_{T_{sat}}^{T_1} Q_s(T) dT$$

For the S₂H sequence, the equilibrium primary system pressure is approximately 200 psia after core recovery. Assuming that the core will quench to approximately T_{sat} for 200 psia system pressure (≈ 467 °K) we have the following equation for the energy storage term:

$$(9) \quad Q_{s12} = \int_{467}^{2173} Q_s(T) dT$$

$$(10) \quad Q_{s12} = 6.87 \times 10^4 \text{ MW-sec}$$

$$(11) \quad Q_{loss} = Q_{top} + Q_{bottom} + Q_{sides}$$

$$\begin{aligned} \text{Upward heat loss} &= 2.99 \text{ MW/m}^2 \\ \text{Downward heat loss} &= 0.310 \text{ MW/m}^2 \\ \text{Side heat loss} &= 0.488 \text{ MW/m}^2 \end{aligned}$$

$$(12) \quad Q_{loss} = 57.7 \text{ MW}$$

$$(13) \quad Q_{loss} t_{12} = Q_{dh12} + Q_{ox12} + Q_{s12}$$

$$(14) \quad 57.7 (t_2 - t_1) \text{ MW-sec} = 282.1 \left[t_2^{0.794} - t_1^{0.794} \right] \text{ MW-sec} + 6.63 \times 10^4 \text{ MW-sec} + 6.87 \times 10^4 \text{ MW-sec}$$

t₁ occurs at 2.80 hours (10080 seconds)

$$(15) \quad 0.204537 t_2 = t_2^{0.794} + 1031.1$$

which, when solved iteratively, yields:

$$t_2 = 15339 \text{ seconds}$$

Therefore, for the S₂H sequence, the average rate of hydrogen production over the time span of t₁₂ to reach a total hydrogen production equal to 75% MWR is:

$$\dot{M}_{H12} = \frac{M_{H12}}{t_{12}} = \frac{994.6 \text{ lbs}}{15339 - 10080 \text{ secs}}$$

or

$$\dot{M}_{H12} = 0.189 \text{ lbm/sec}$$

for a period of 15339-10080 secs = 5259 secs (1.46 hrs.)

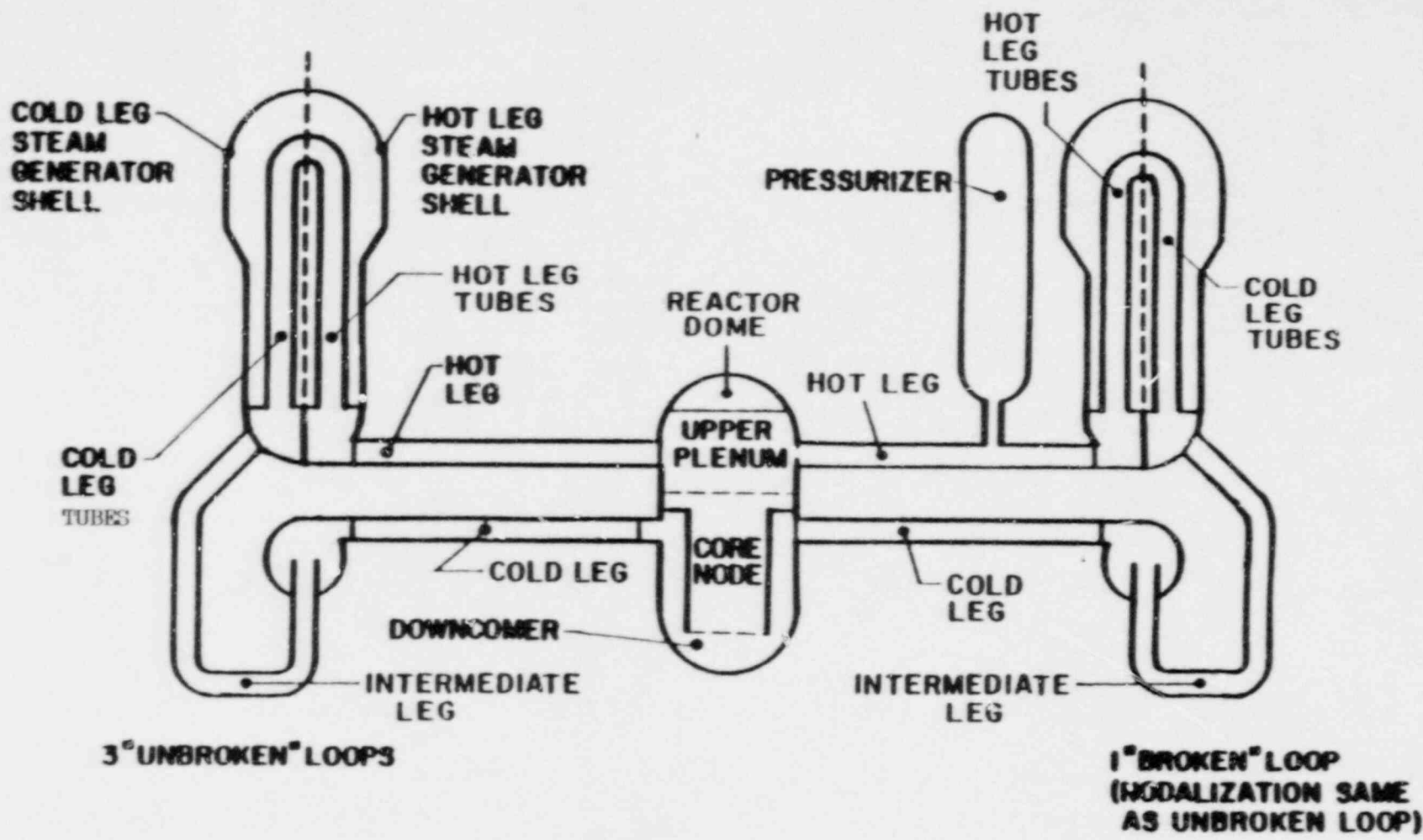


Figure 1: Application of PWR primary system nodalization to a Westinghouse 4 loop design.

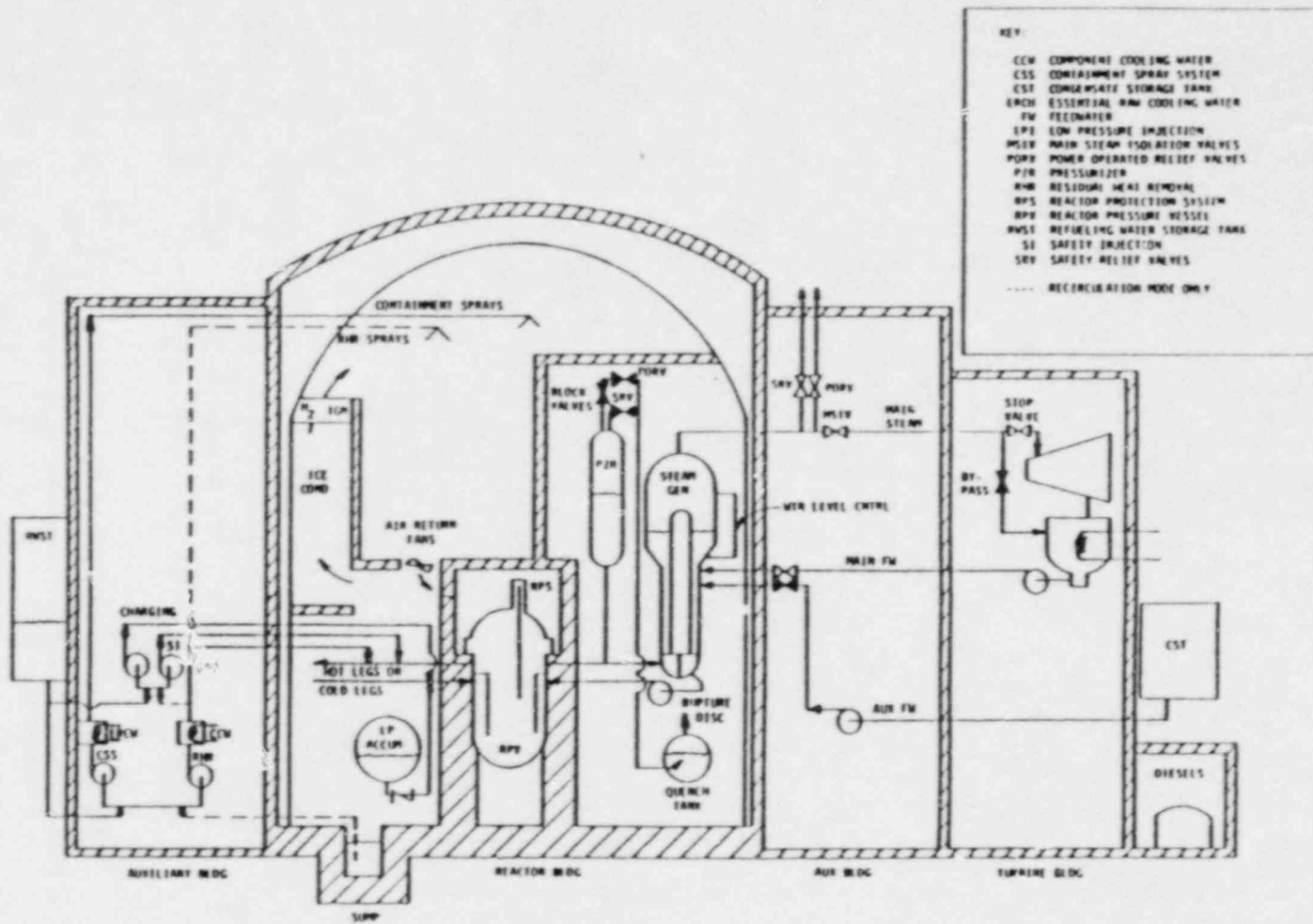


Figure 2 Catawba Safety System Features

APPENDIX 1

S₁D Sequence Plots - 10CFR50.44 Analysis

SID SEQUENCE - 10CFR50.44 ANALYSIS

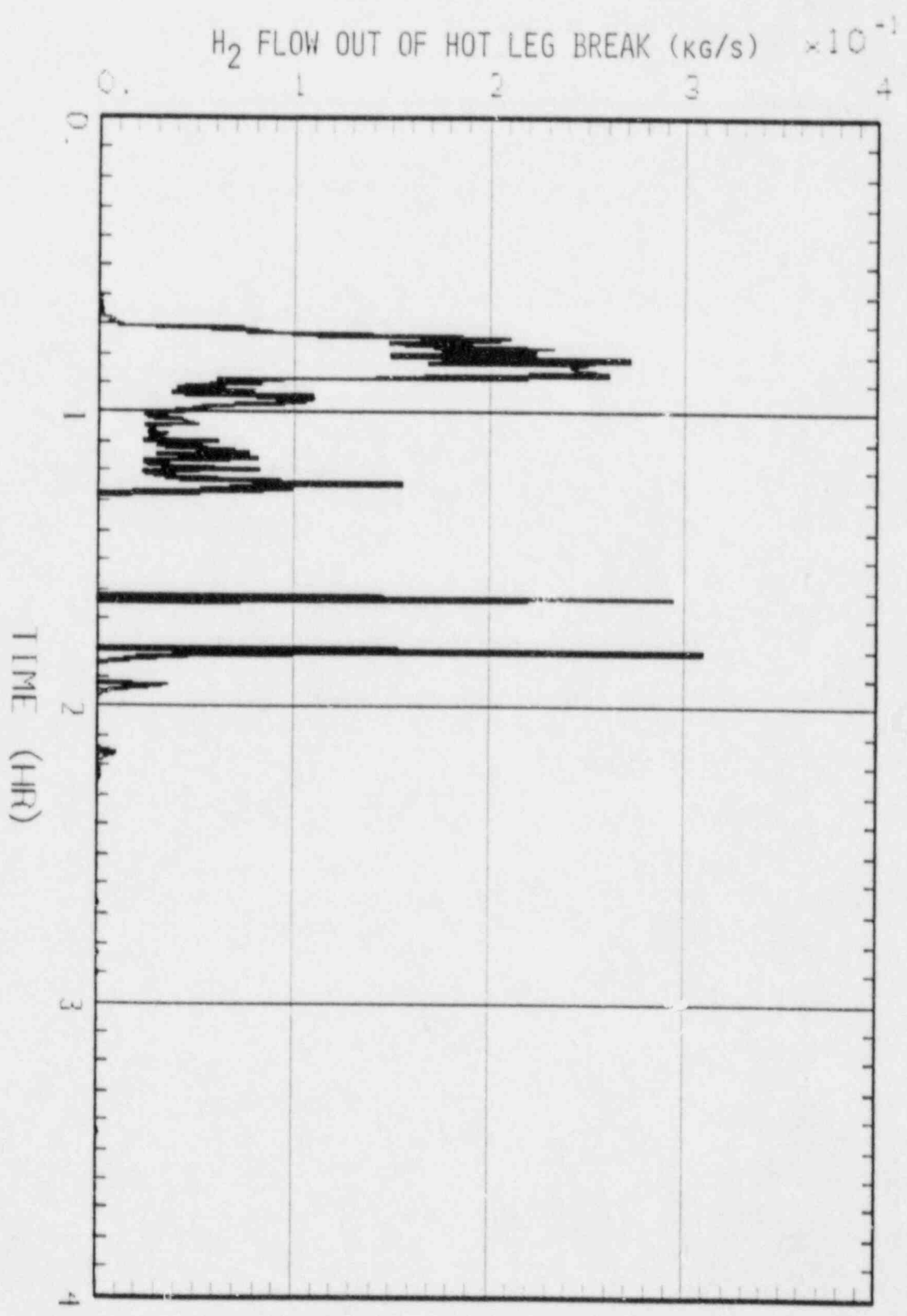
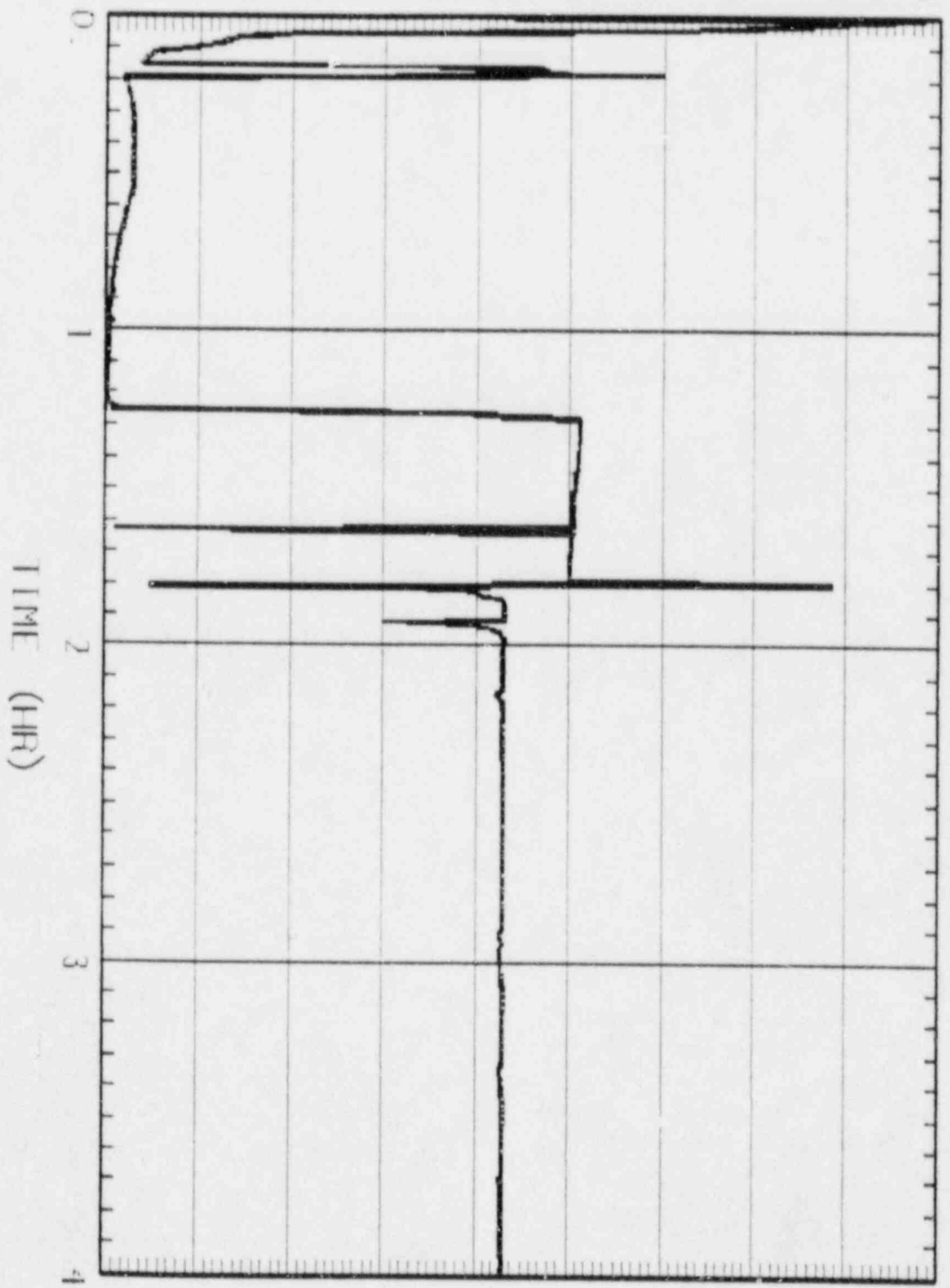


Figure 1.01 H₂ Flow Out of Hot Leg Break

WATER/STEAM FLOW OUT OF HOT LEG BREAK (kg/s) $\times 10^2$
0. 1.0 2.0 3.0 4.0 5.0 6.0 7.0 8.0 9.0



SIB SEQUENCE - 10CFR50.44 ANALYSIS

Figure 1.02 Water/Steam Flow Out of Hot Leg Break

S1D SEQUENCE - 10CFR50.44 ANALYSIS

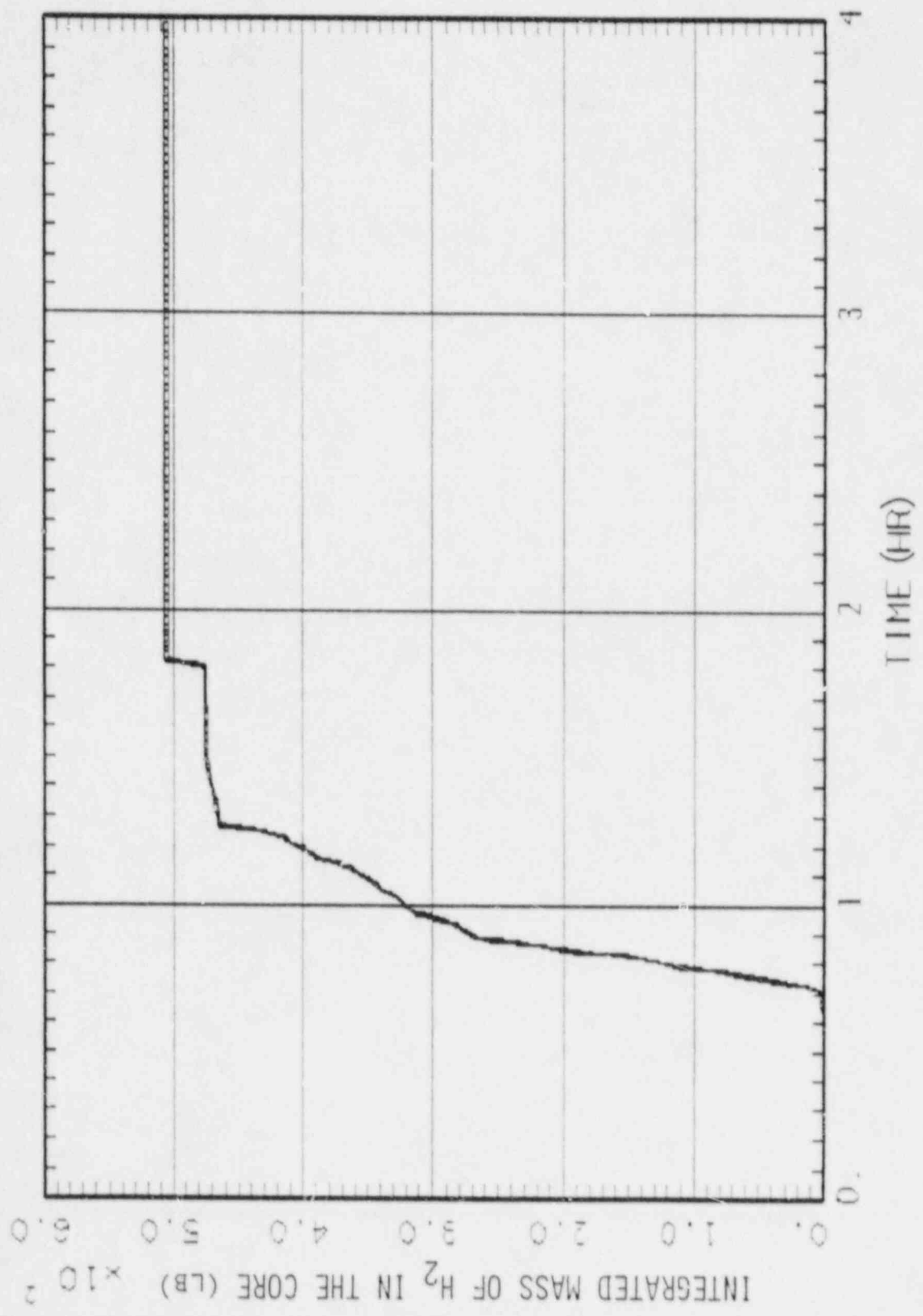


Figure 1.03 Integrated Mass of H₂ Generated in the Core

SID SEQUENCE - 10CFR50.44 ANALYSIS

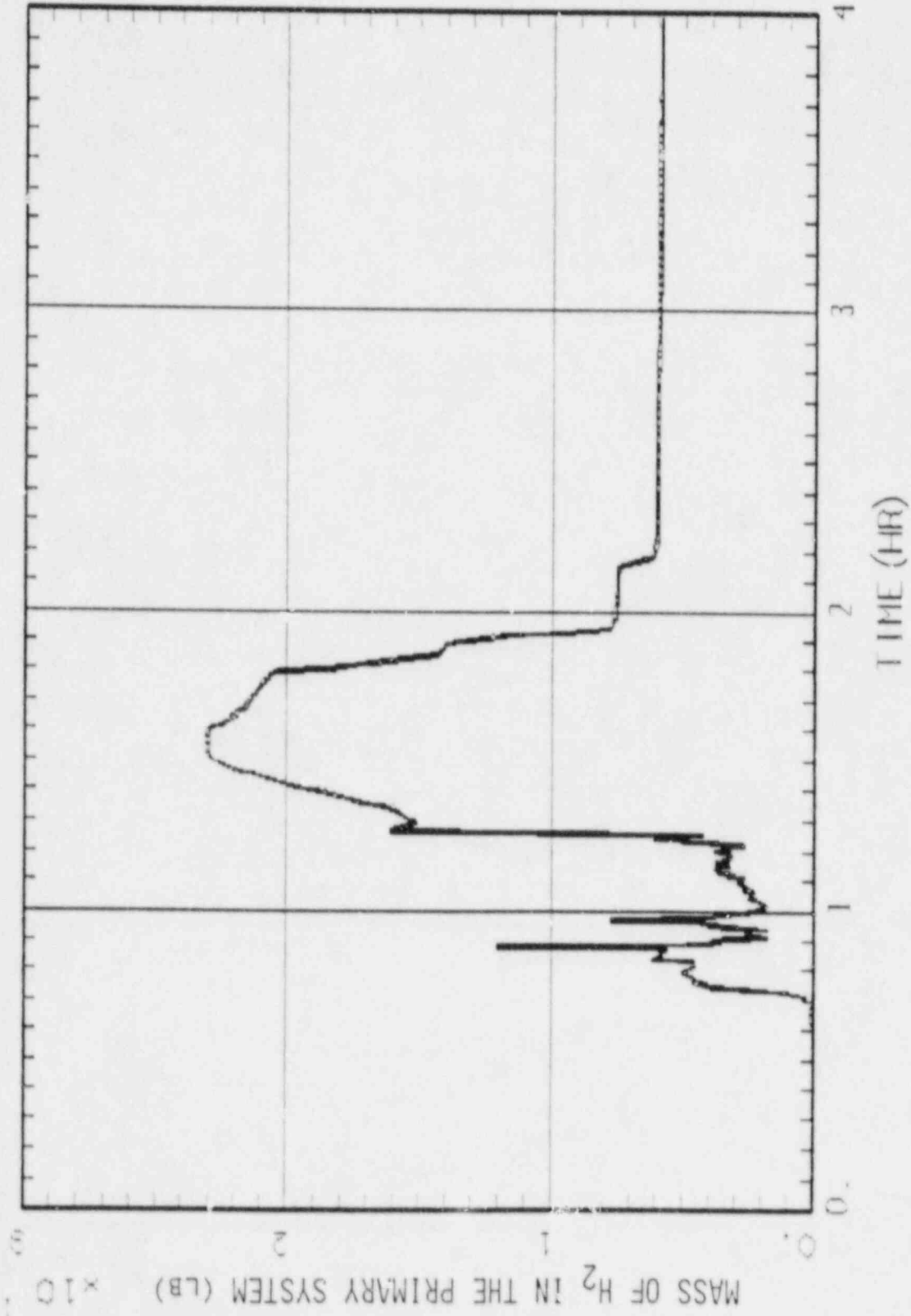


Figure 1.04 Mass of H₂ in the Primary System

SID SEQUENCE - 10CFR50.44 ANALYSIS

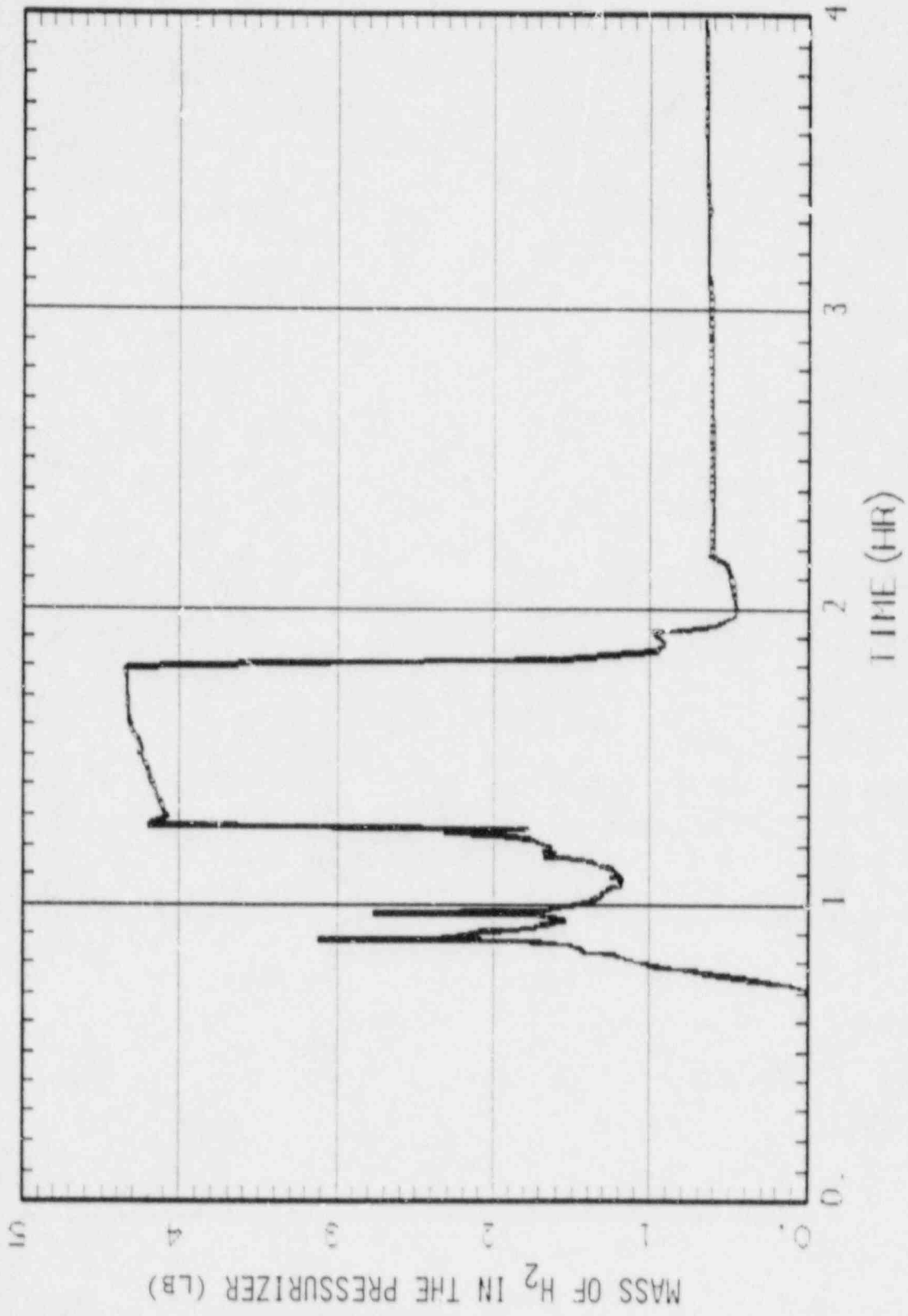
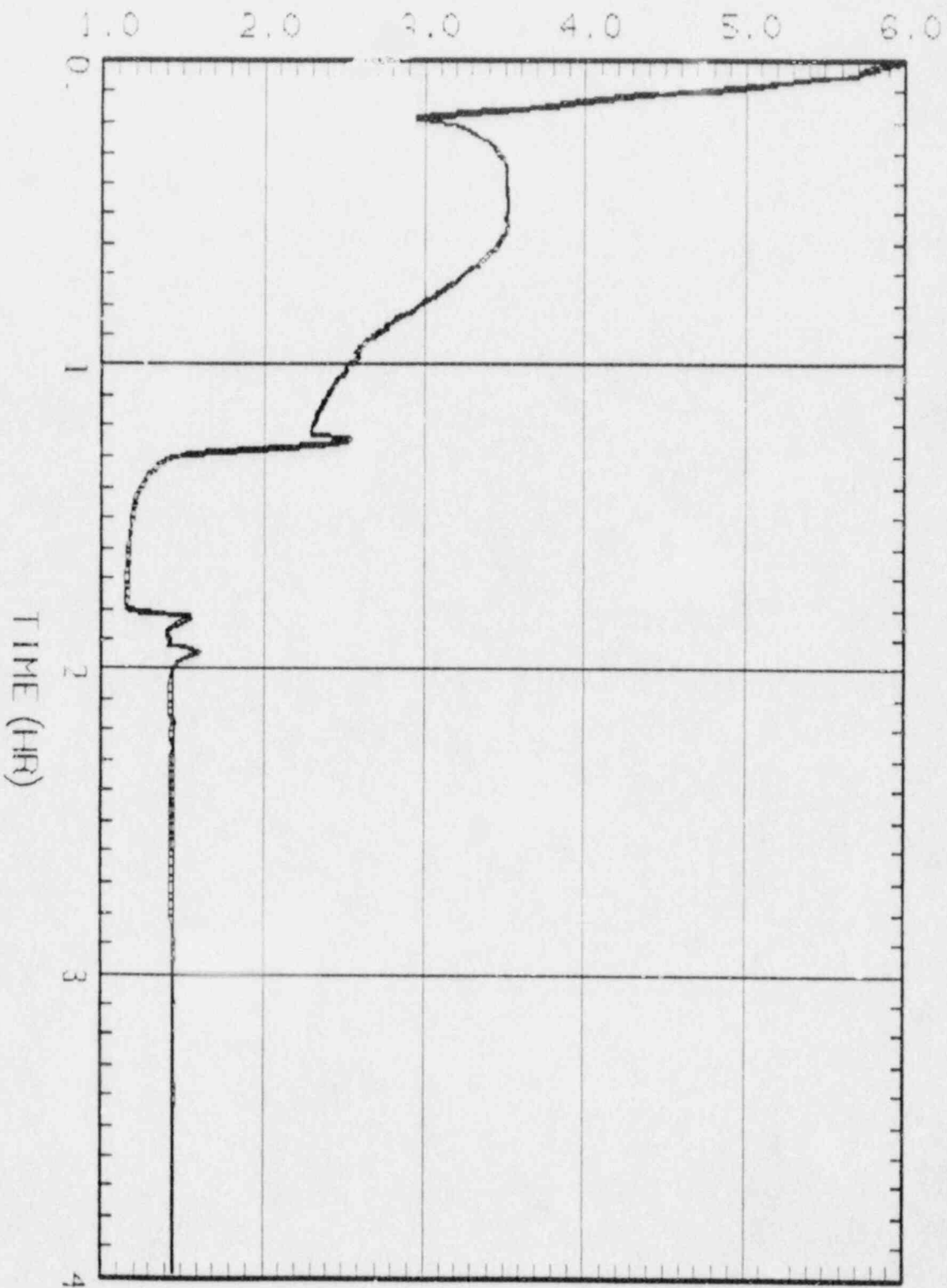


Figure 1.05 Mass of H₂ in the Pressurizer

WATER TEMPERATURE IN THE CORE (°F) $\times 10^{-2}$



SID SEQUENCE - 10CFR50.44 ANALYSIS

F are 1.06 Water Temperature in the Core

SID SEQUENCE - 10CFR50.44 ANALYSIS

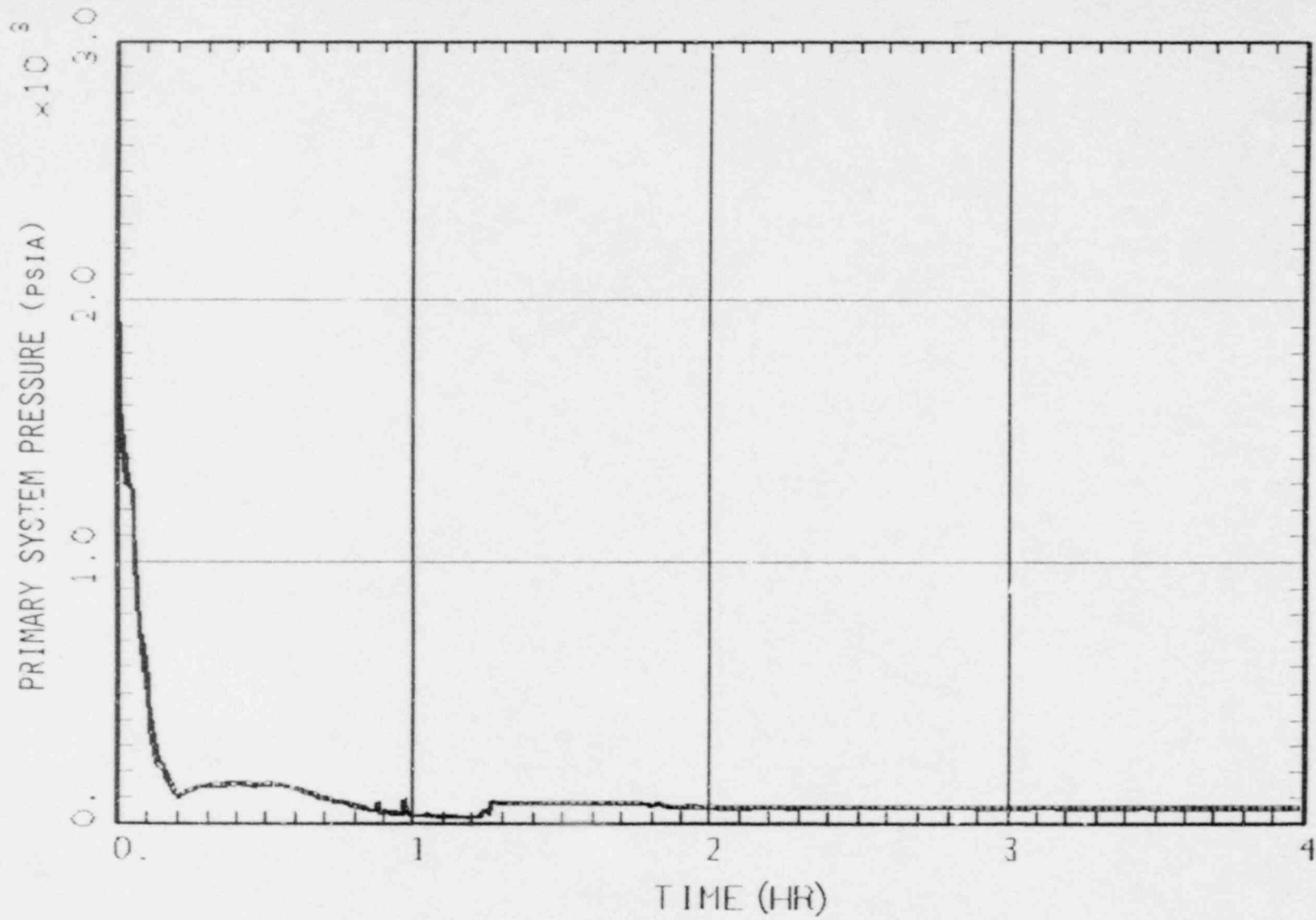


Figure 1.07 Primary System Pressure

SID SEQUENCE - 10CFR50.44 ANALYSIS

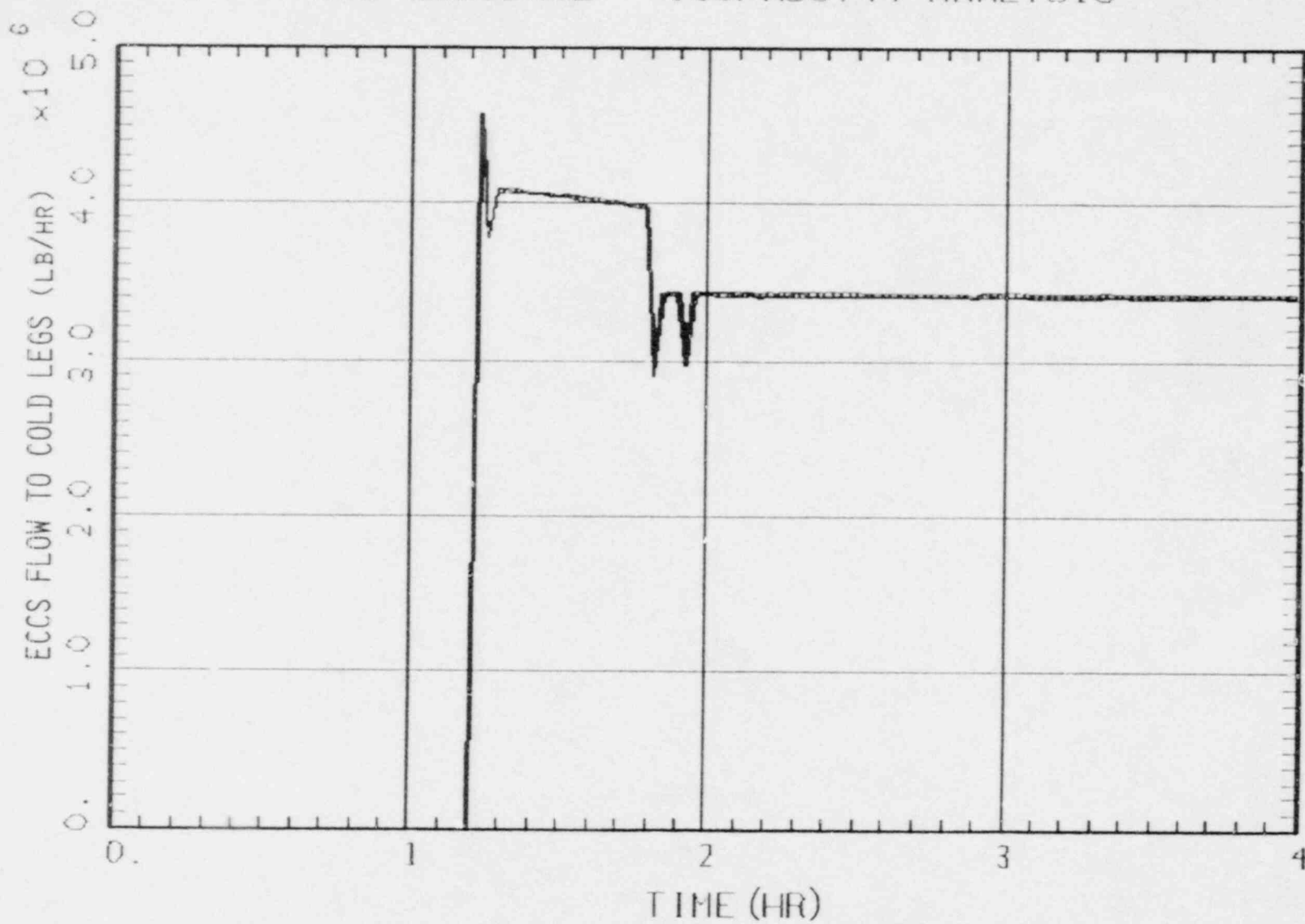


Figure 1.08 ECCS Flow to Cold Legs

SID SEQUENCE - 10CFR50.44 ANALYSIS

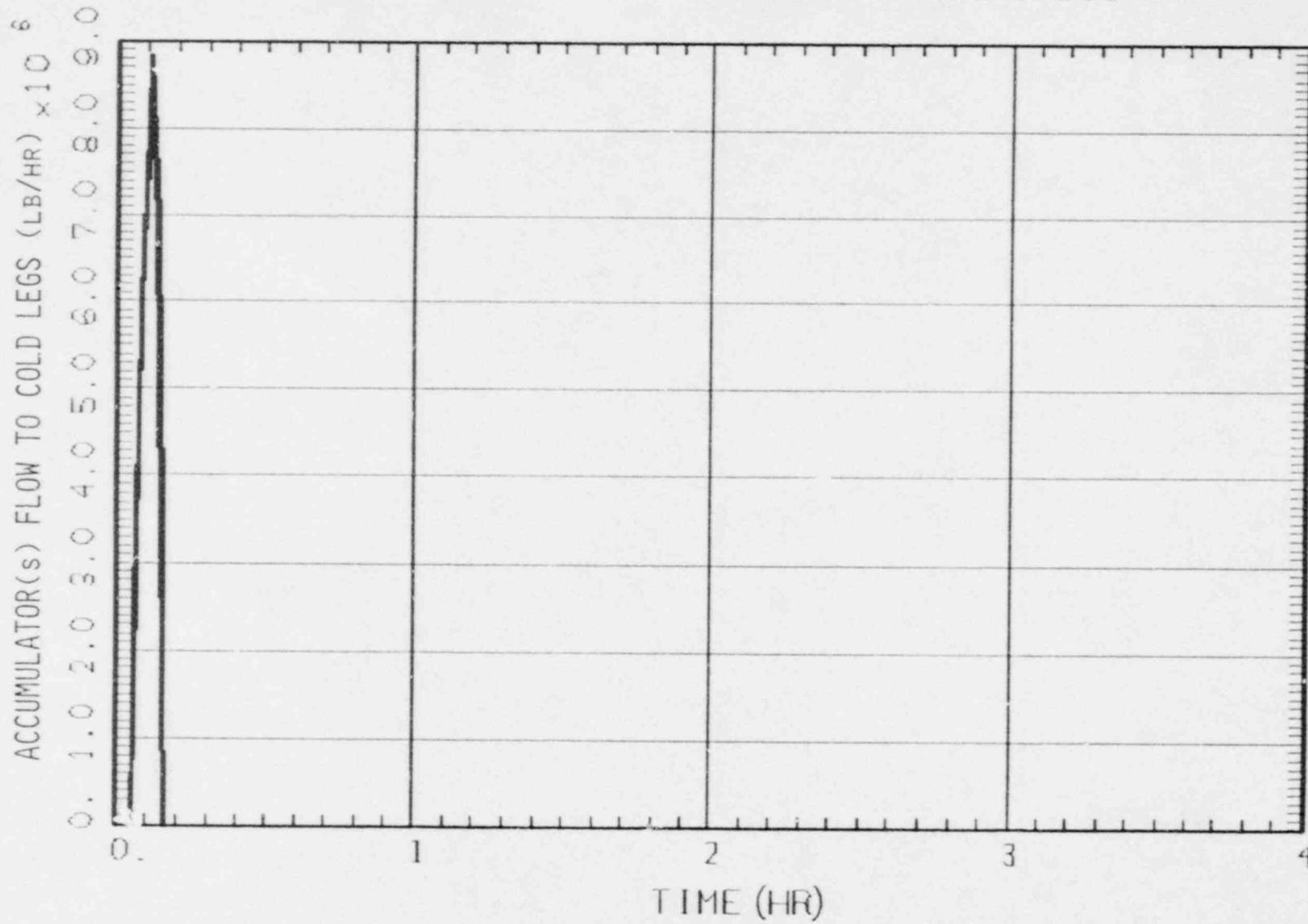


Figure 1.09 Accumulator(s) Flow to Cold Legs

SID SEQUENCE - 10CFR50.44 ANALYSIS

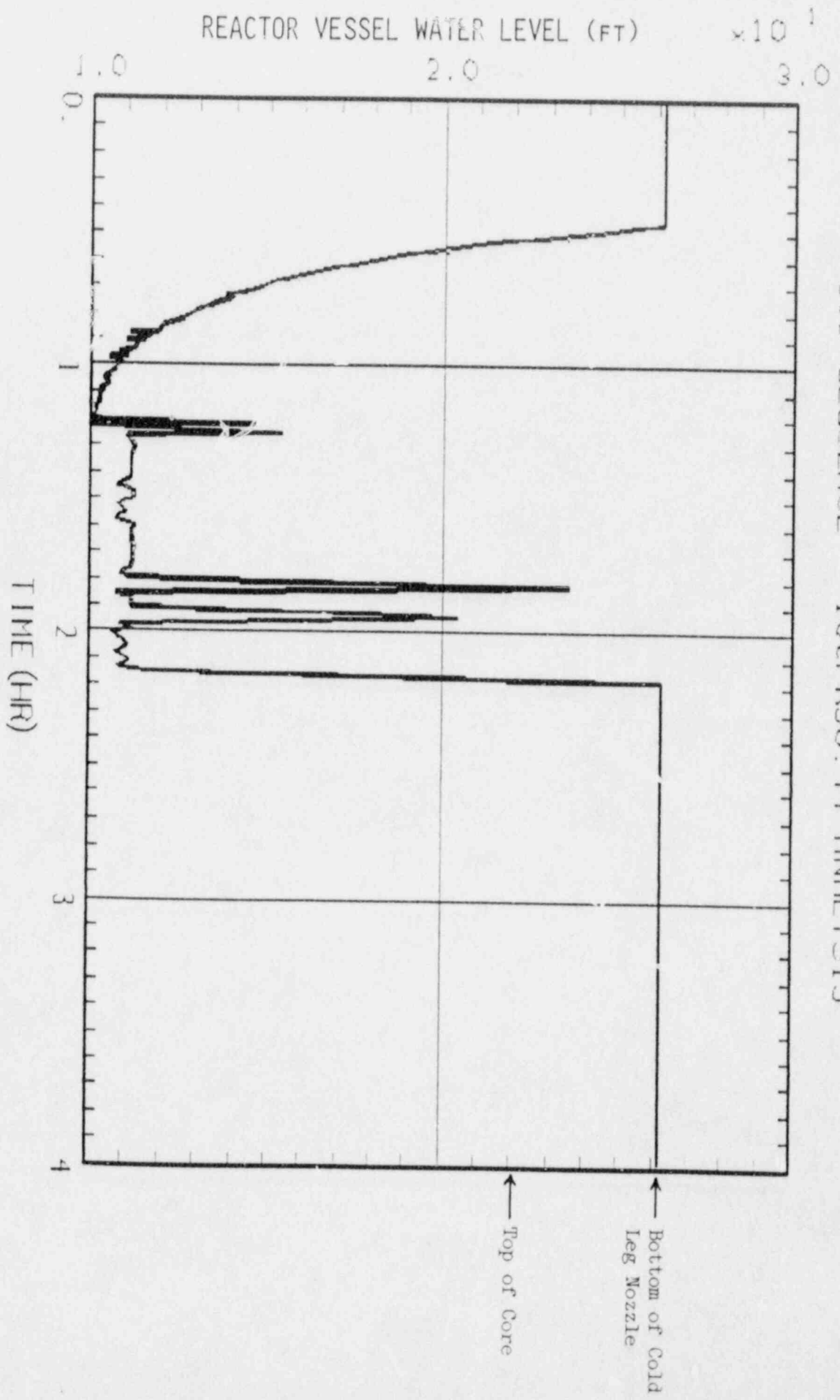


Figure 1.10 Reactor Vessel Water Level

SID SEQUENCE - 10CFR50.44 ANALYSIS

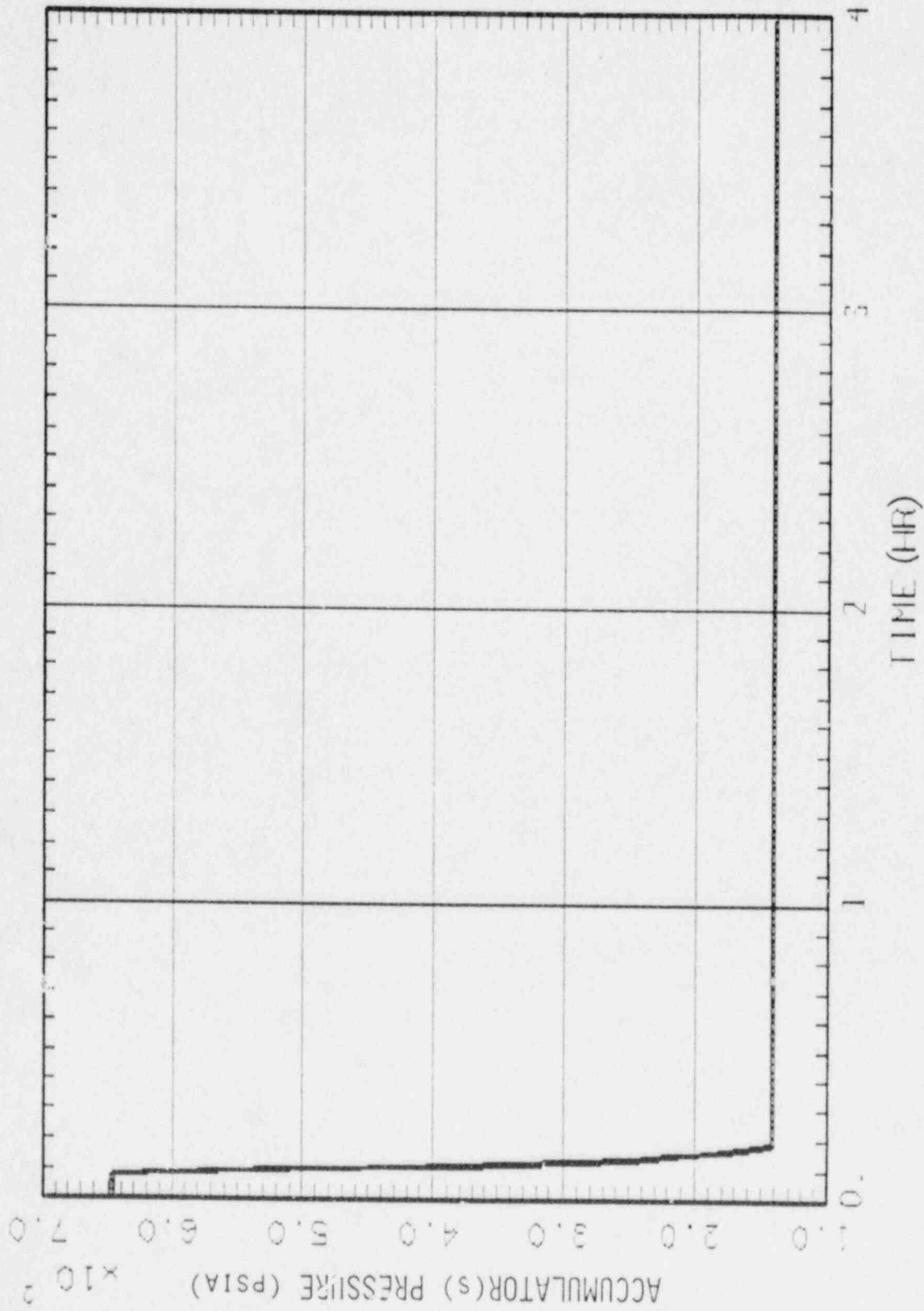


Figure 1.11 Accumulator(s) Pressure

SID SEQUENCE - 10CFR50.44 ANALYSIS

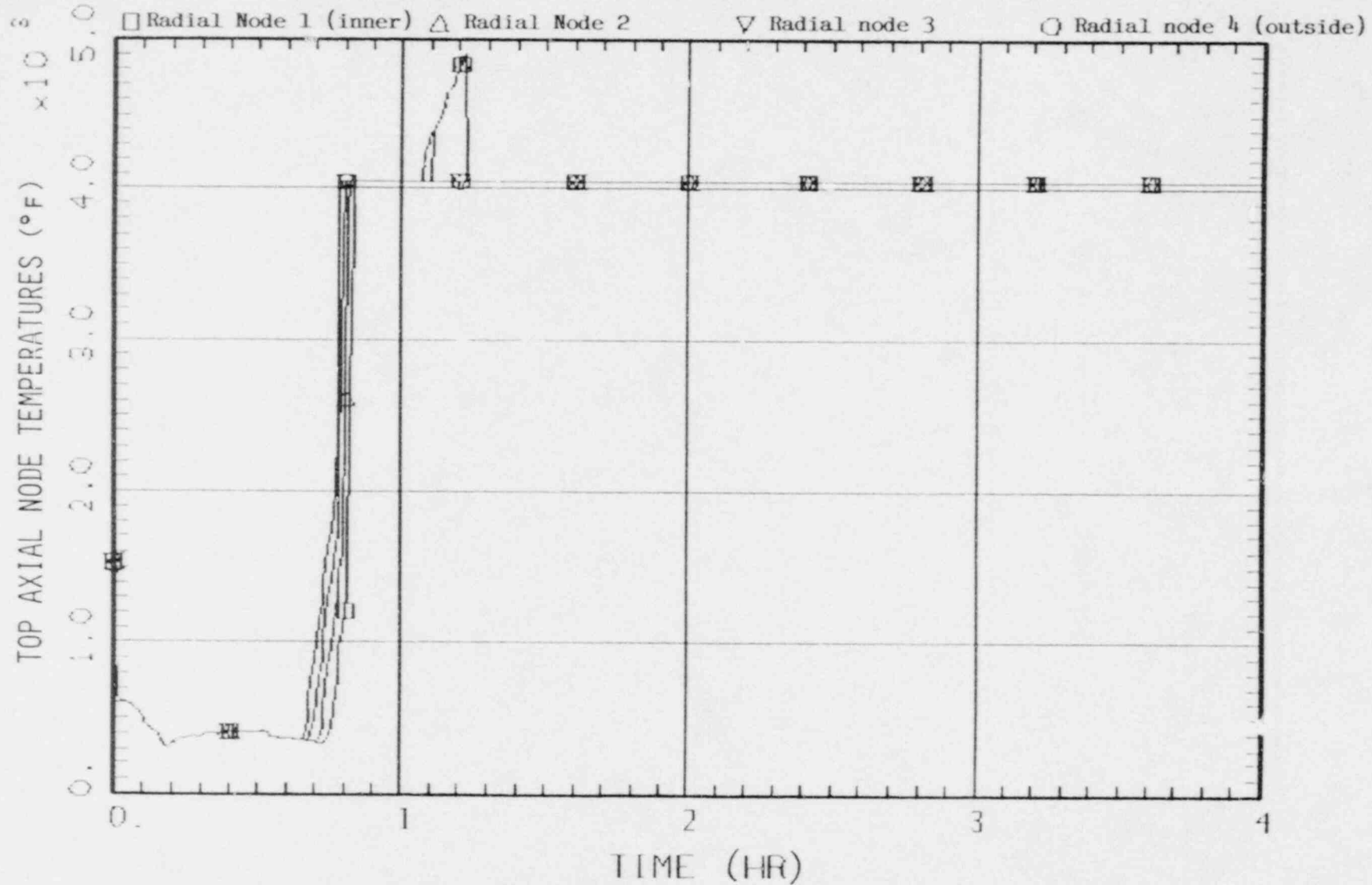


Figure 1.12 Top of Active Fuel Axial Node X 4 Top Radial Nodes

SID SEQUENCE - 10CFR50.44 ANALYSIS

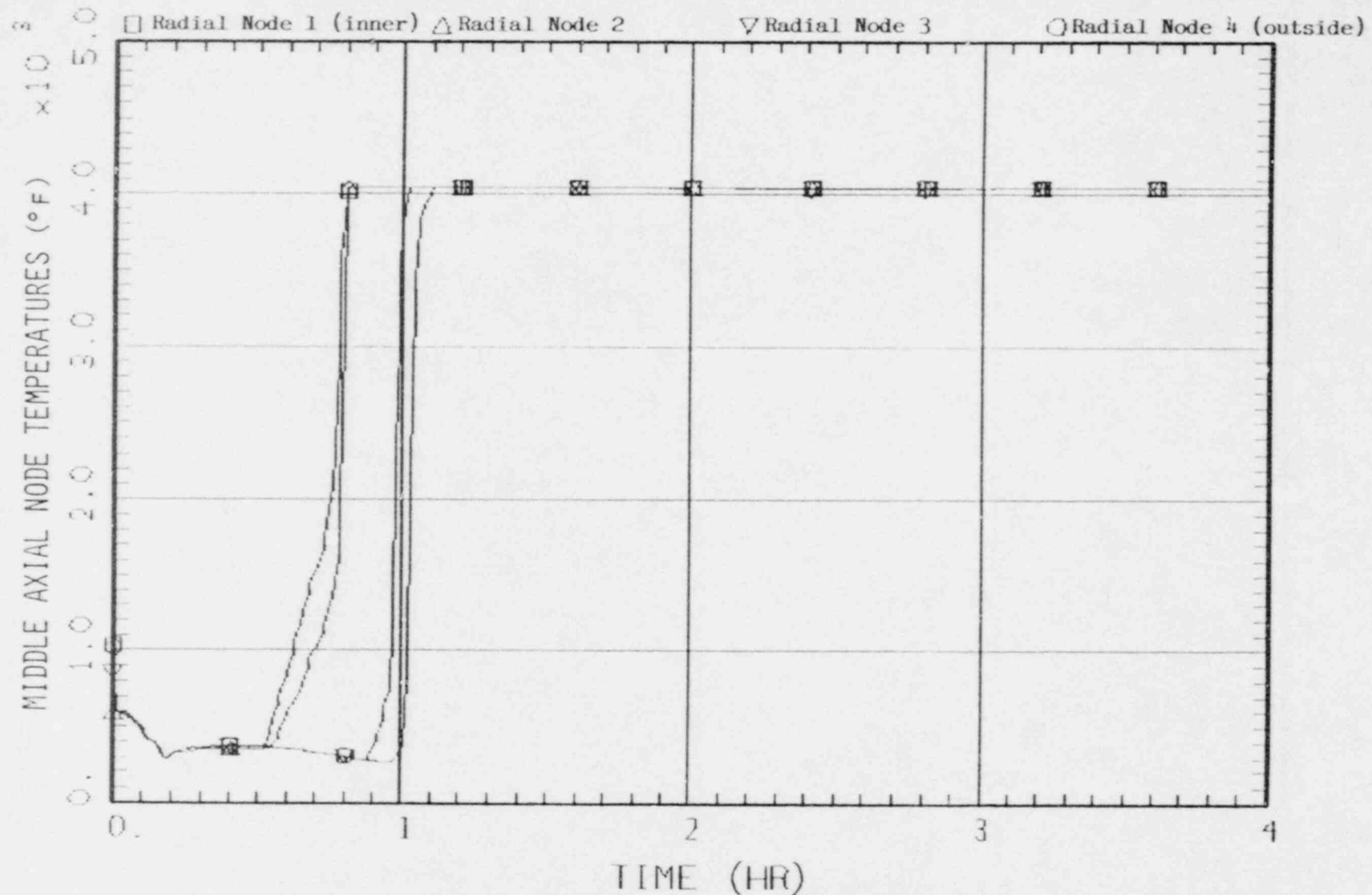


Figure 1.13 Middle of Active Fuel Axial Node X 4 Middle Radial Nodes

SID SEQUENCE - 10CFR50.44 ANALYSIS

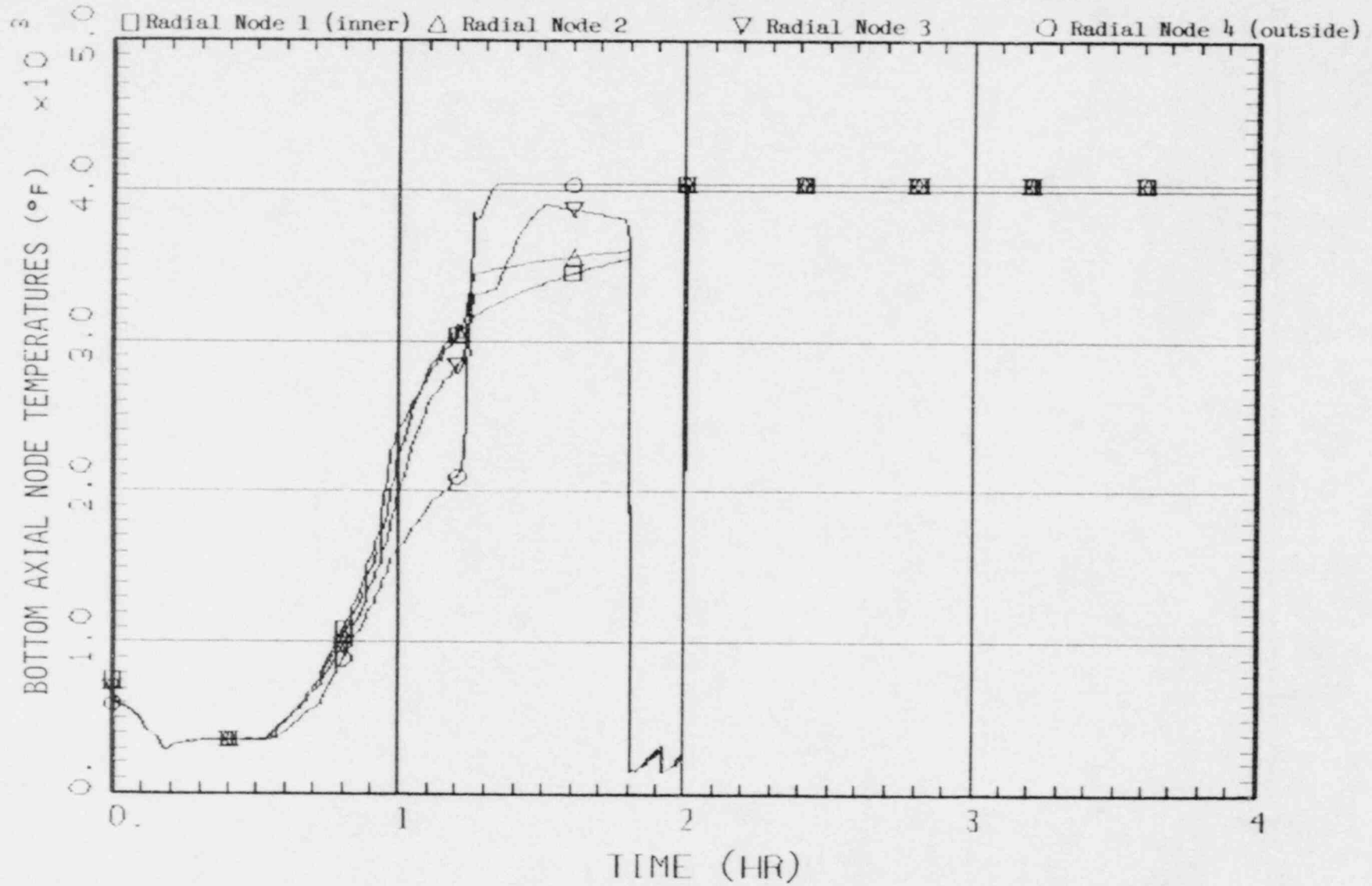


Figure 1.14 Bottom of Active Fuel Axial Node X 4 Bottom Radial Nodes

APPENDIX 2

S₂D Sequence Plots - 10CFR50.44 Analysis

S2D SEQUENCE - 10CFR50.44 ANALYSIS

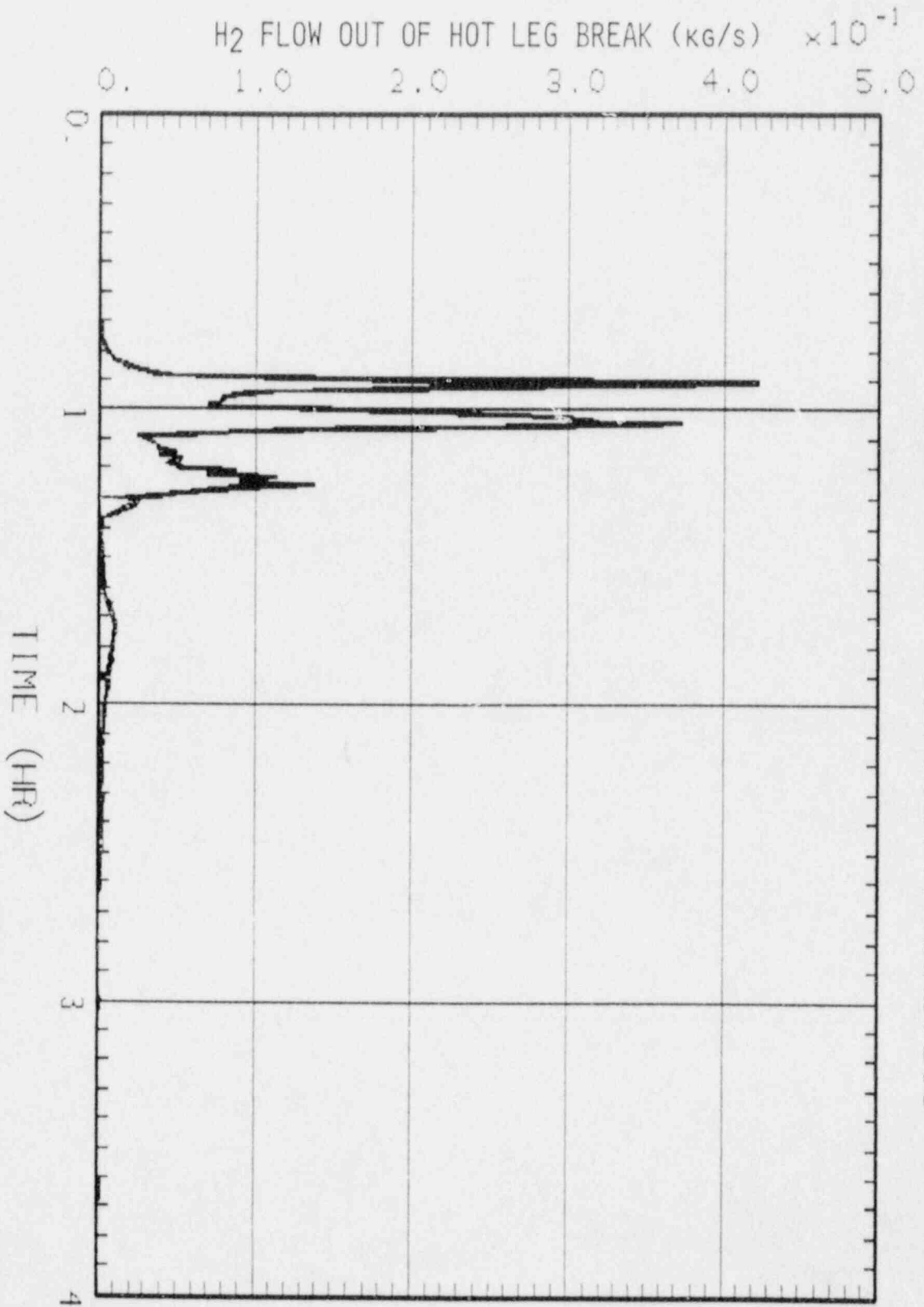


Figure 2.01 H₂ Flow Out of Hot Leg Break

52D SEQUENCE - 10CFR50.44 ANALYSIS

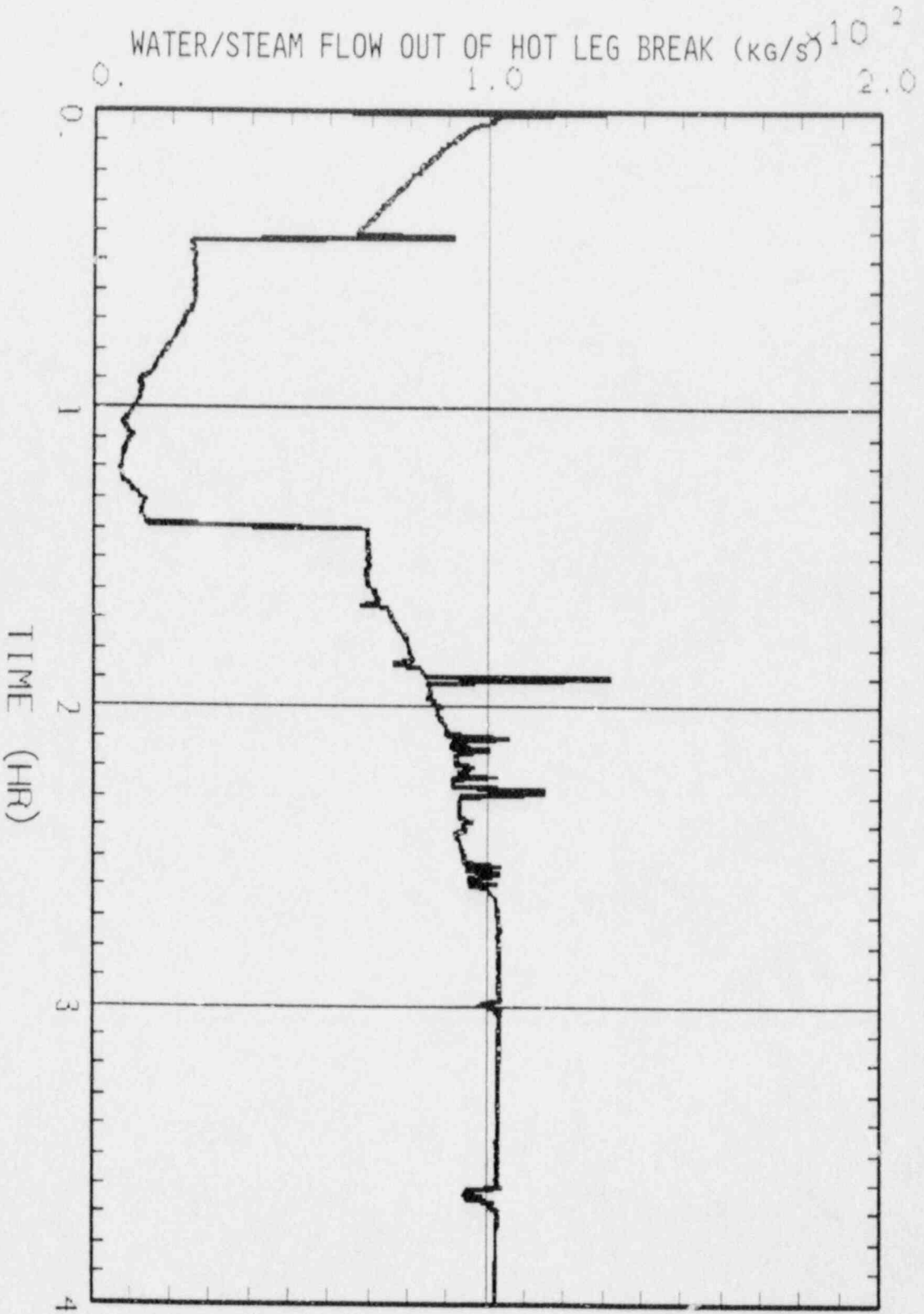


Figure 2.02 Water/Steam Flow Out of Hot Leg Break

S2D SEQUENCE - 10CFR50.44 ANALYSIS

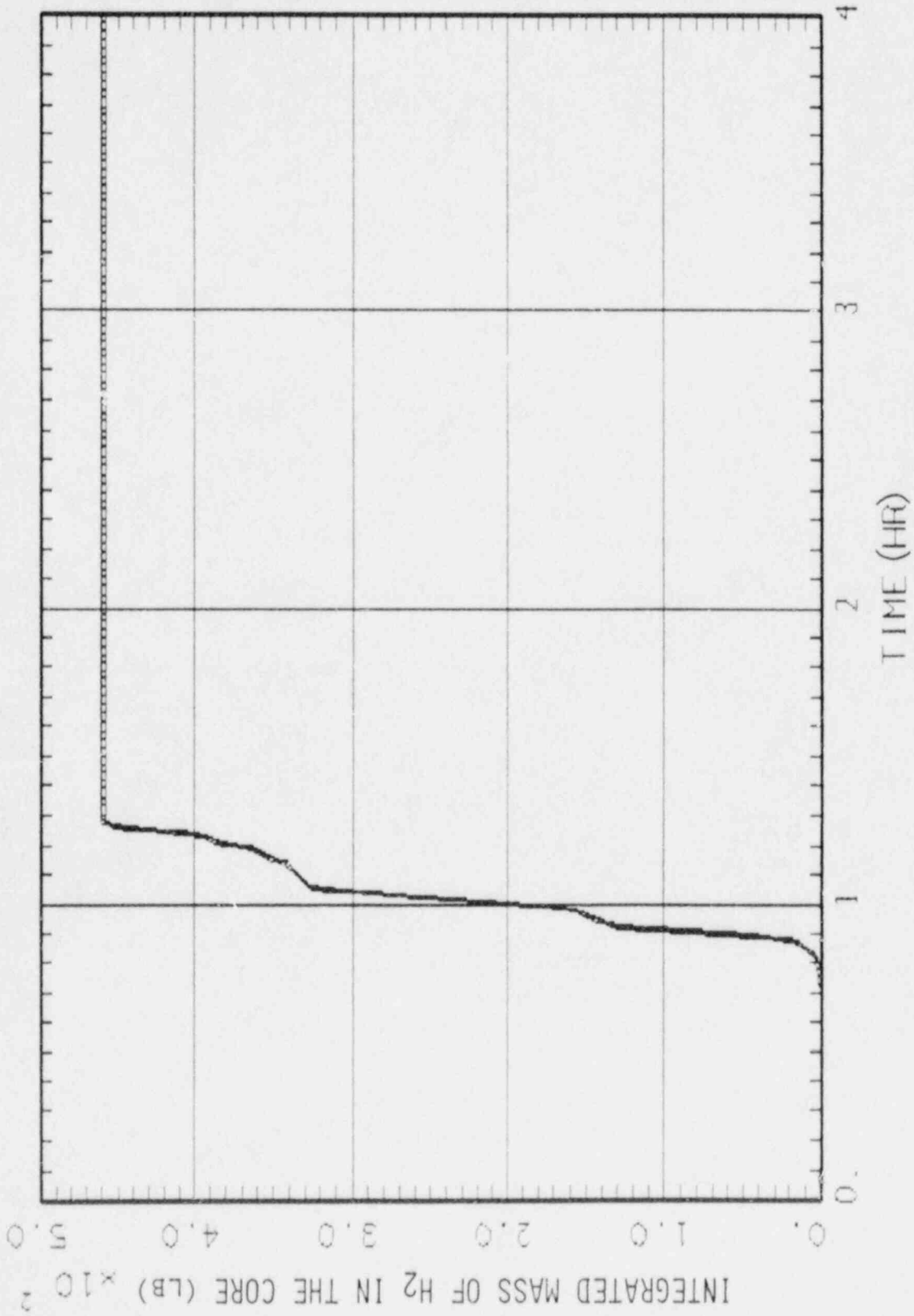


Figure 2.03 Integrated Mass of H₂ Generated in the Core

S2D SEQUENCE - 10CFR50.44 ANALYSIS

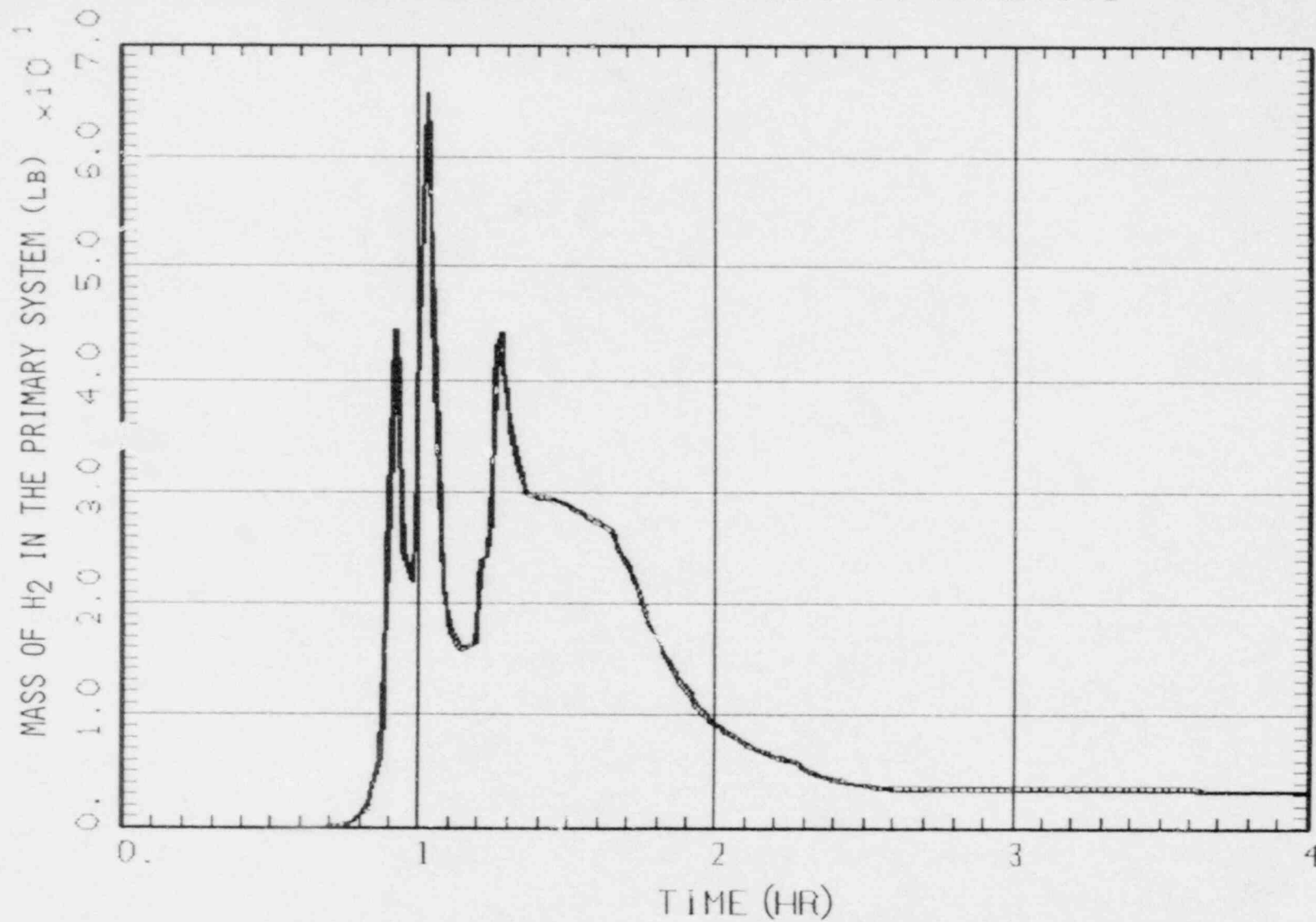


Figure 2.04 Mass of H₂ in the Primary System

S2D SEQUENCE - 10CFR50.44 ANALYSIS

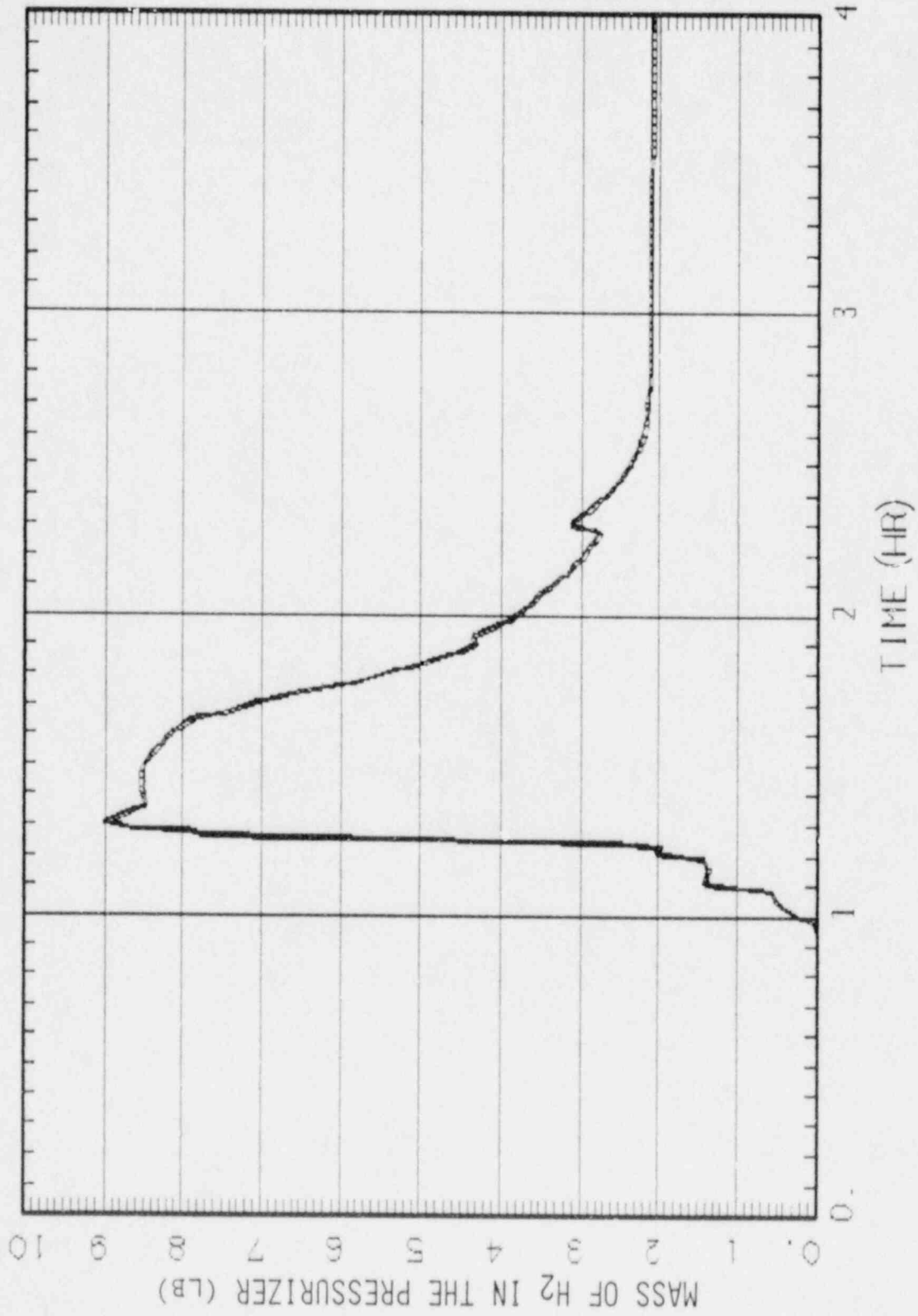


Figure 2.05 Mass of H₂ in the Pressurizer

S2D SEQUENCE - 10CFR50.44 ANALYSIS

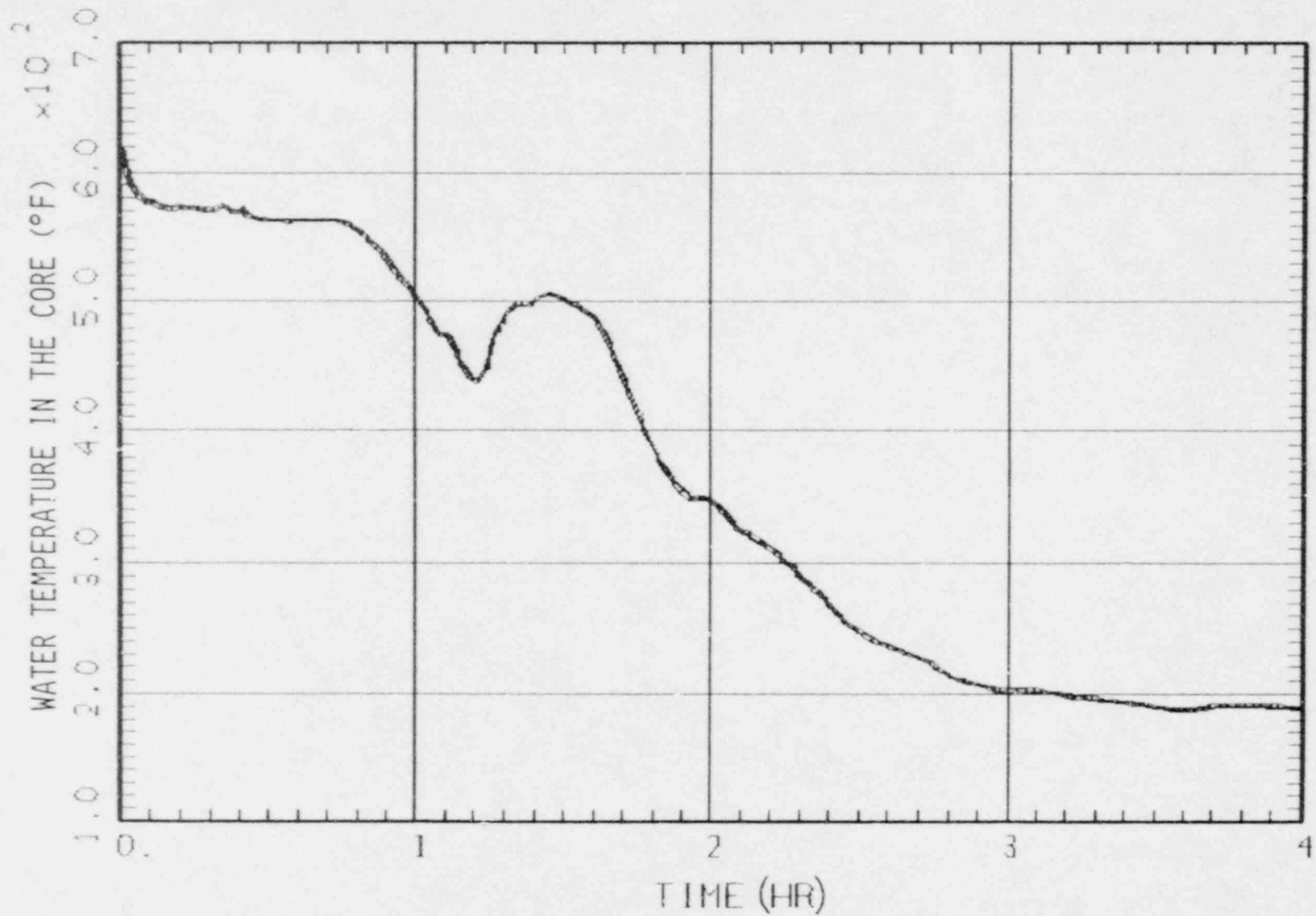


Figure 2.06 Water Temperature in the Core

52D SEQUENCE - 10CFR50.44 ANALYSIS

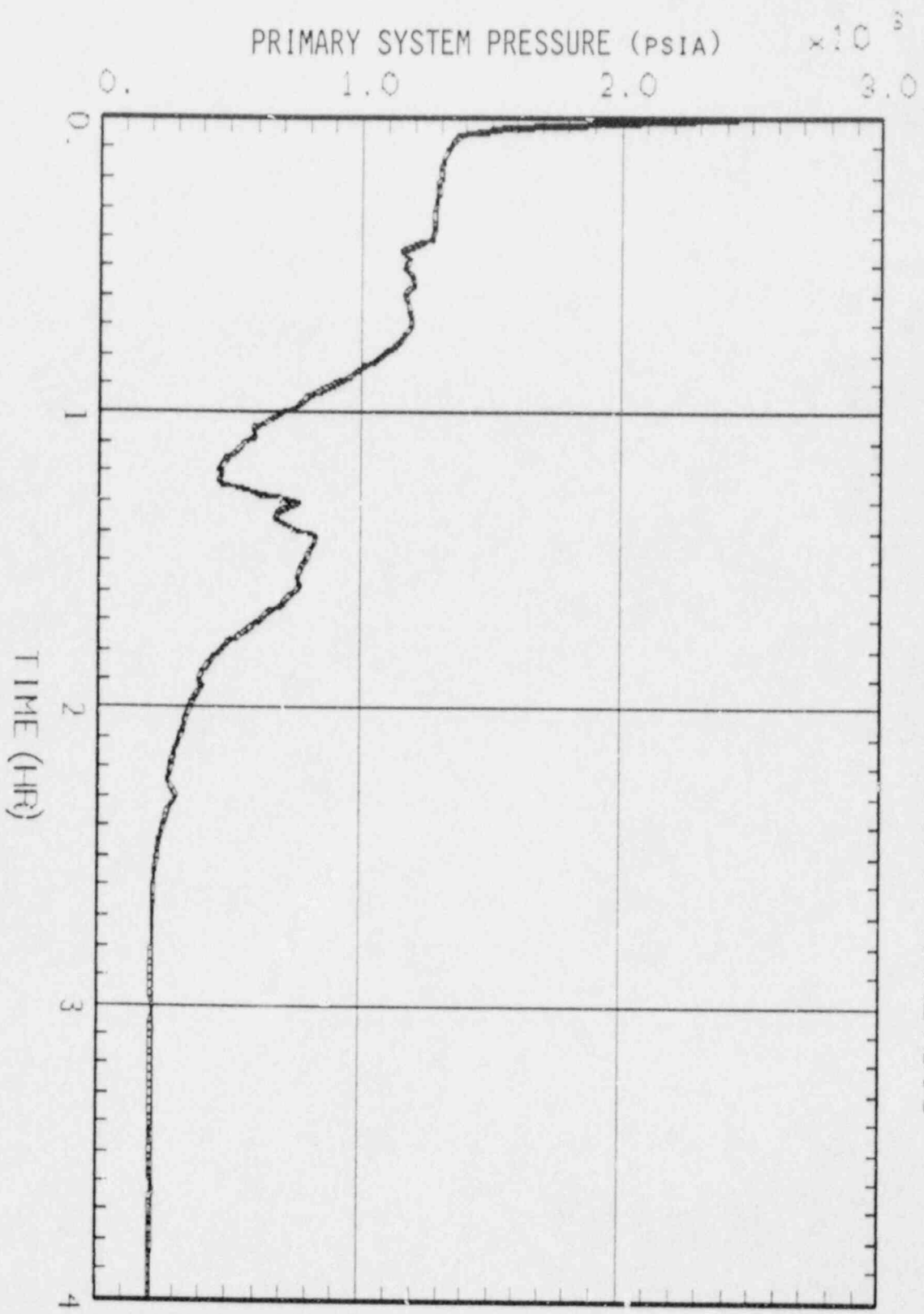


Figure 2.07 Primary System Pressure

S2D SEQUENCE - 10CFR50.44 ANALYSIS

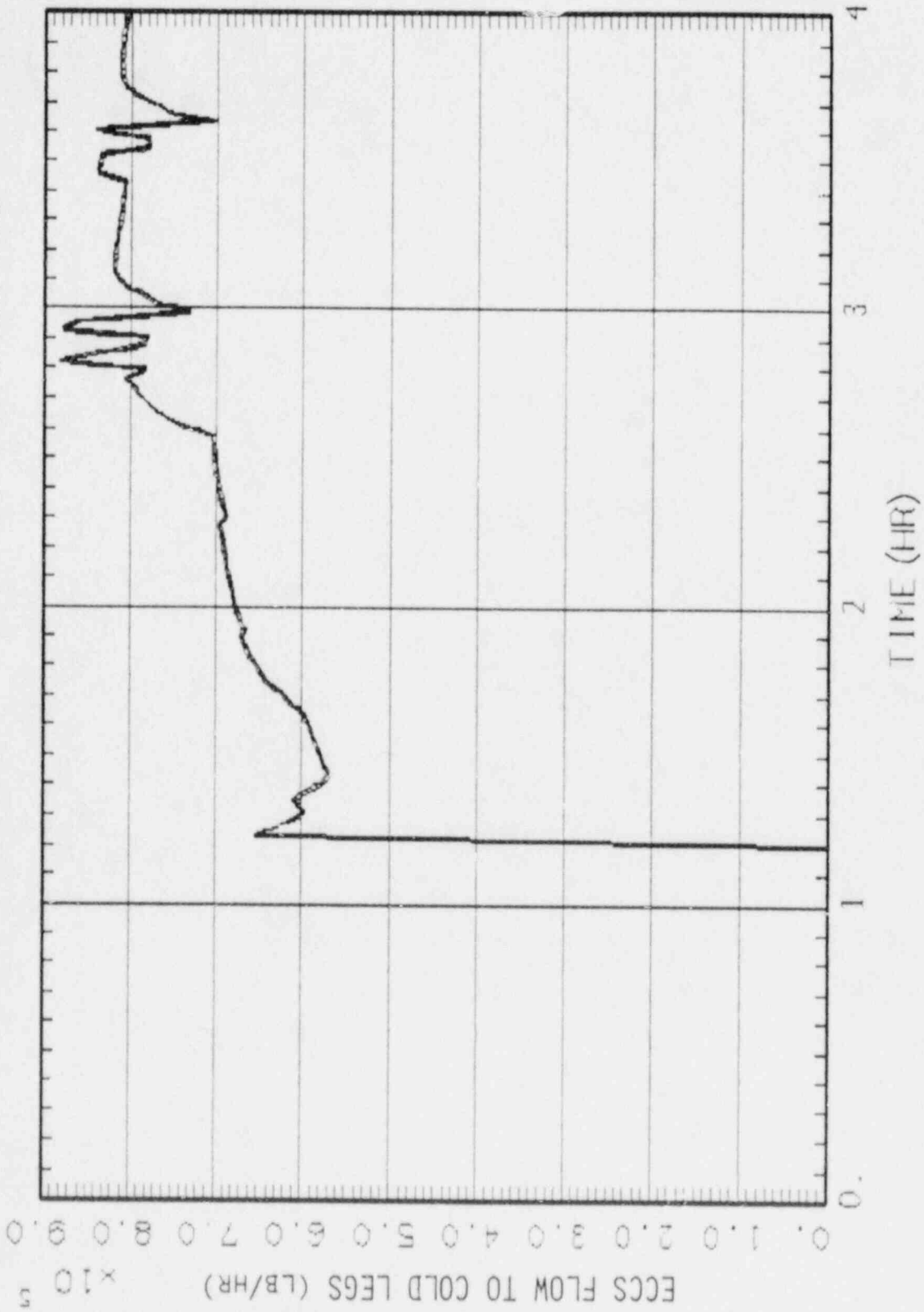


Figure 2.08 ECCS Flow to Cold Legs

S2D SEQUENCE - 10CFR50.44 ANALYSIS

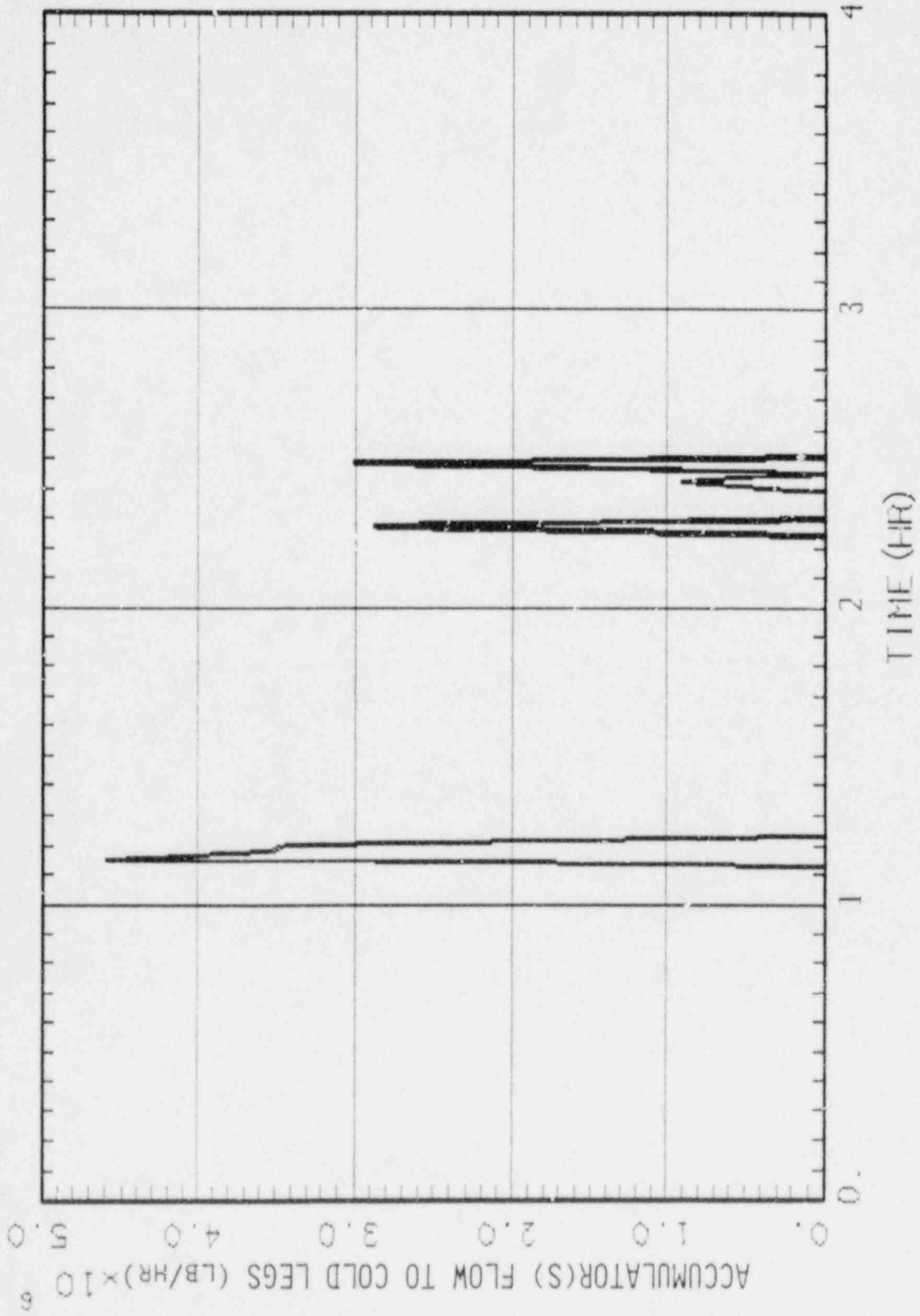


Figure 2.09 Accumulator(s) Flow to Cold Legs

S2D SEQUENCE - 10CFR50.44 ANALYSIS

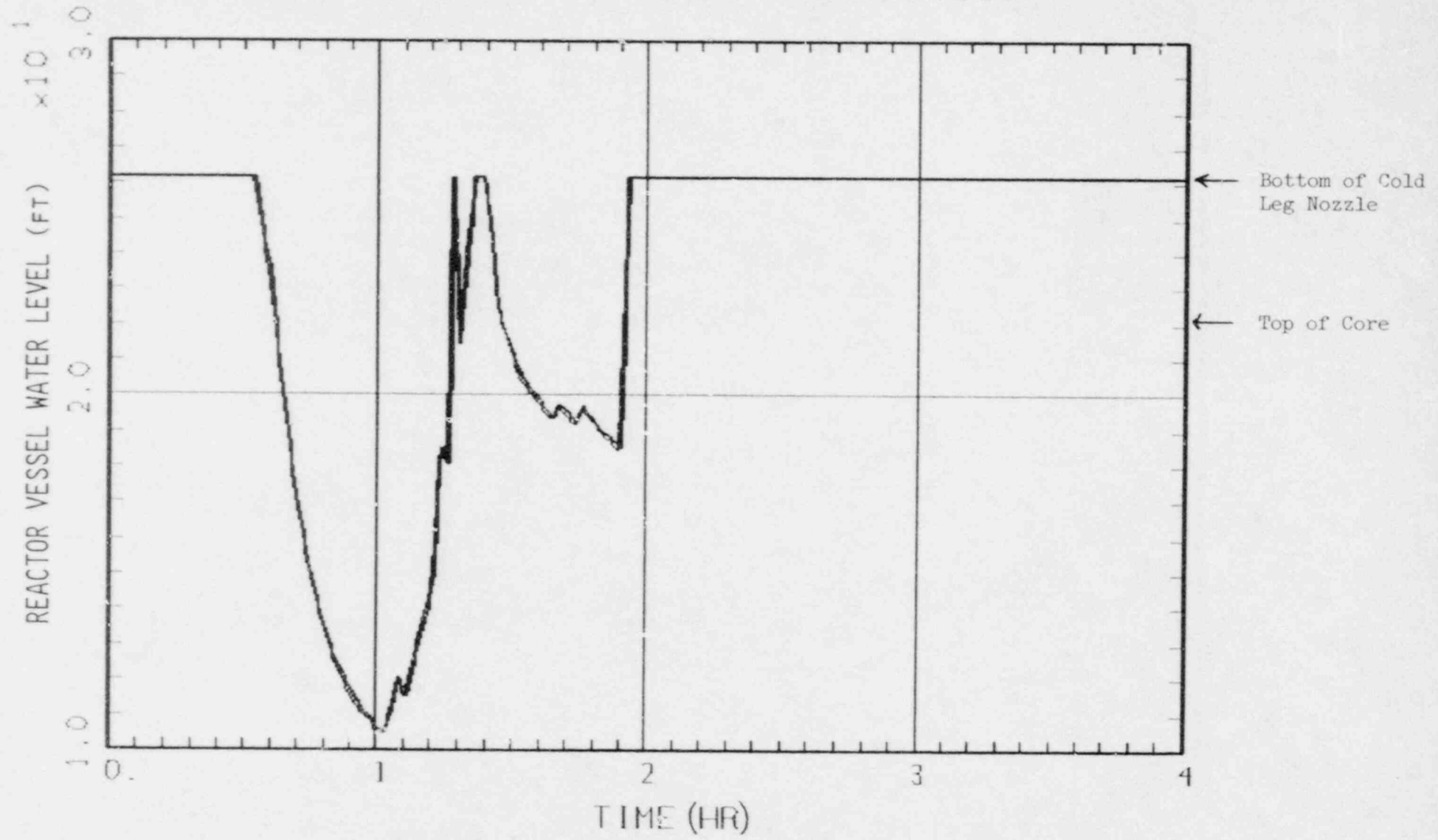


Figure 2.10 Reactor Vessel Water Level

S2D SEQUENCE - 10CFR50.44 ANALYSIS

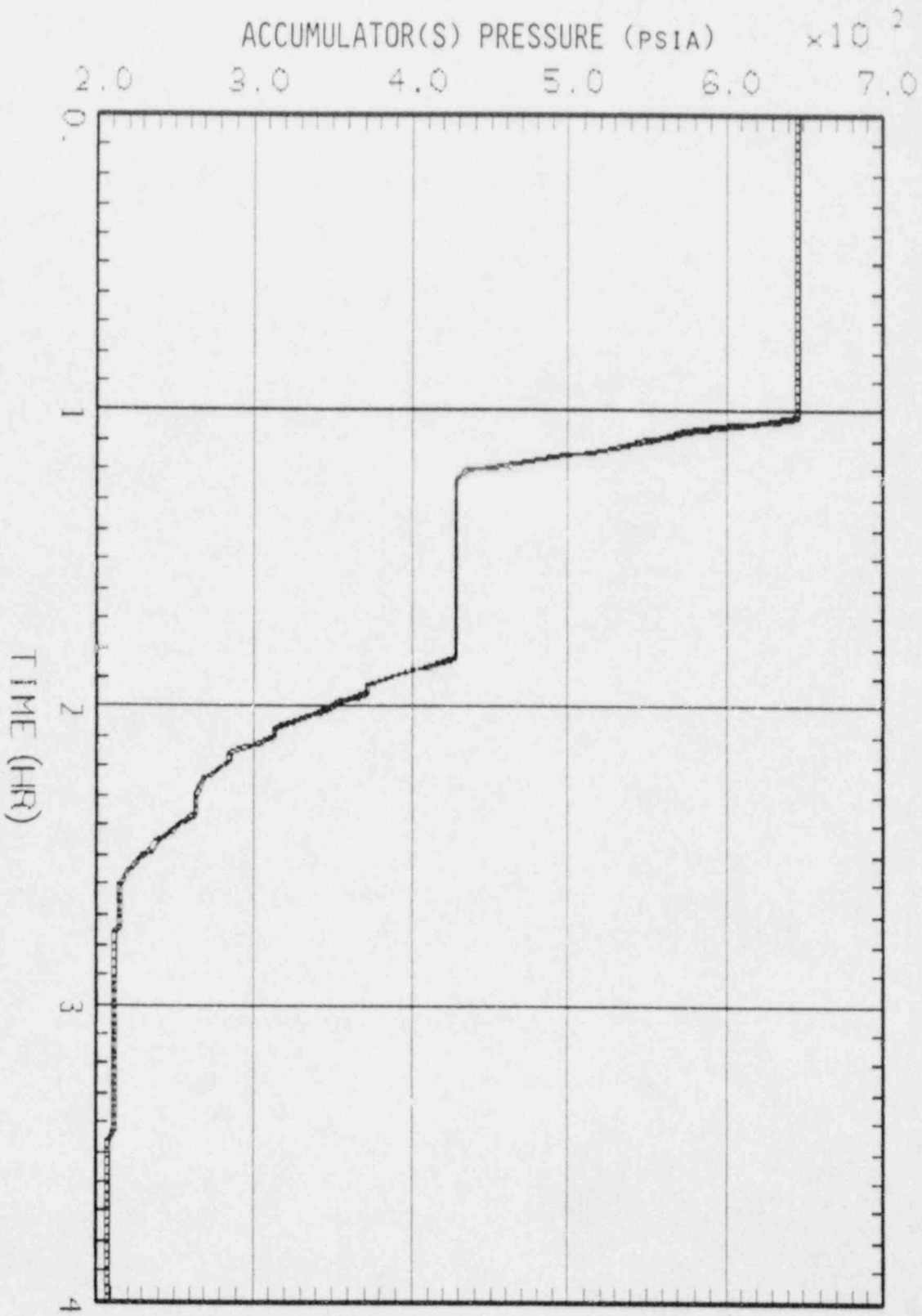


Figure 2.11 Accumulator(s) Pressure

S2D SEQUENCE - 10CFR50.44 ANALYSIS

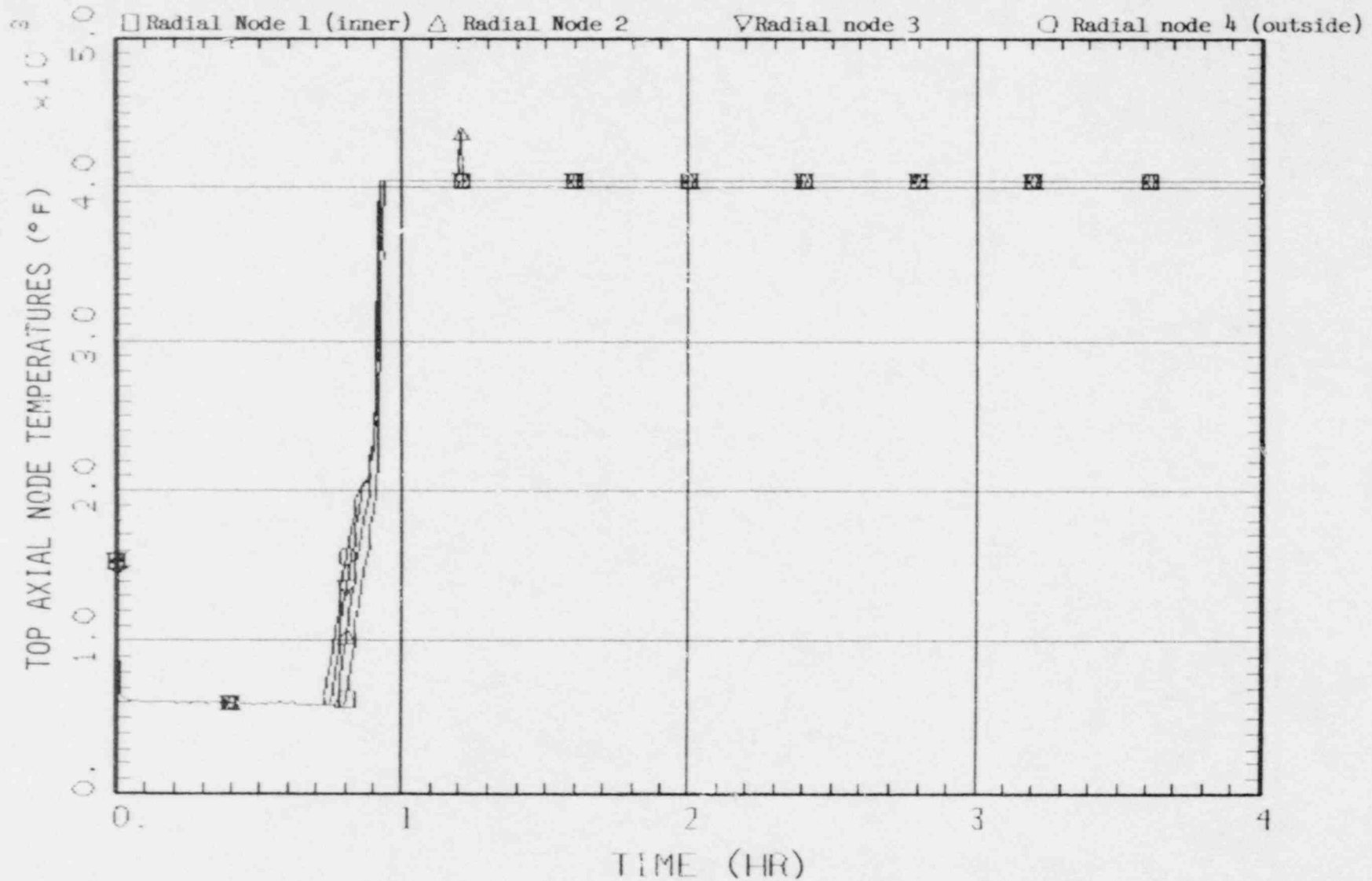


Figure 2.12 Top of Active Fuel Axial Node X 4 Top Radial Nodes

S2D SEQUENCE - 10CFR50.44 ANALYSIS

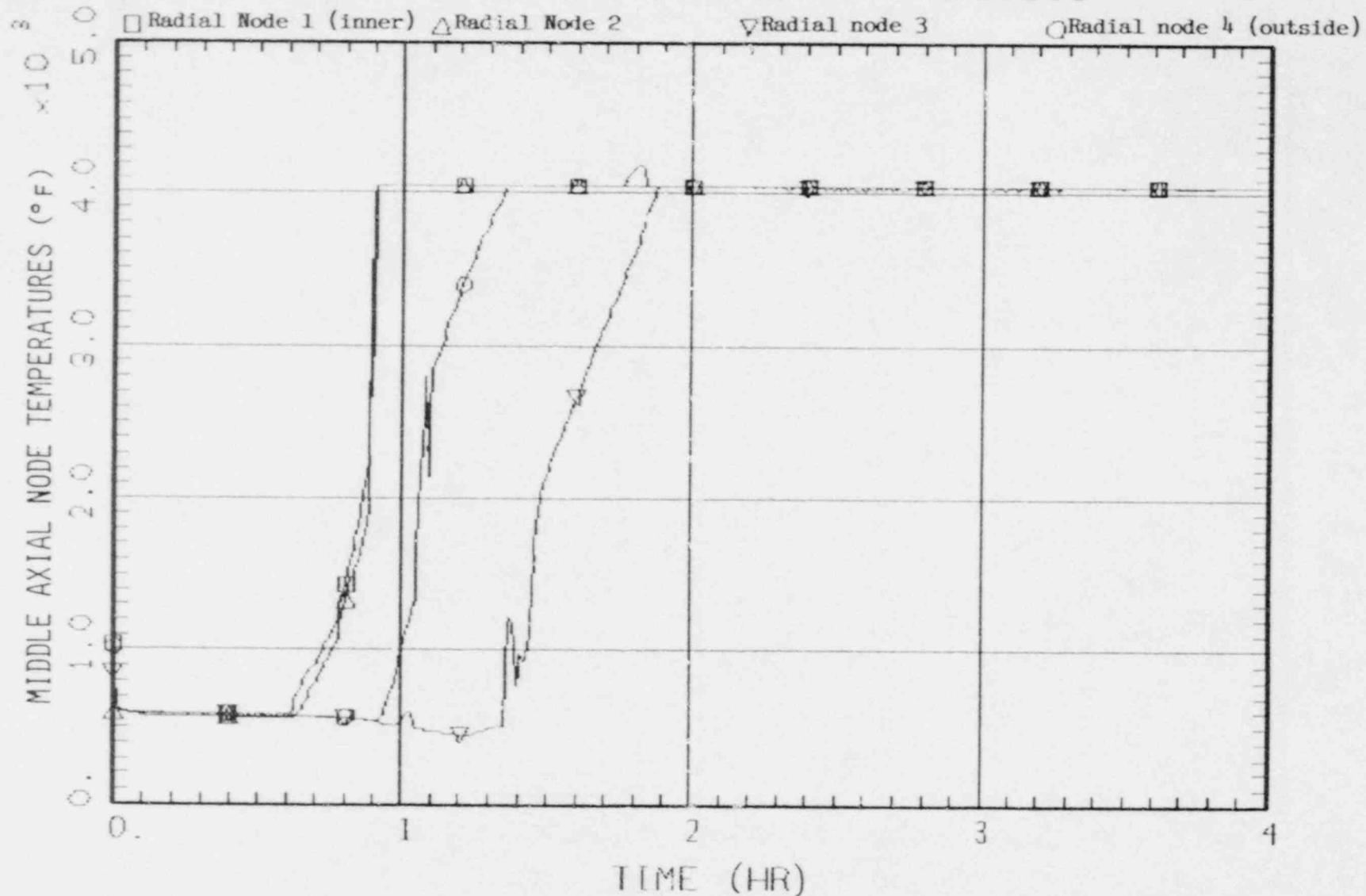


Figure 2.13 Middle of Active Fuel Axial Node X 4 Middle Radial Nodes

S2D SEQUENCE - 10CFR50.44 ANALYSIS

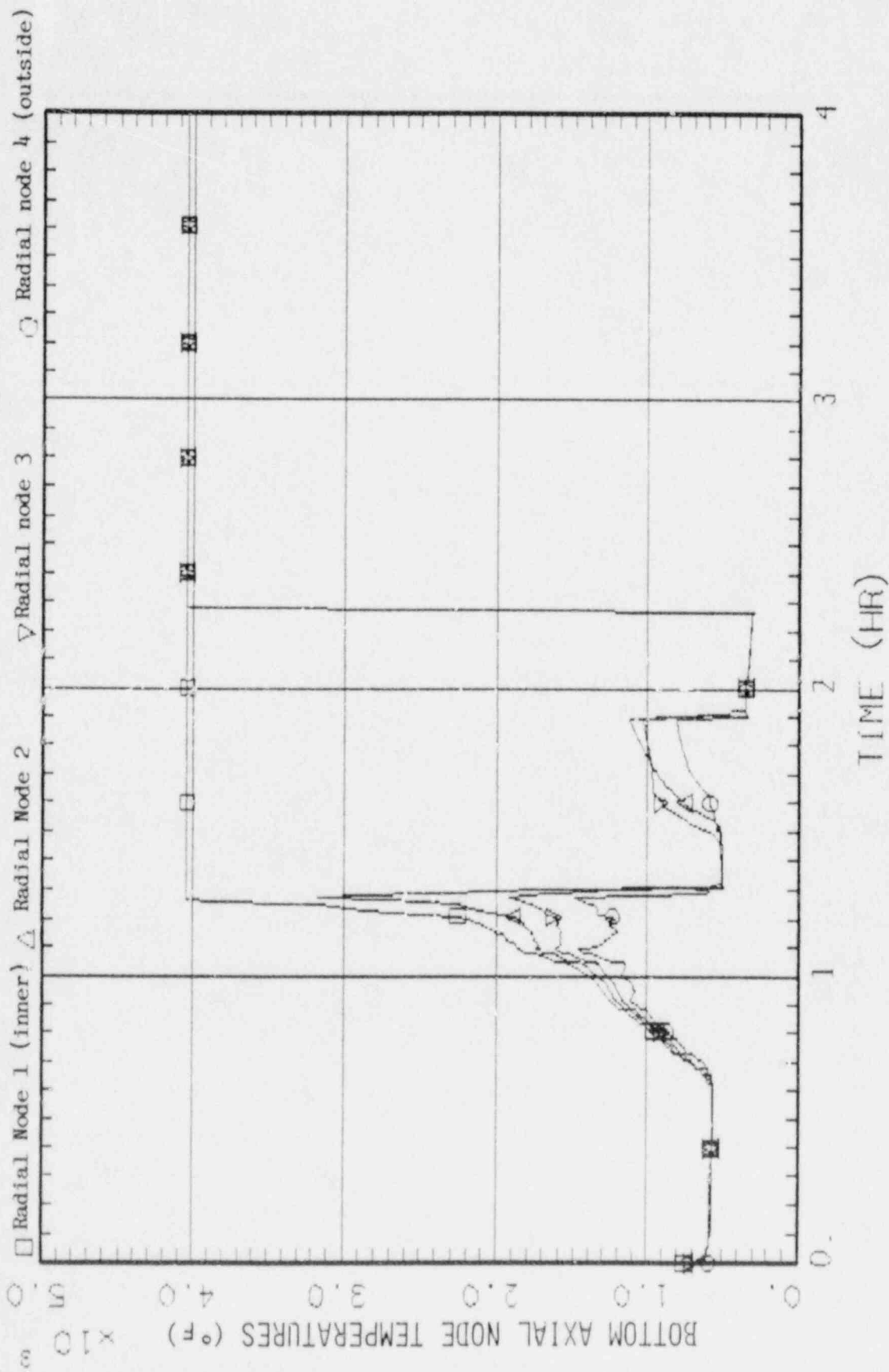


Figure 2.14 Bottom of Active Fuel Axial Node X 4 Bottom Radial Nodes

APPENDIX 3

TMLU Sequence Plots - 10CFR50.44 Analysis

TMLU SEQUENCE - 10CFR50.44 ANALYSIS

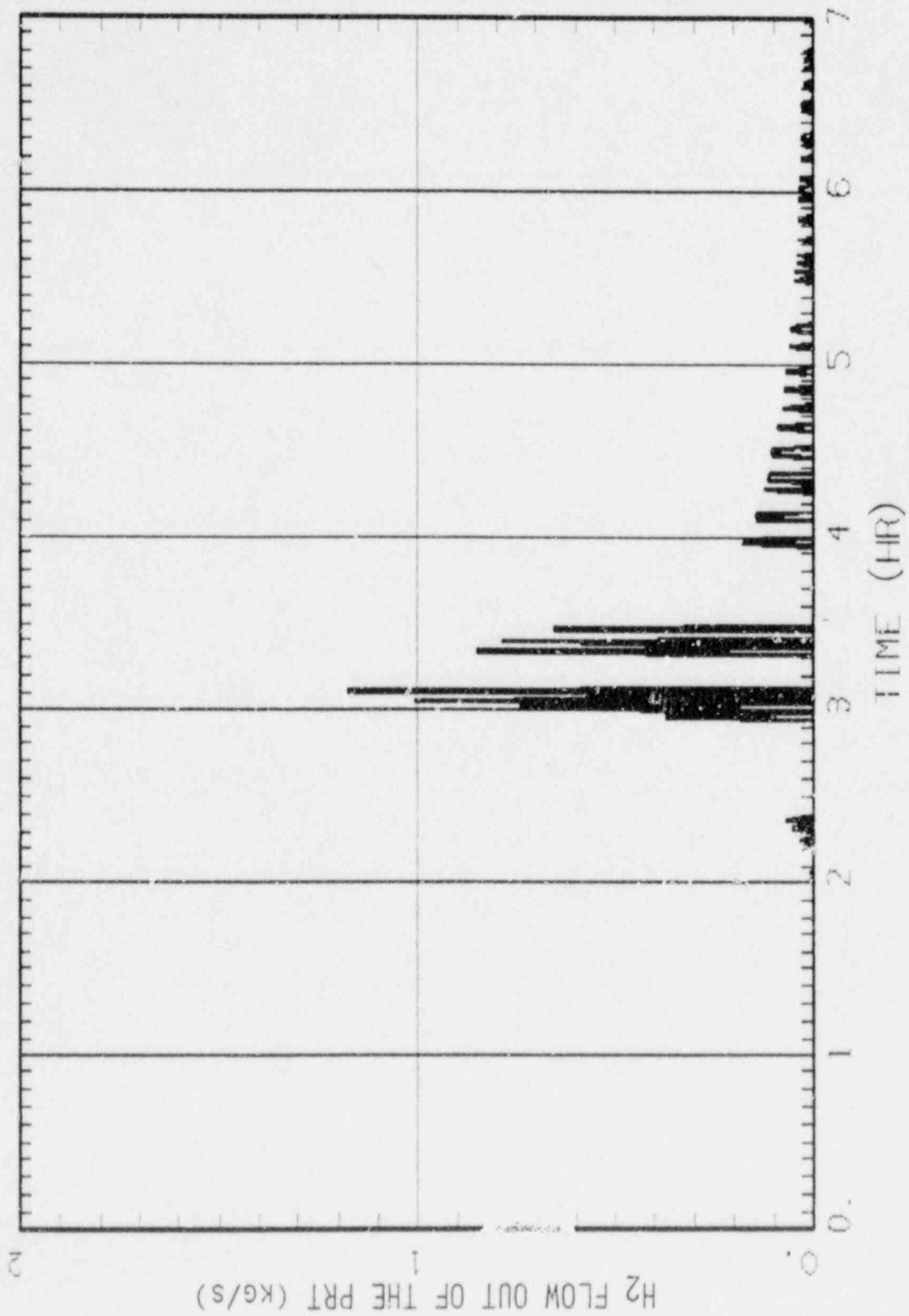


Figure 3.01 H₂ Flow Out of the PRT

TMU SEQUENCE - 10CFR50.44 ANALYSIS

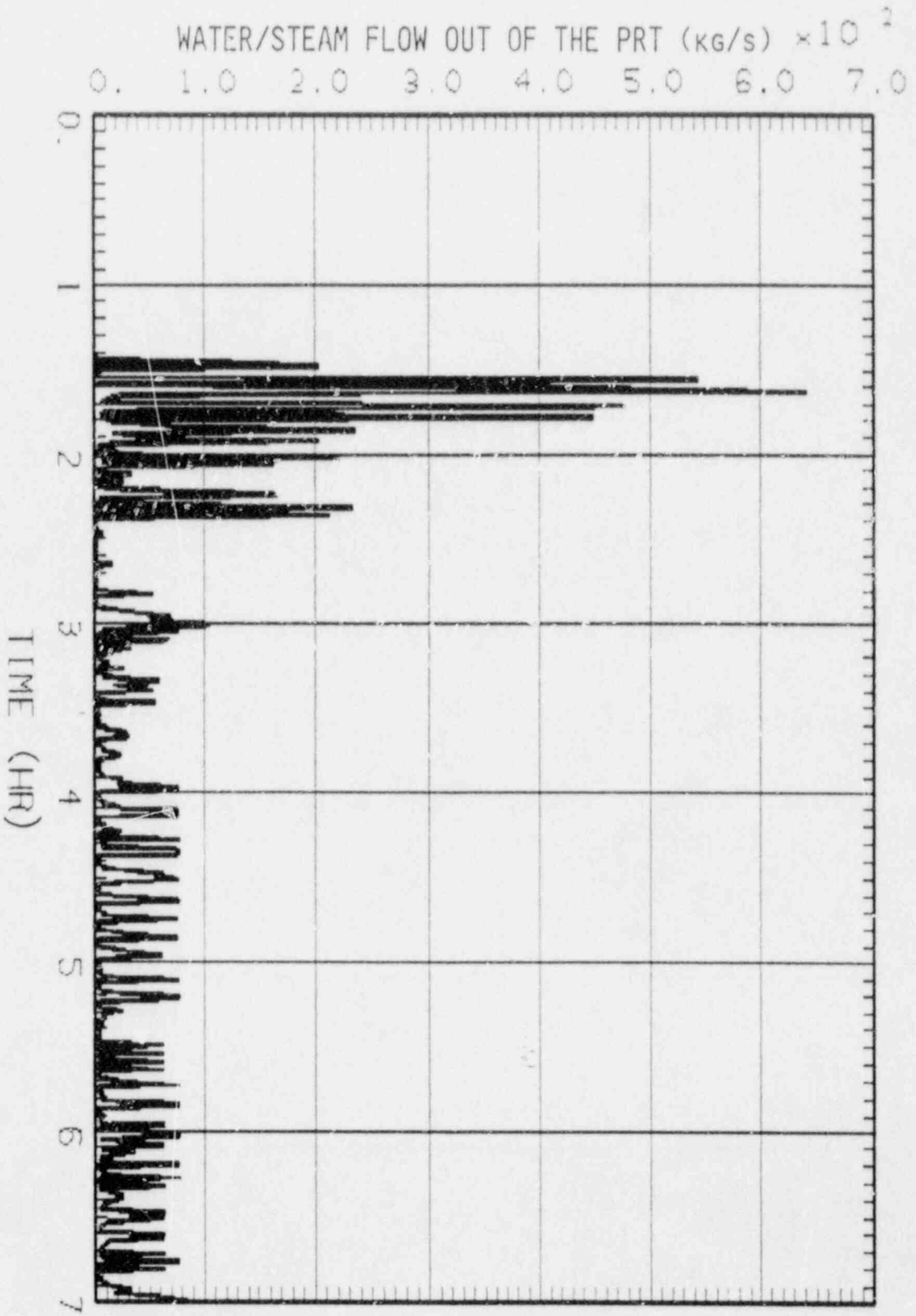


Figure 3.02 Water/Steam Flow Out of the PRT

TIME SEQUENCE - ITCFR50.44 ANALYSIS

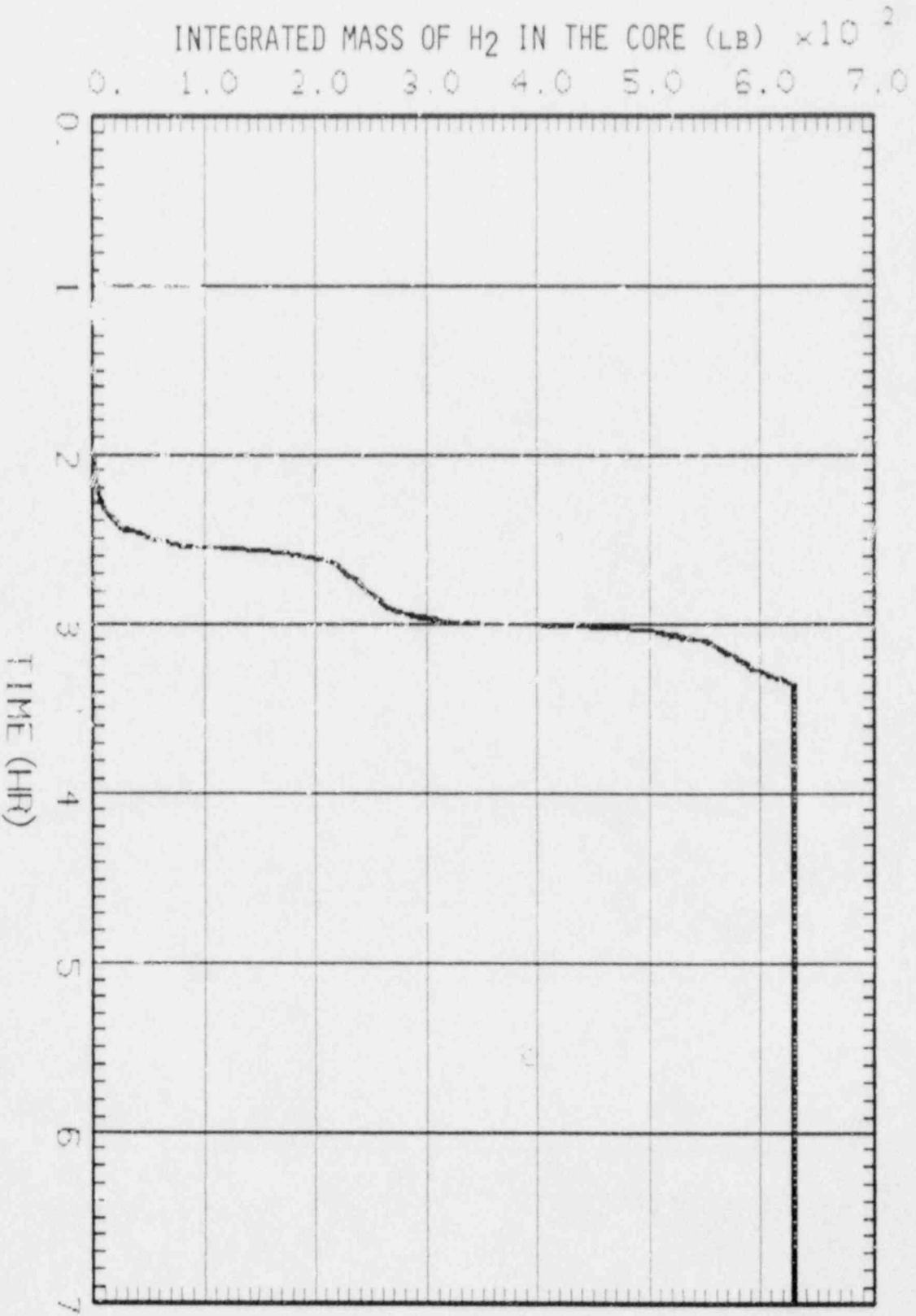


Figure 3.03 Integrated Mass of H₂ Generated in the Core

TMLU SEQUENCE - 10CFR50.44 ANALYSIS

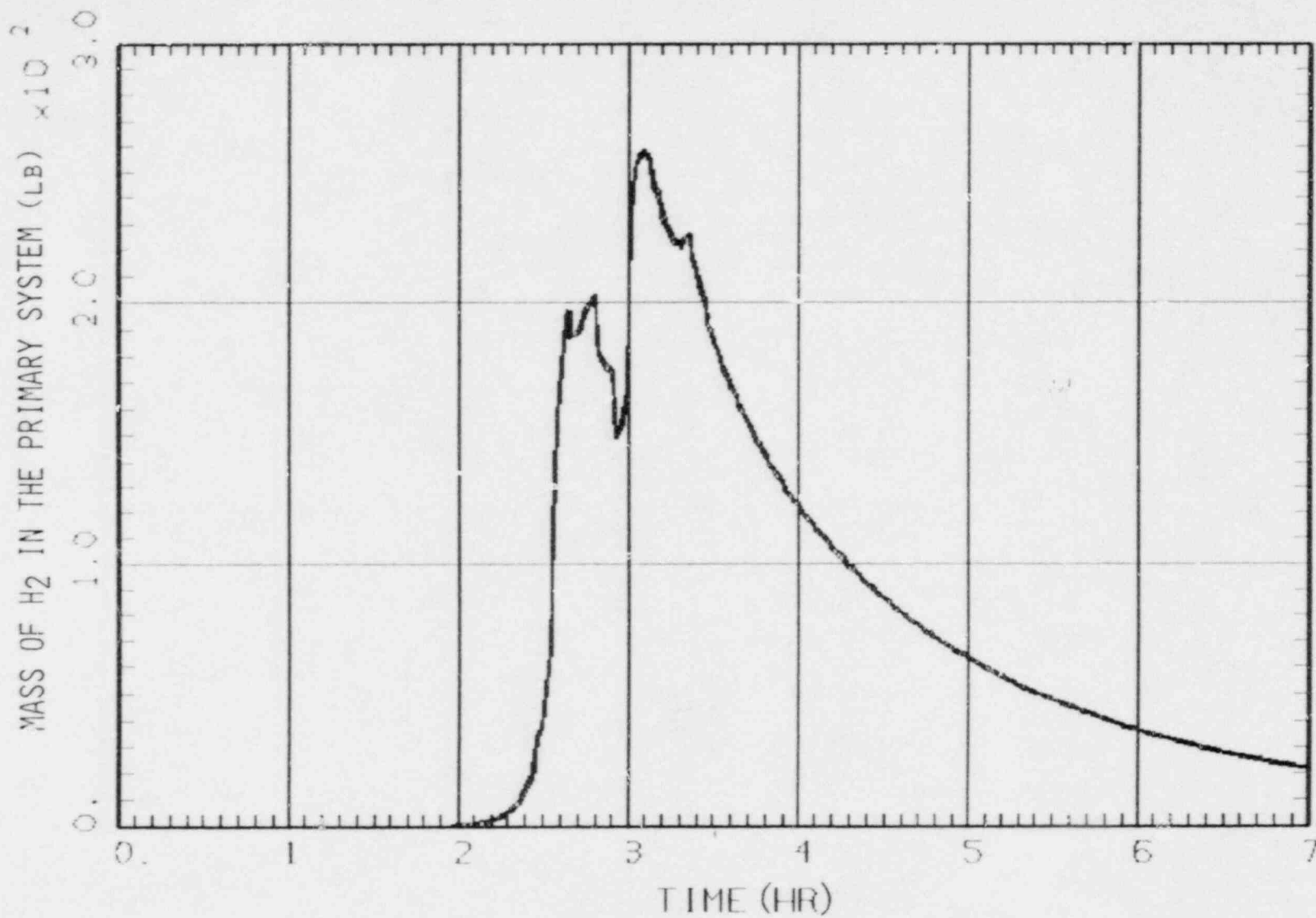


Figure 3.04 Mass of H₂ in the Primary System

TMLU SEQUENCE - 10CFR50.44 ANALYSIS

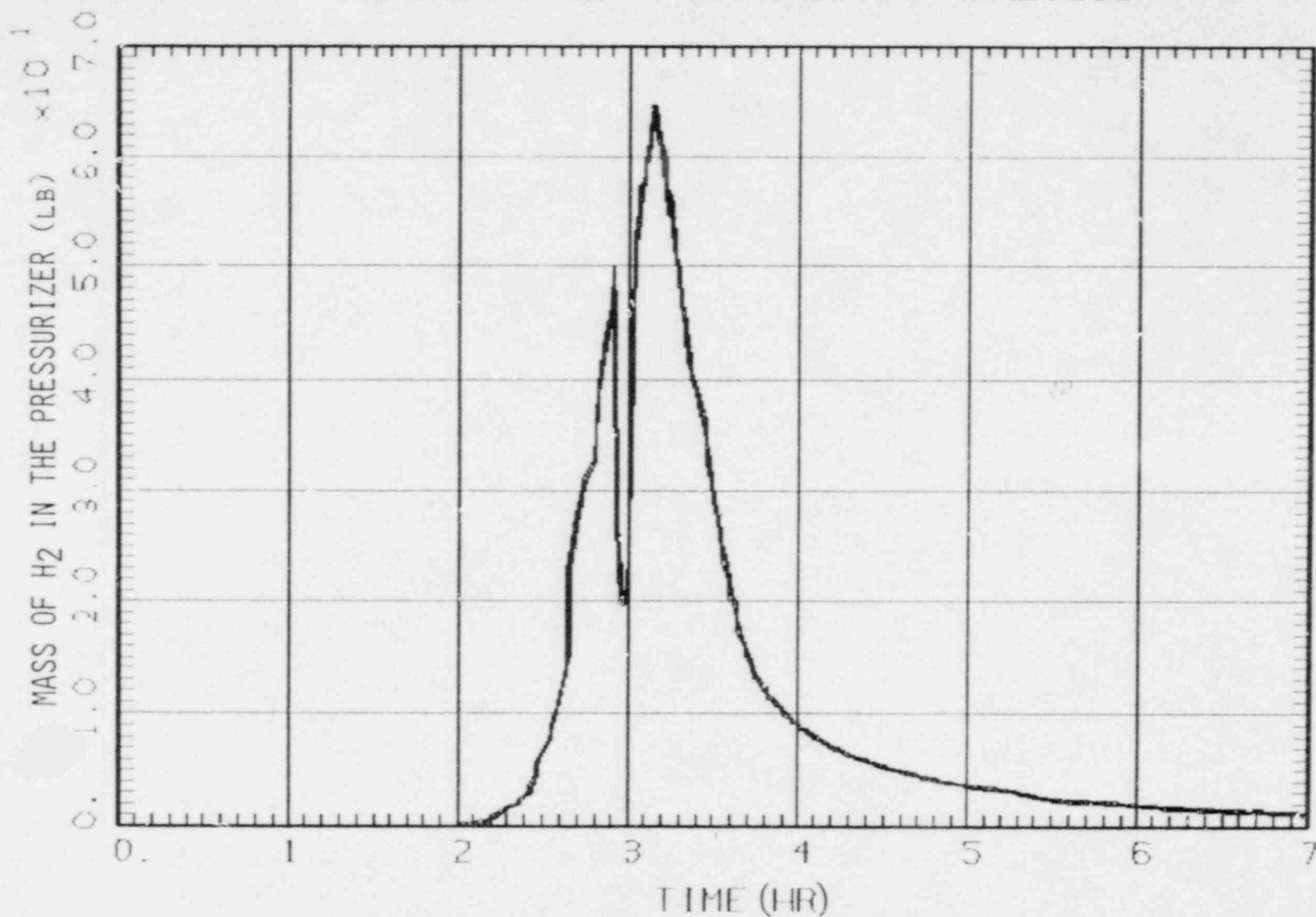


Figure 3.05 Mass of H₂ in the Pressurizer

TMLU SEQUENCE - 10CFR50.44 ANALYSIS

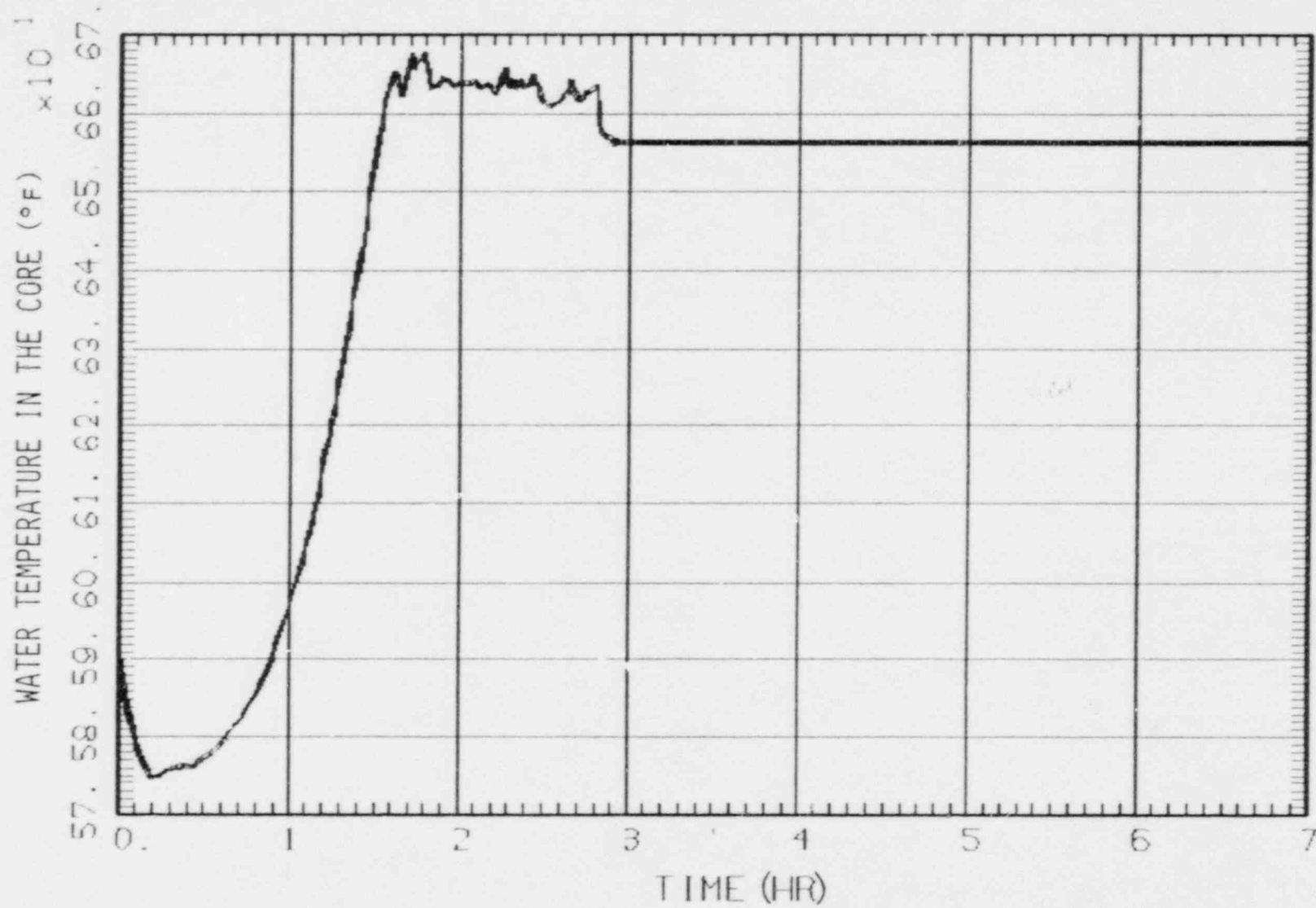


Figure 3.06 Water Temperature in the Core

TMI.U SEQUENCE - 10CFR50.44 ANALYSIS

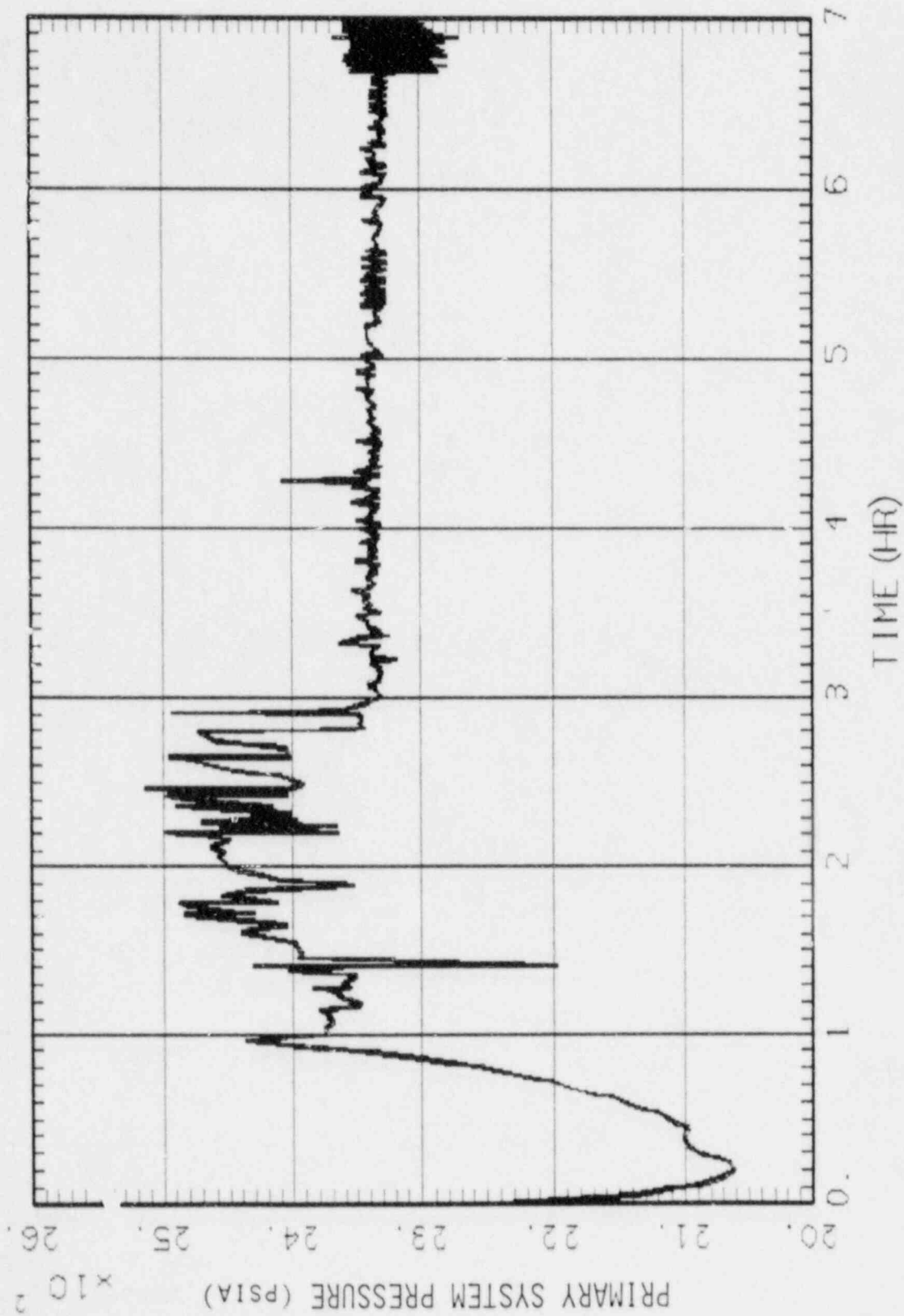


Figure 3.07 Primary System Pressure

TMLU SEQUENCE - 10CFR50.44 ANALYSIS

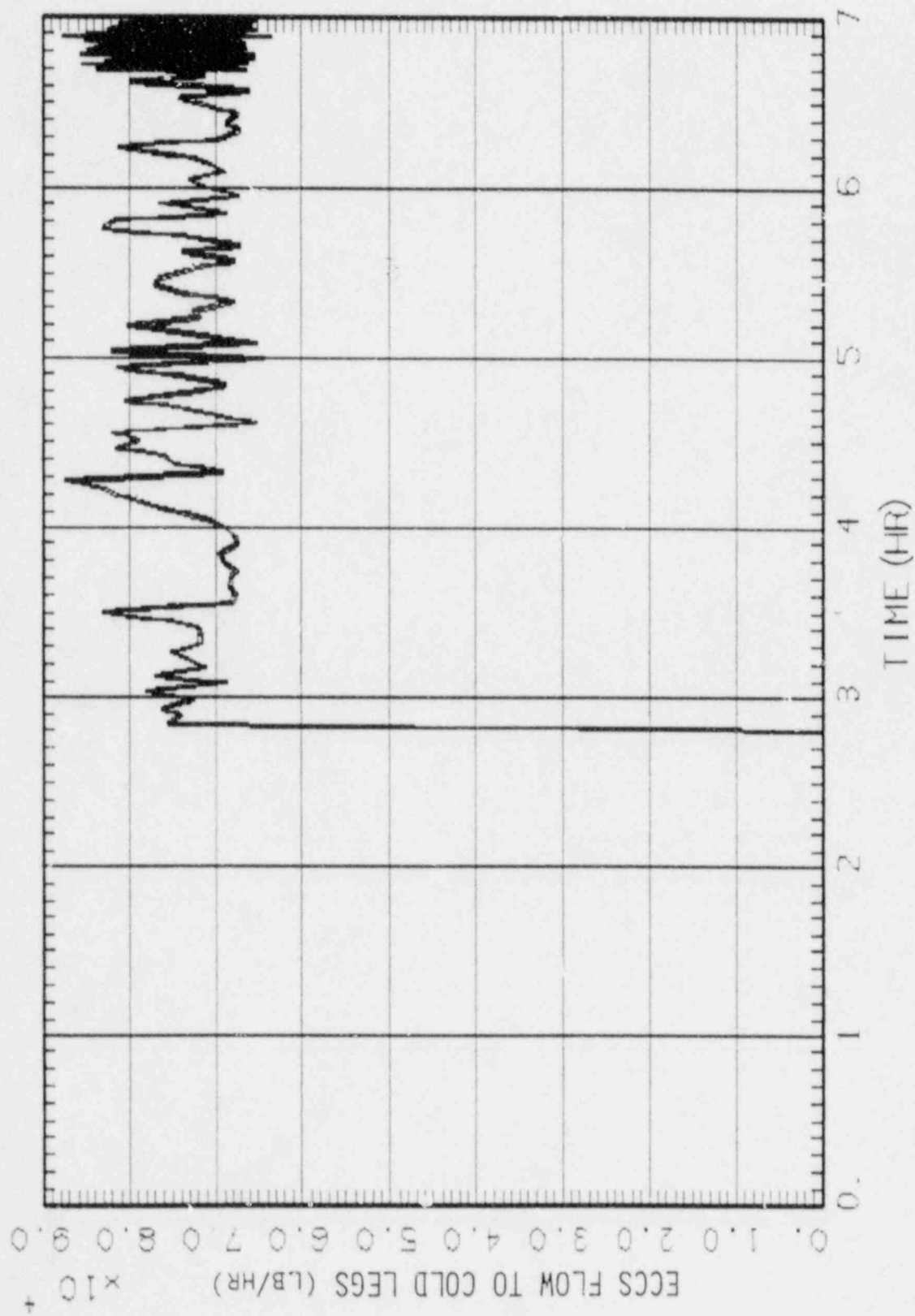


Figure 3.08 ECCS Flow to Cold Legs

TMLU SEQUENCE - 10CFR50.44 ANALYSIS

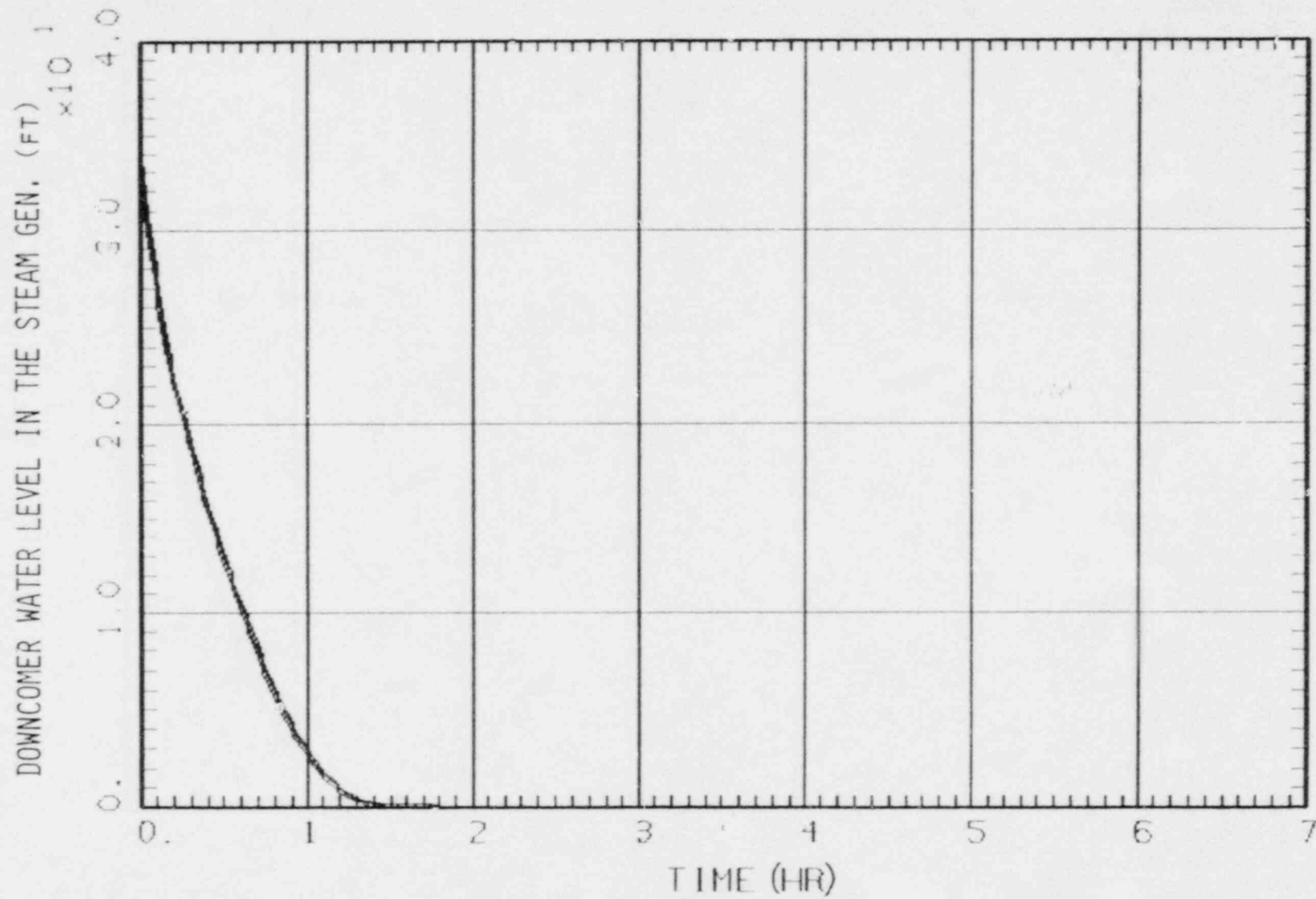


Figure 3.09 Downcomer Water Level in the Steam Generator(s)

TMLU SEQUENCE - 10CFR50.44 ANALYSIS

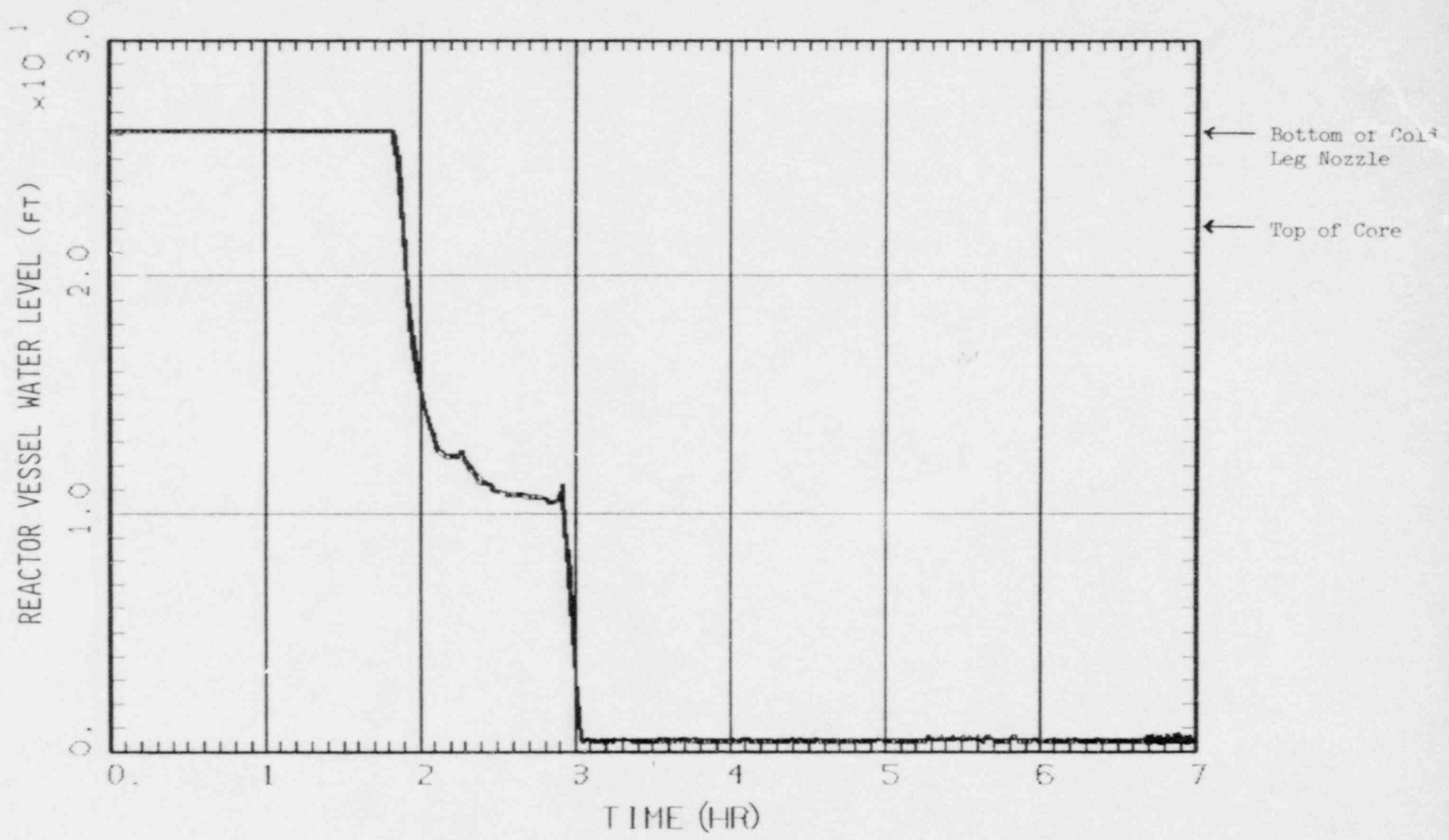


Figure 3.10 Reactor Vessel Water Level

TMLU SEQUENCE - 10CFR50.44 ANALYSIS

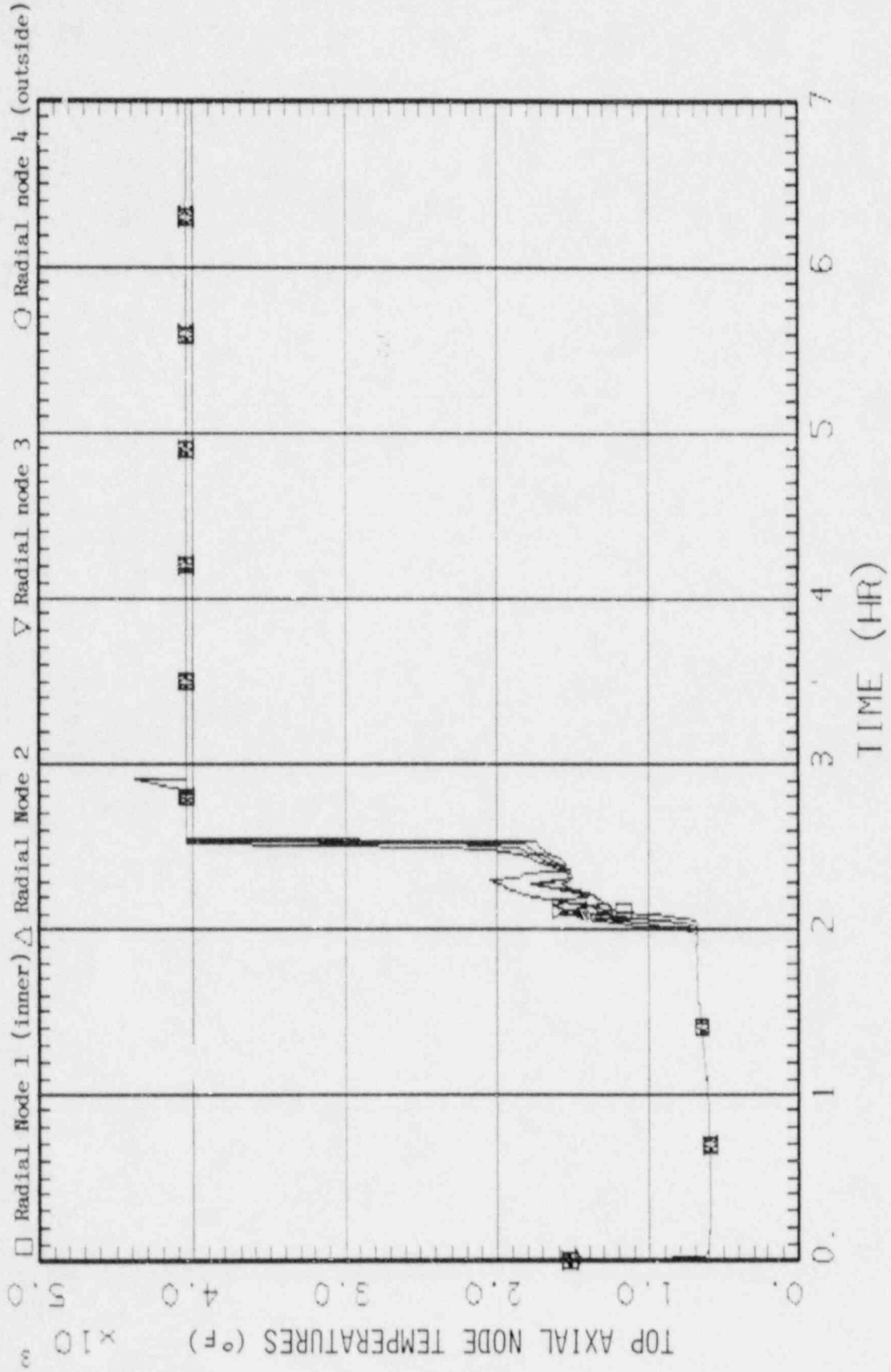


Figure 3.11 Top of Active Fuel Axial Node X 4 Top Radial Nodes

TMLU SEQUENCE - 10CFR50.44 ANALYSIS

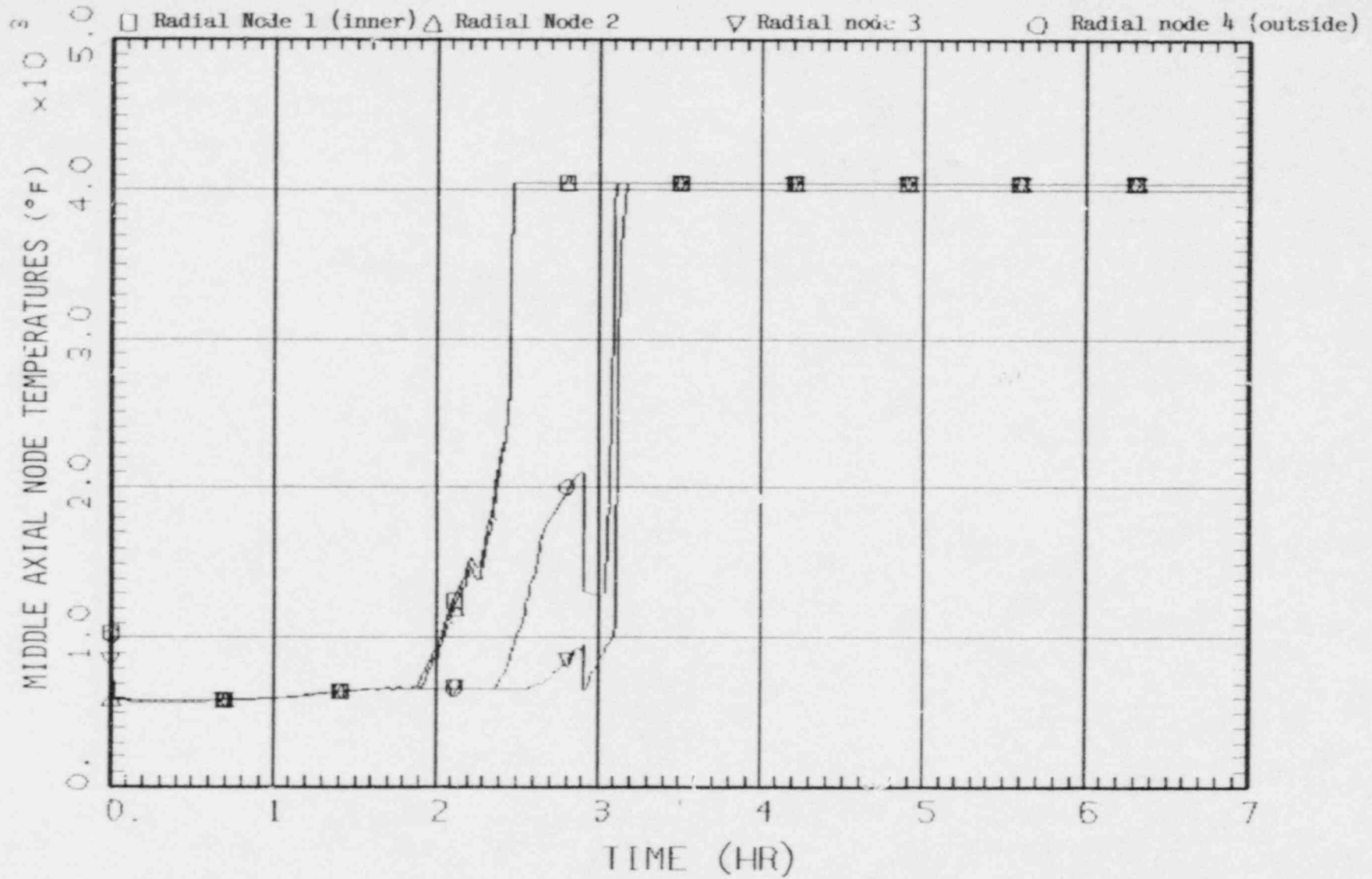


Figure 3.12 Middle of Active Fuel Axial Node X 4 Middle Radial Nodes

TMLU SEQUENCE - 10CFR50.44 ANALYSIS

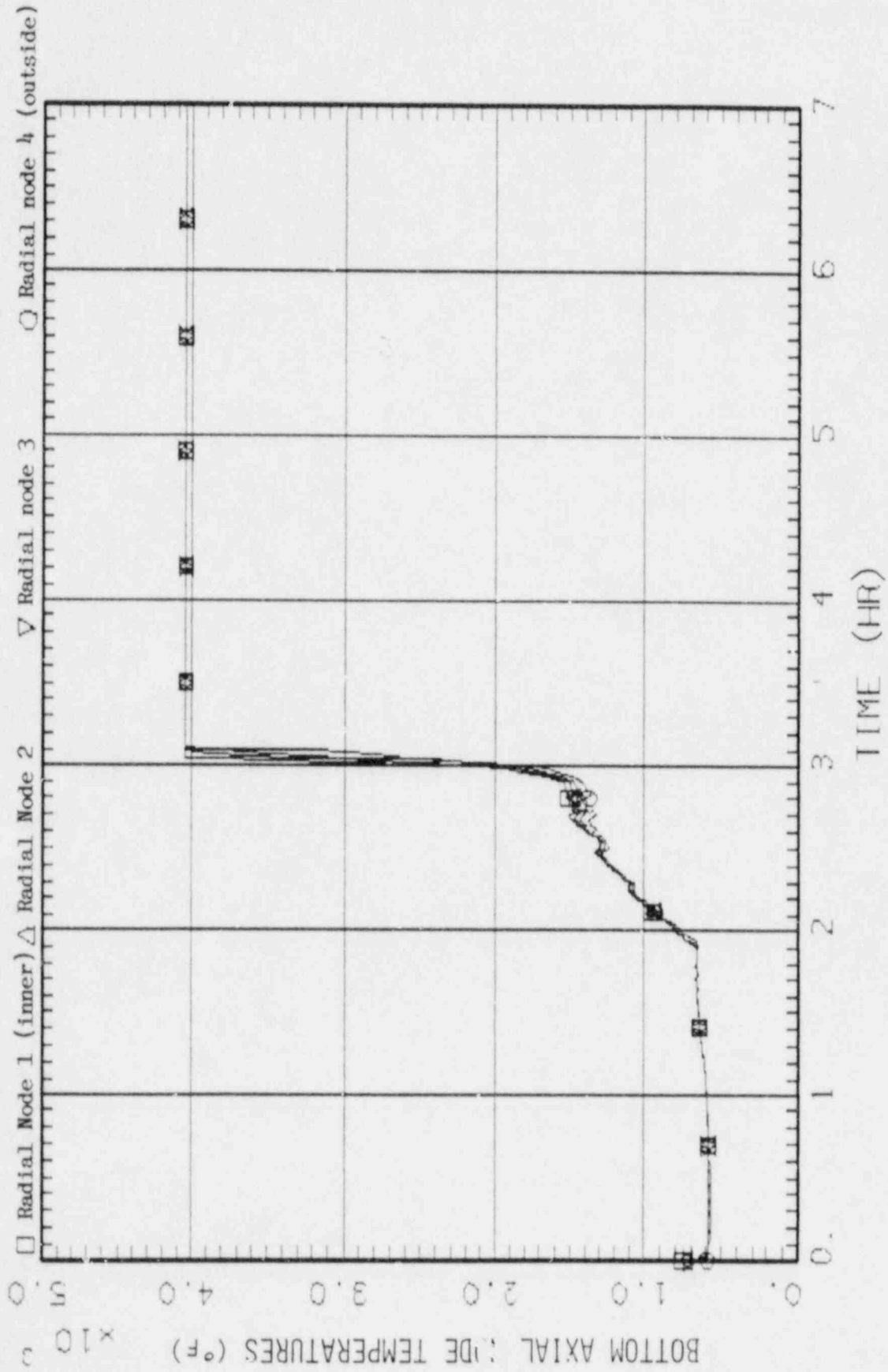


Figure 3.13 Bottom of Active Fuel Axial Node X 4 Bottom Radial Nodes

APPENDIX 4

S₂H Sequence Plots - 10CFR50.44 Analysis

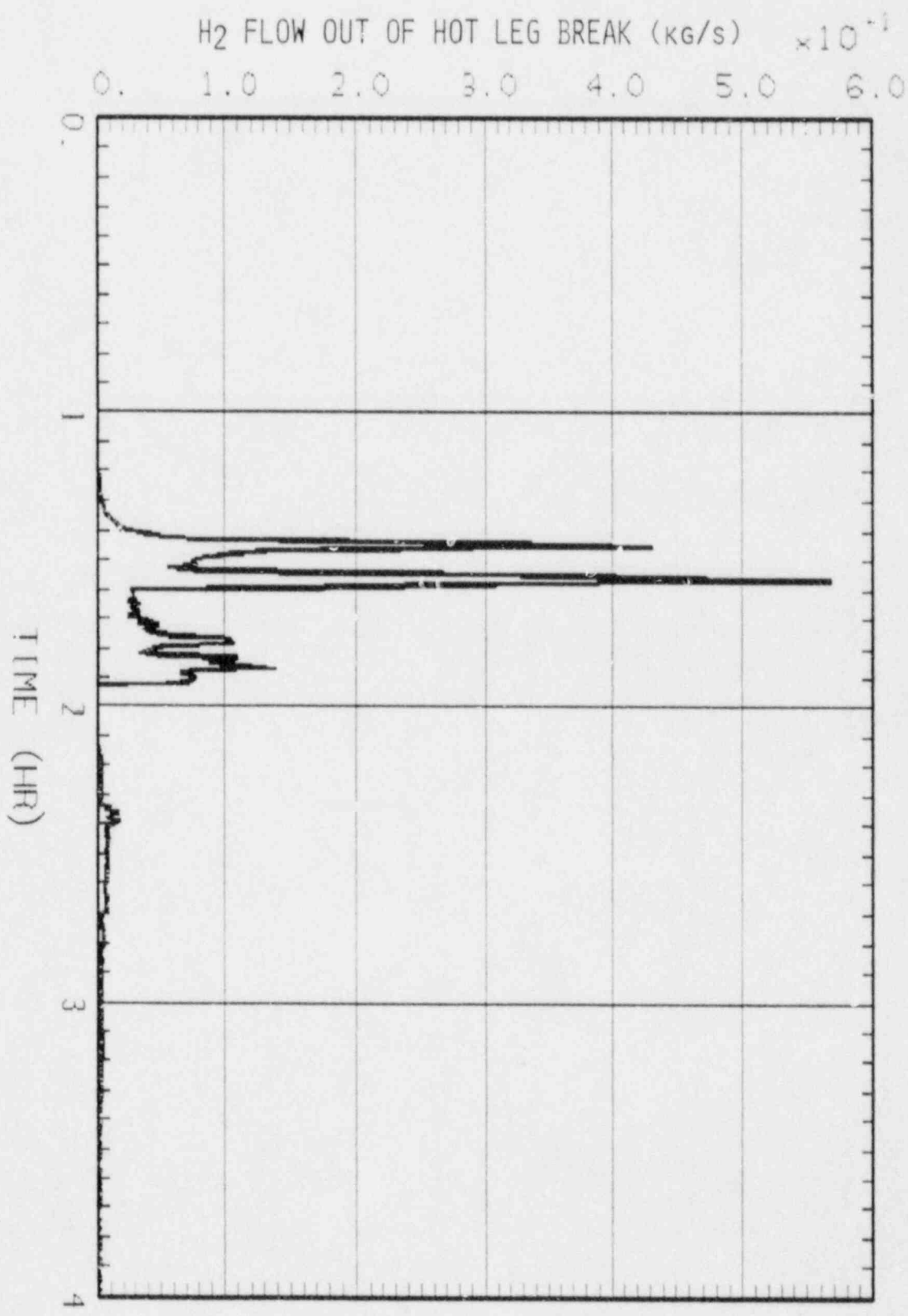


Figure 4.01 H₂ Flow Out of Hot Leg Break

S2H SEQUENCE - 10CFR50.44 ANALYSIS

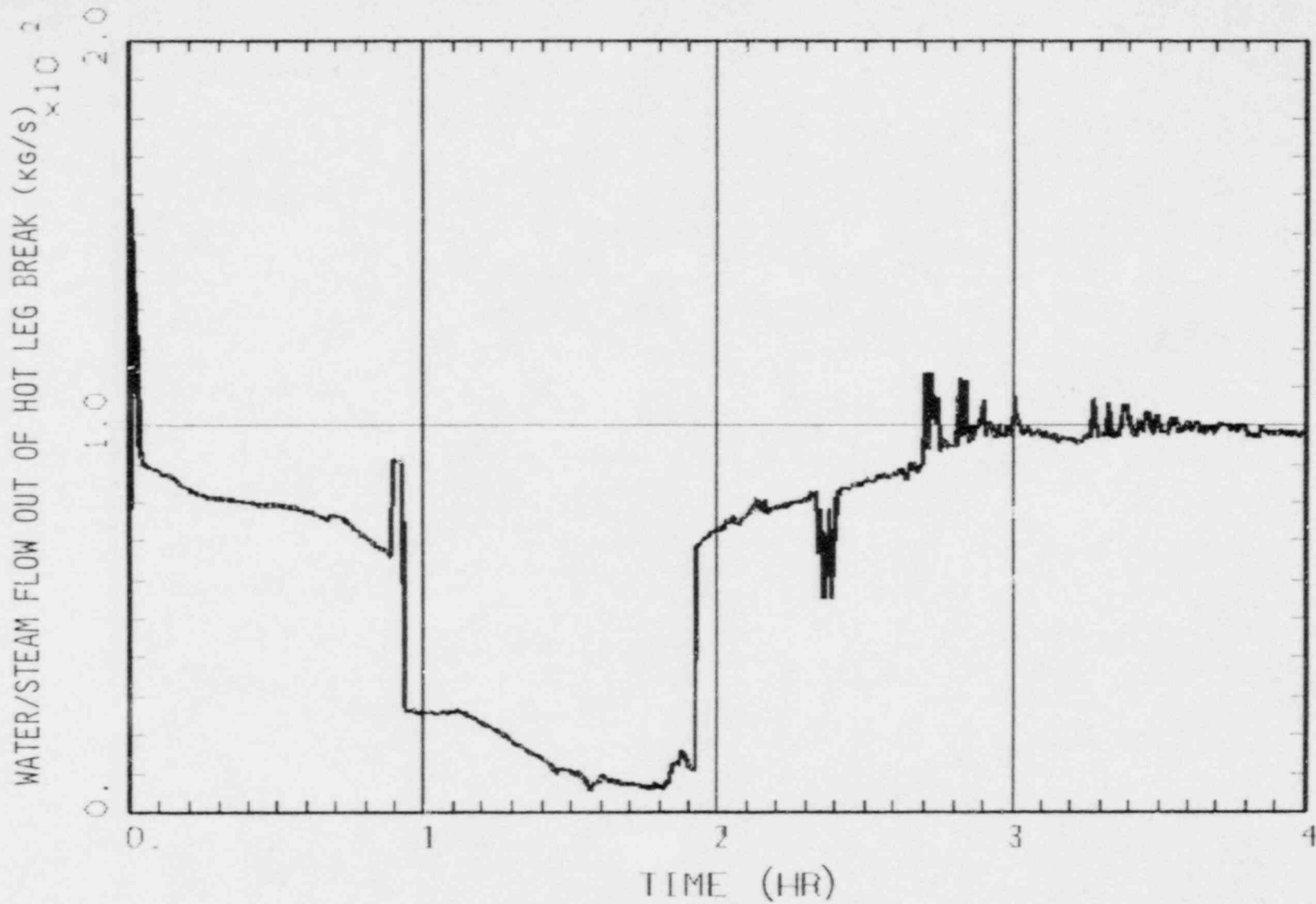


Figure 4.02 Water/Steam Flow Out of Hot Leg Break

S2H SEQUENCE - 10CFR50.44 ANALYSIS

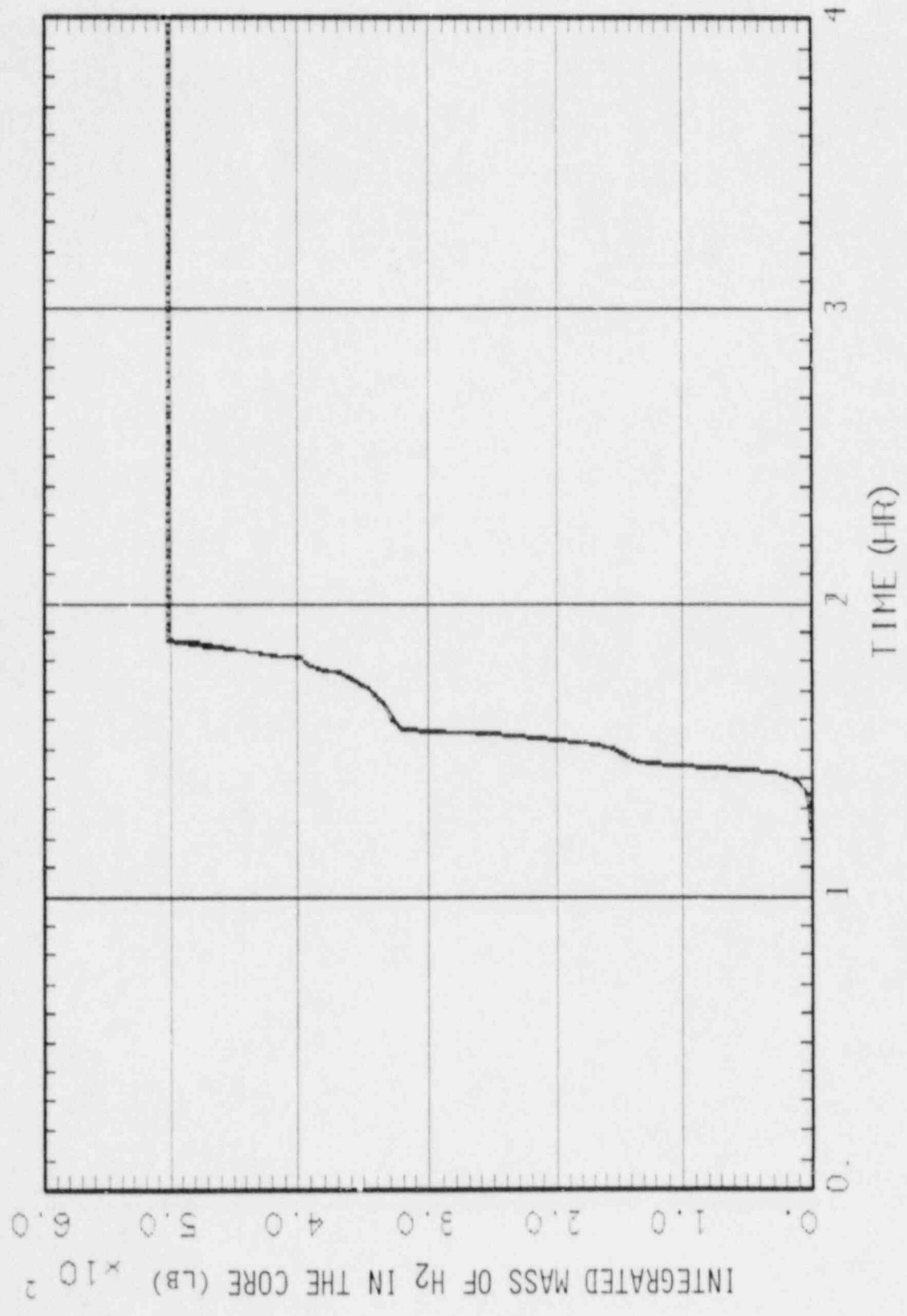


Figure 4.03 Integrated Mass of H₂ Generated in the Core

S2H SEQUENCE - 10CFR50.44 ANALYSIS

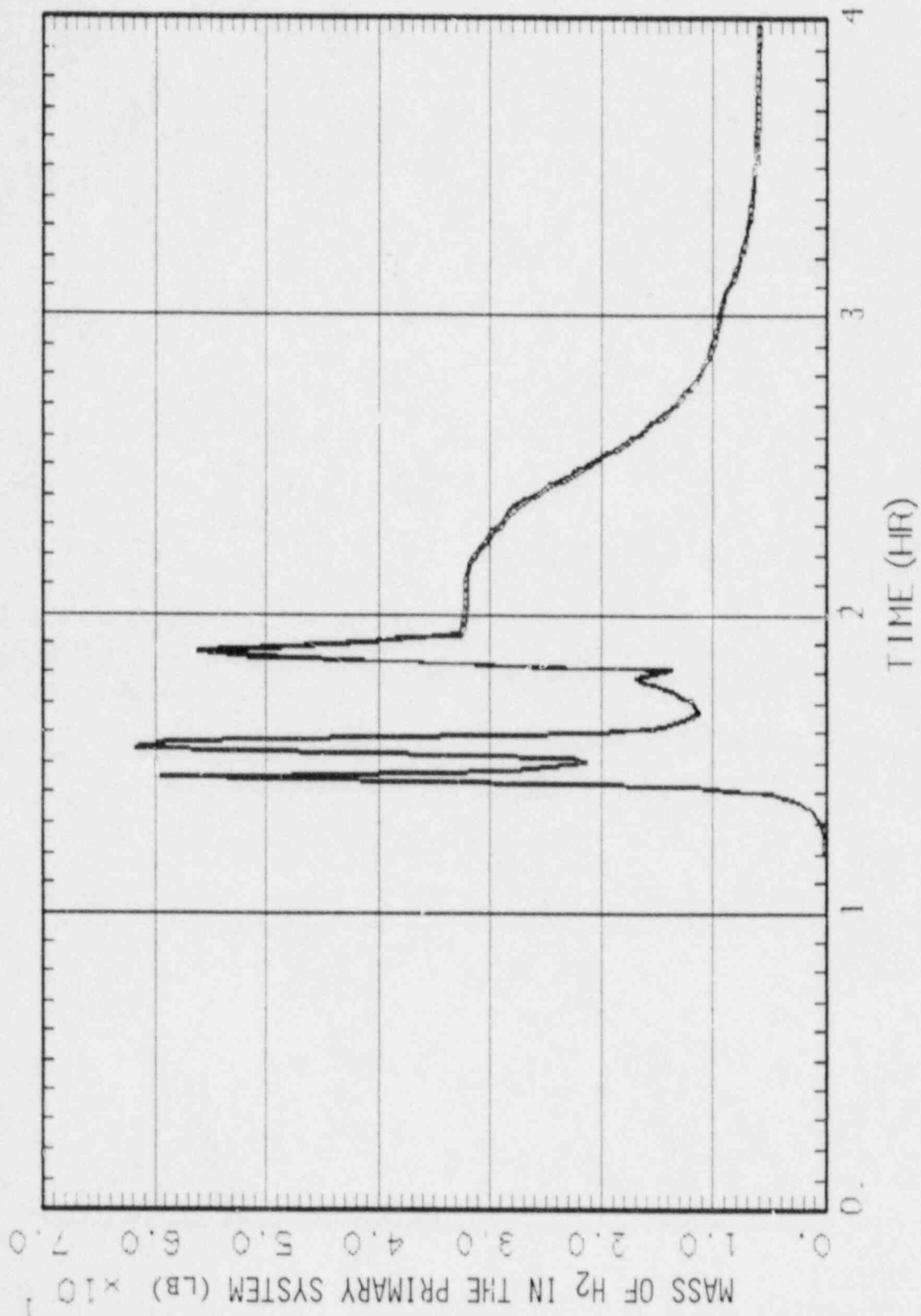


Figure 4.04 Mass of H₂ in the Primary System

S2H SEQUENCE - 10CFR50.44 ANALYSIS

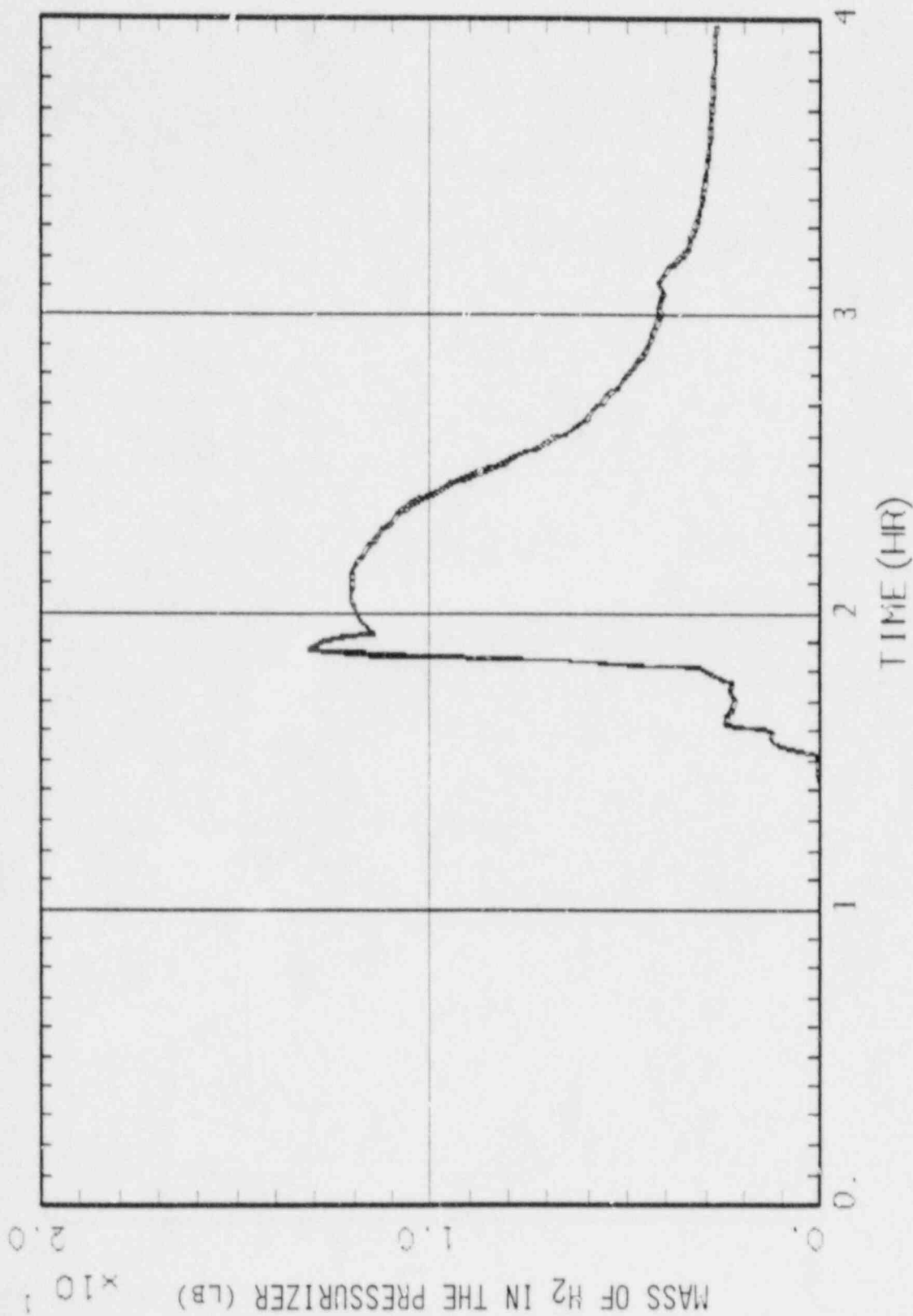


Figure h.05 Mass of H₂ in the Pressurizer

S2H SEQUENCE - 10CFR50.44 ANALYSIS

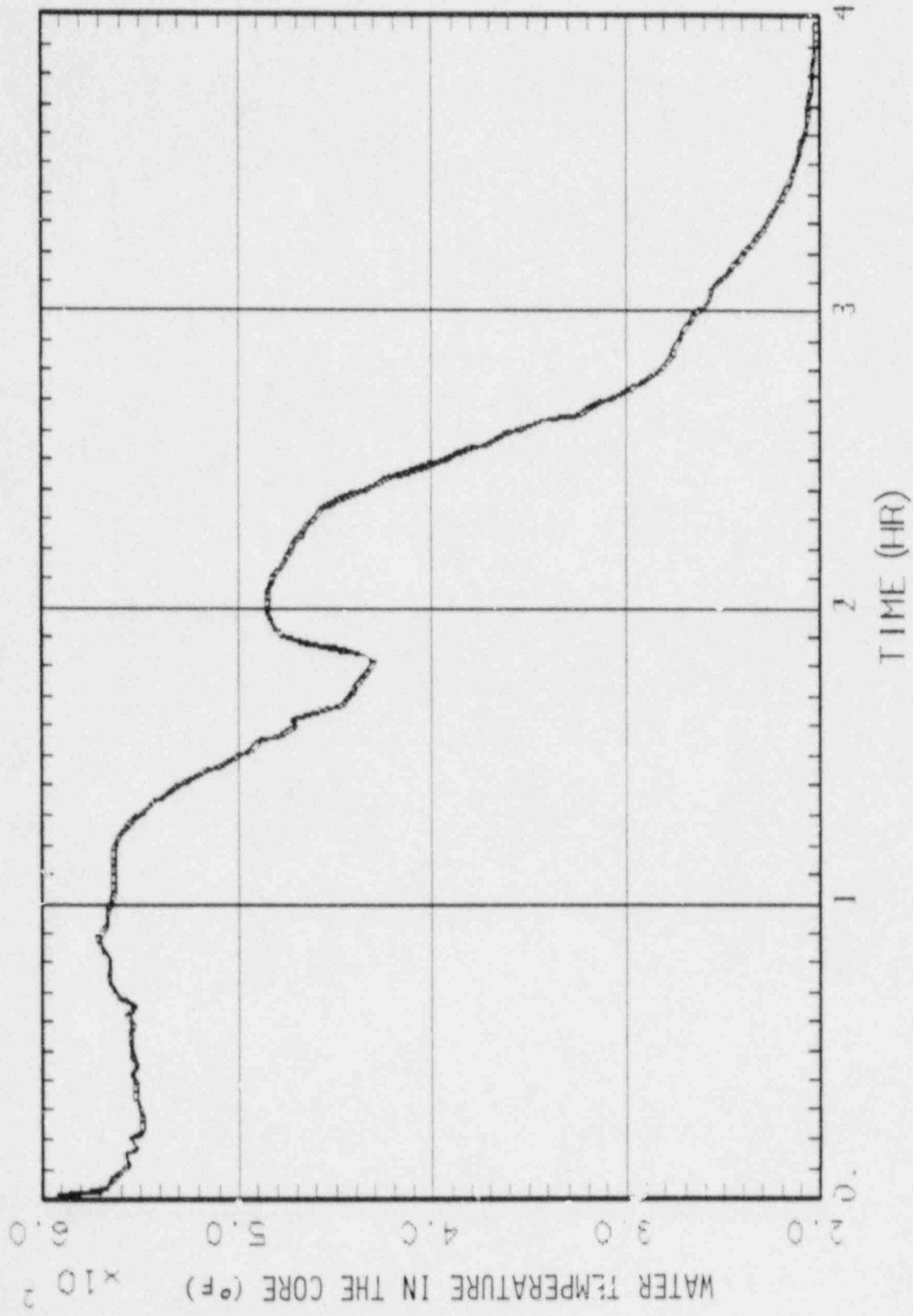


Figure 4.06 Water Temperature in the Core

S2H SEQUENCE - 10CFR50.44 ANALYSIS

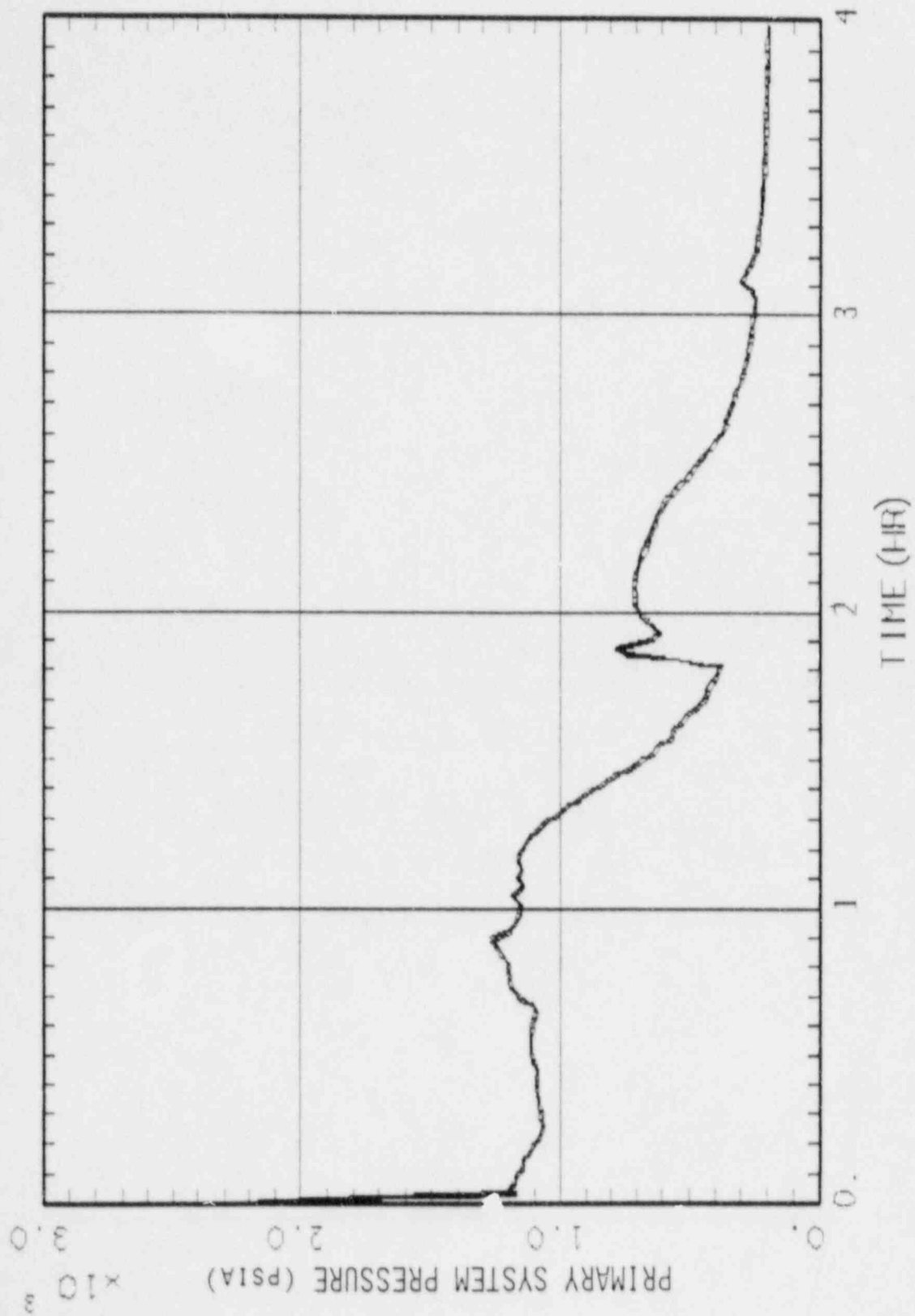


Figure 4.07 Primary System Pressure

S2H SEQUENCE - 10CFR50.44 ANALYSIS

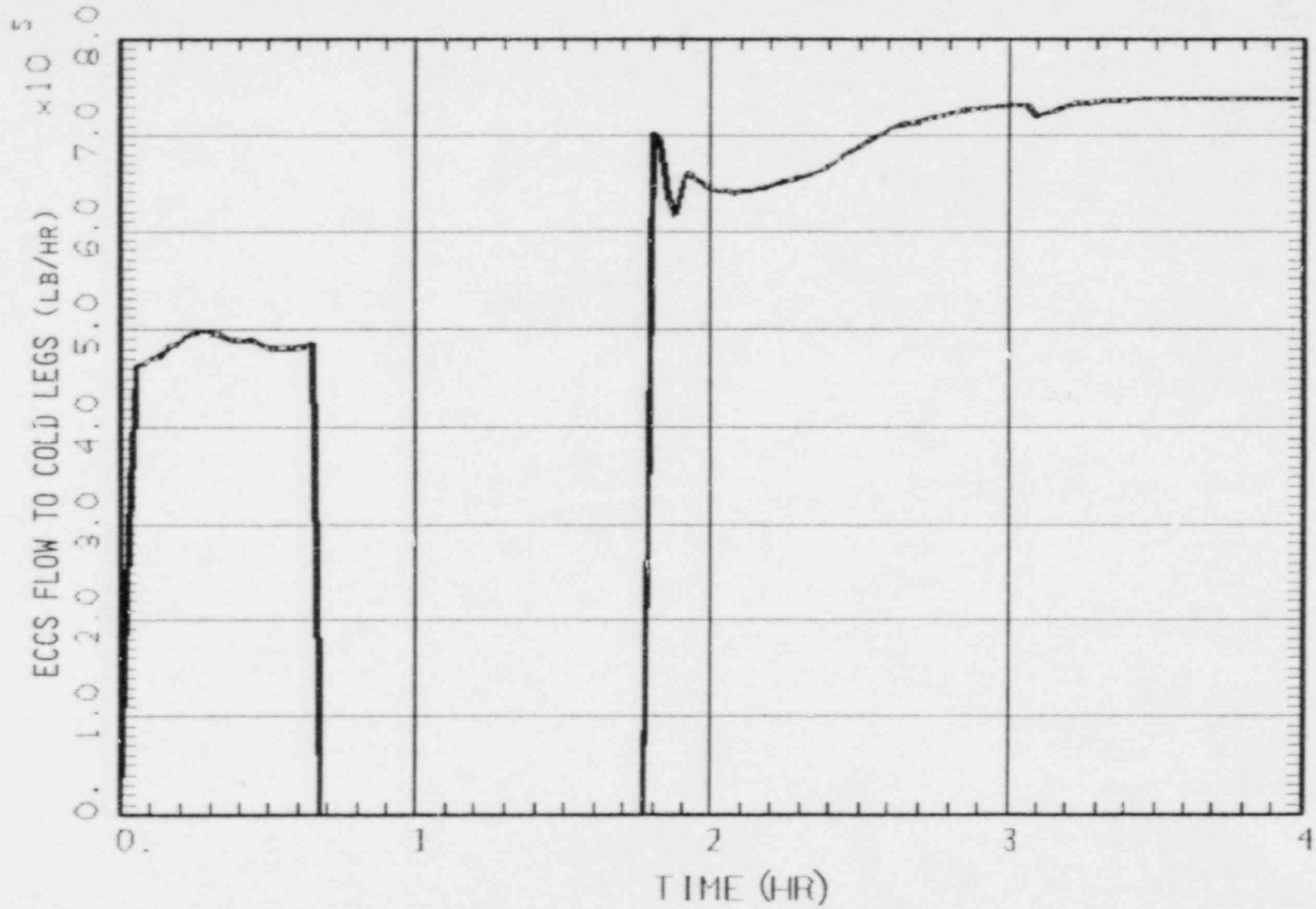


Figure 4.08 ECCS Flow to Cold Legs

S2H SEQUENCE - 10CFR50.44 ANALYSIS

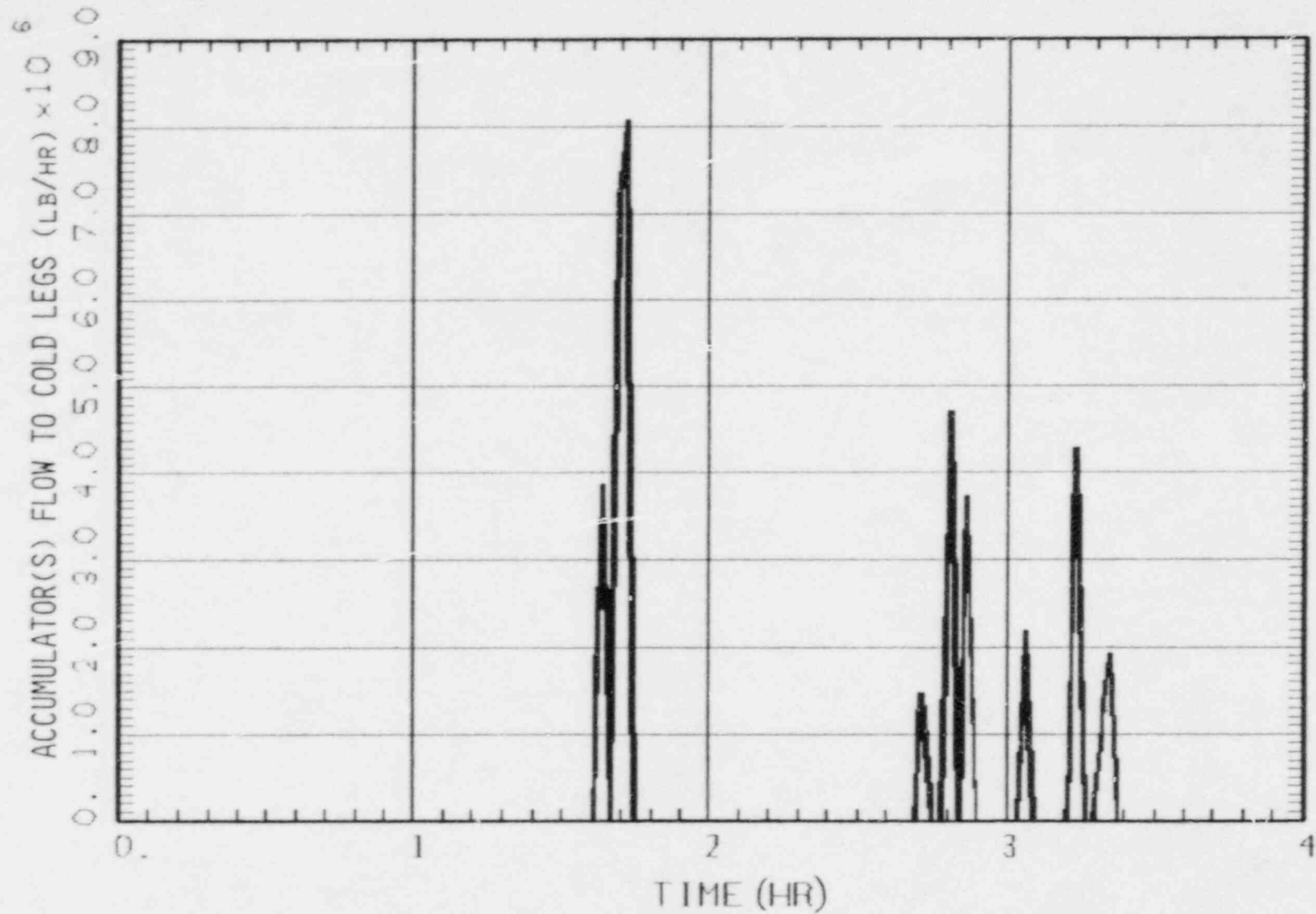


Figure 4.09 Accumulator(s) Flow to Cold Legs

S2H SEQUENCE - 10CFR50.44 ANALYSIS

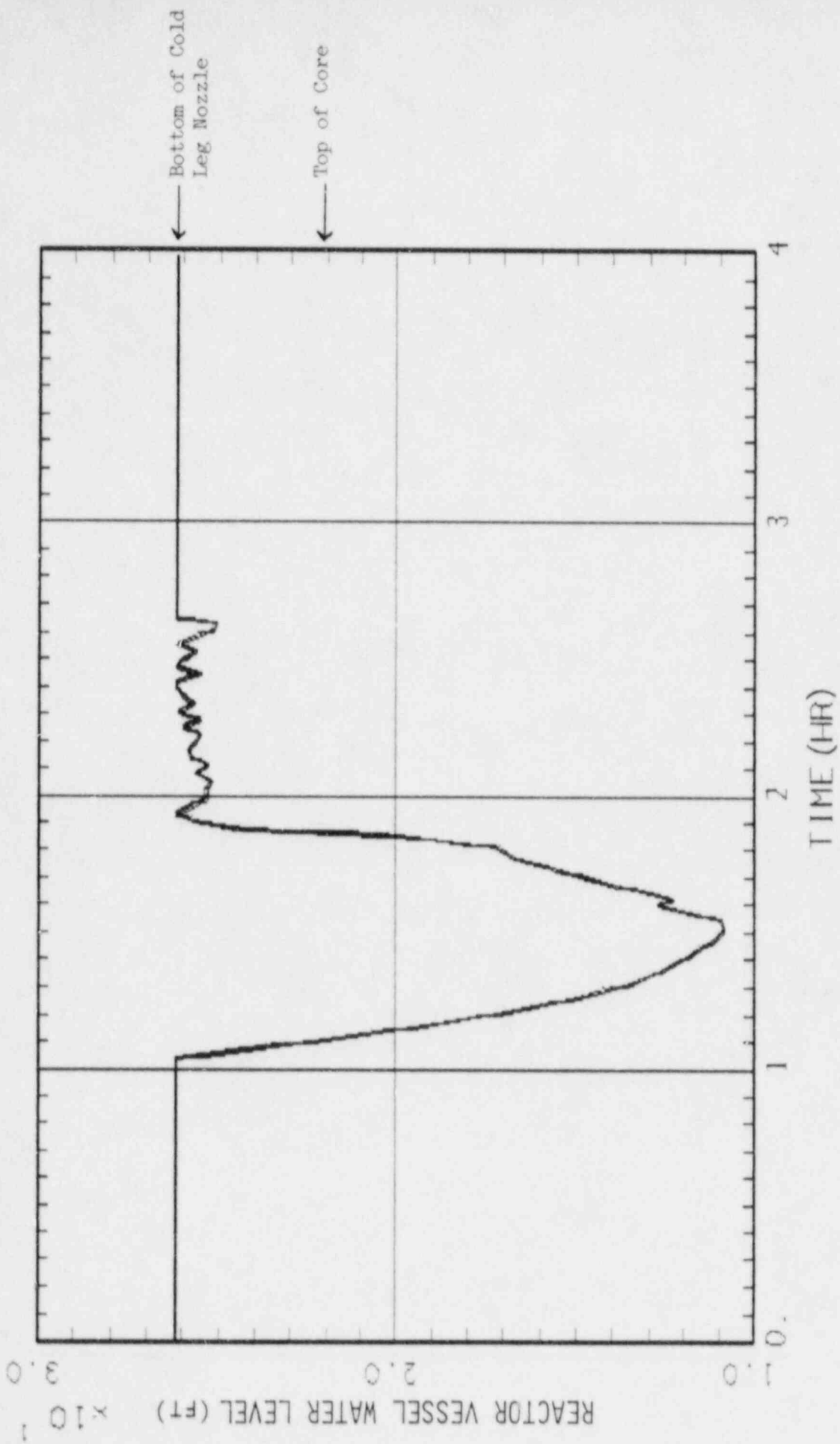


Figure 4.10 Reactor Vessel Water Level

S2H SEQUENCE - 10CFR50.44 ANALYSIS

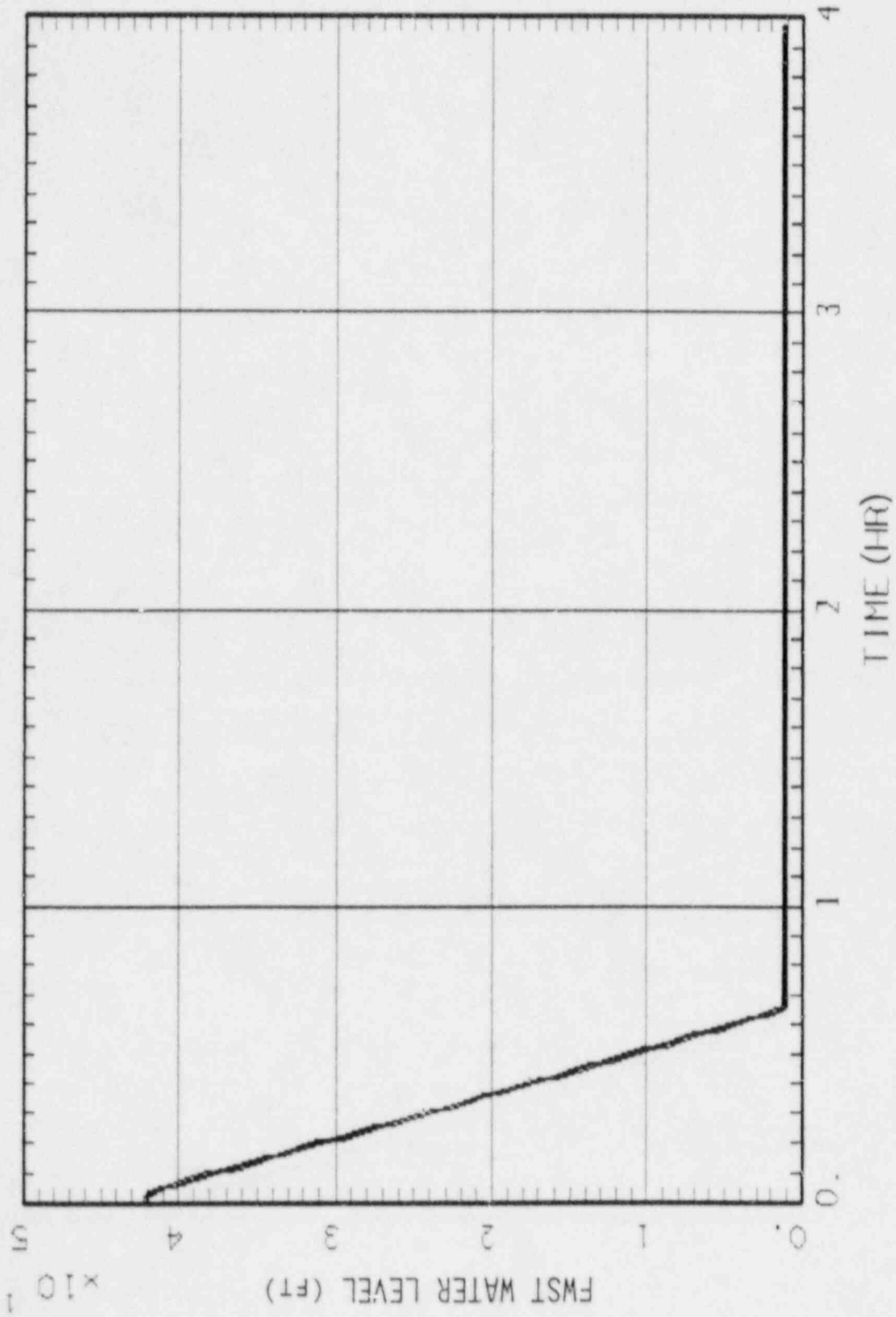


Figure 4.11 FWST Water Level

S2H SEQUENCE - 10CFR50.44 ANALYSIS

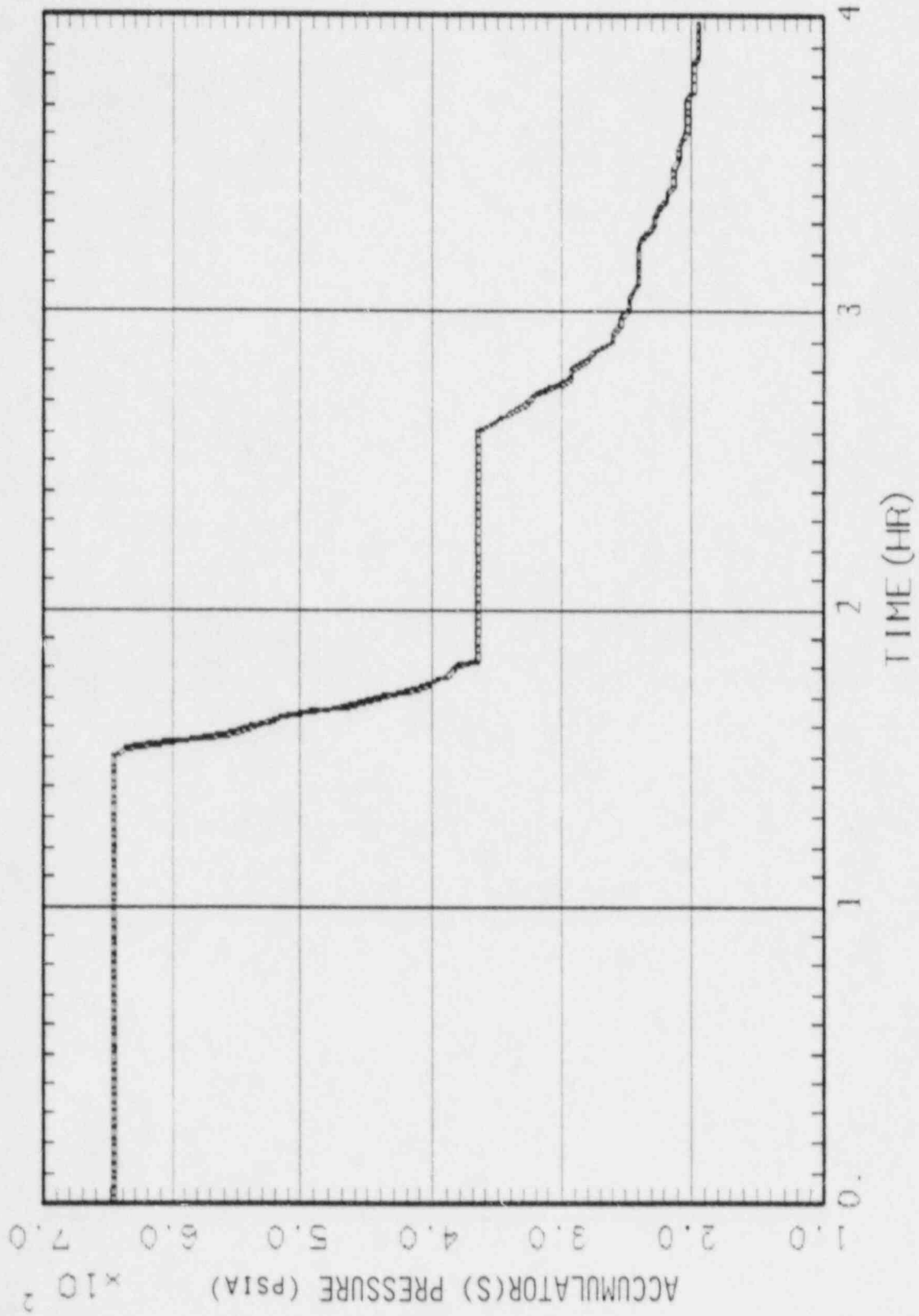


Figure 4.12 Accumulator(s) Pressure

S2H SEQUENCE - 10CFR50.44 ANALYSIS

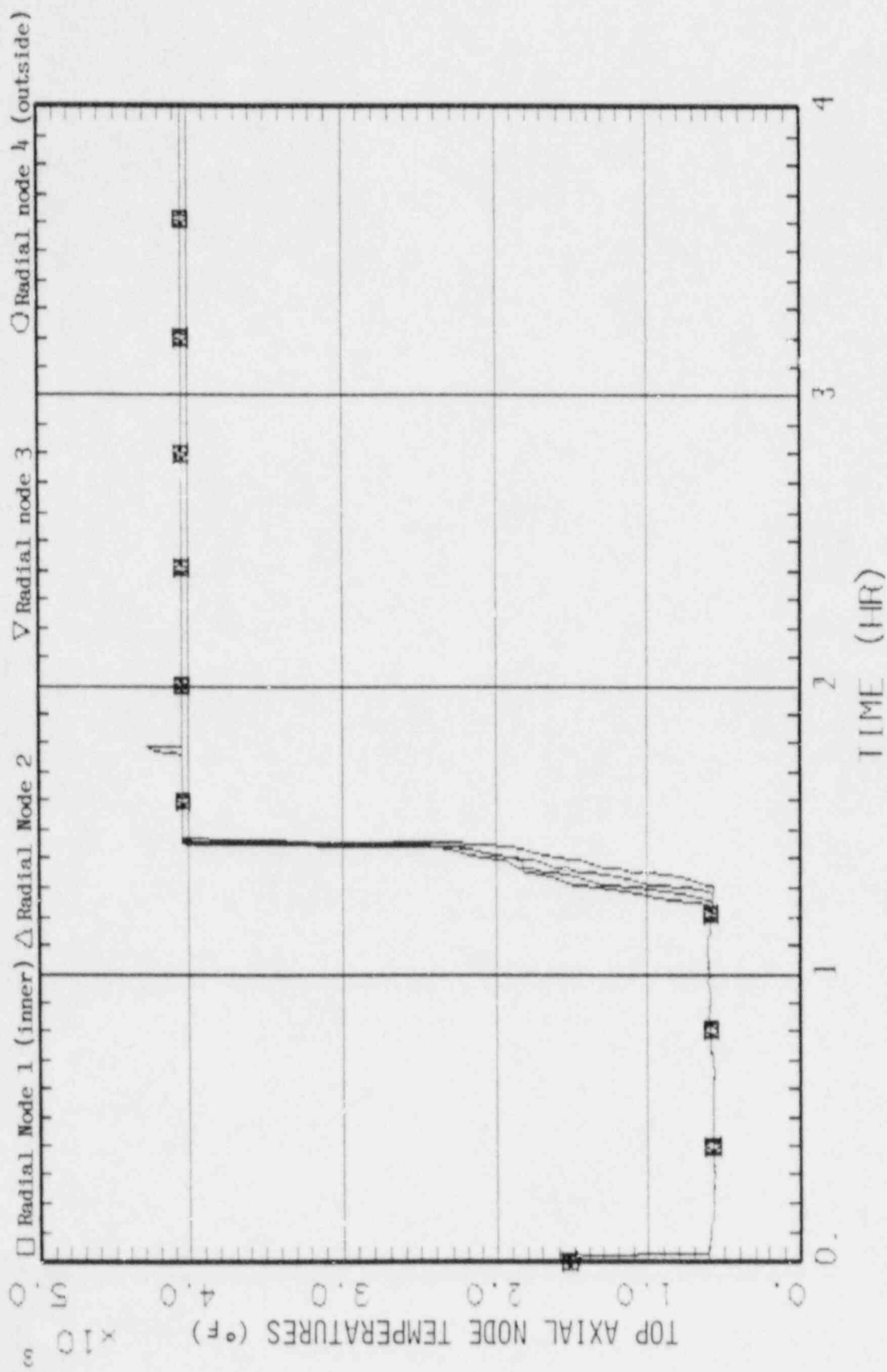


Figure 4.13 Top of Active Fuel Axial Node X 4 Top Radial Modes

S2H SEQUENCE - 10CFR50.44 ANALYSIS

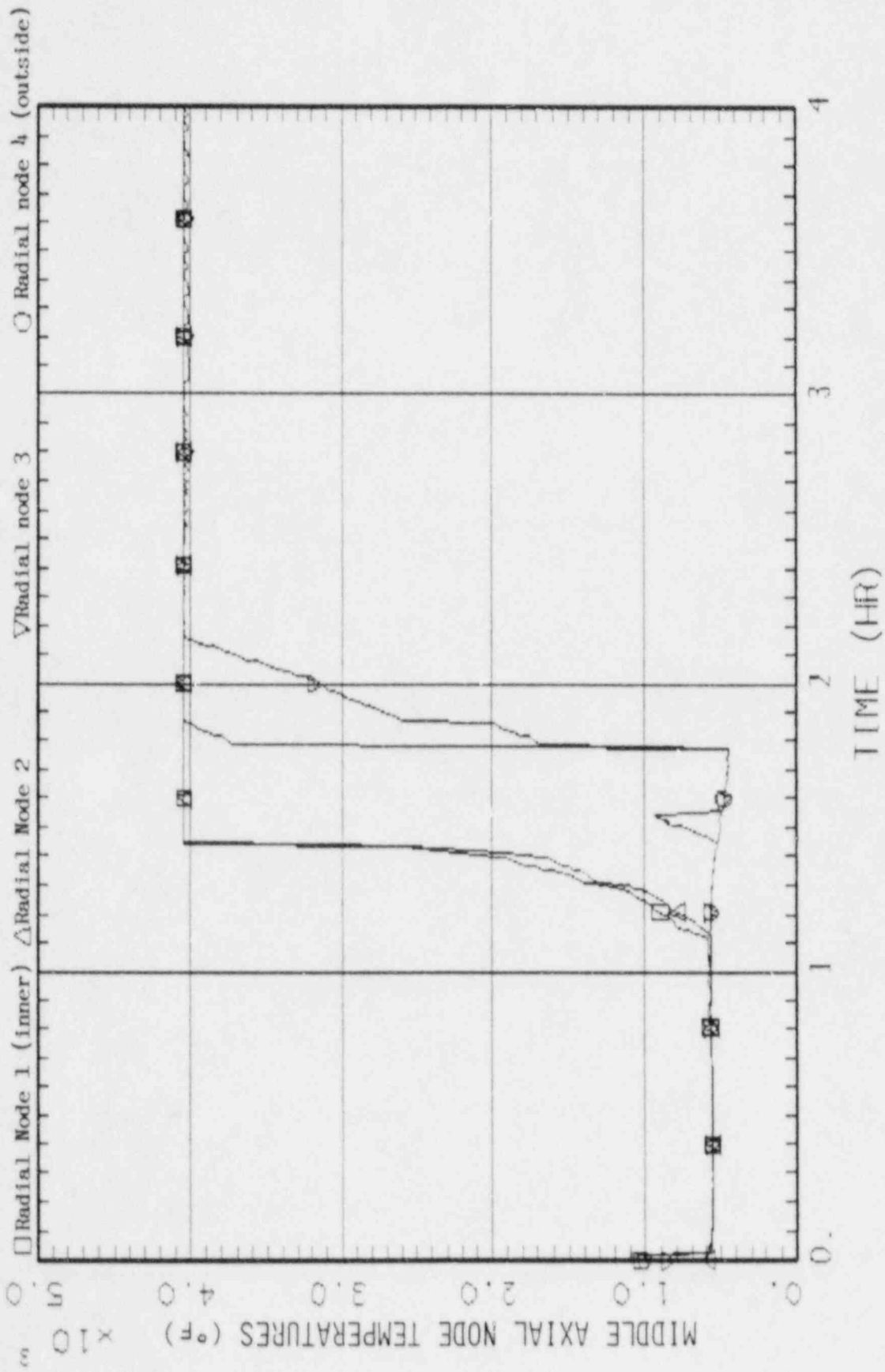


Figure 4.14 Middle of Active Fuel Axial Node X 4 Middle Radial Node

S2H SEQUENCE - 10CFR50.44 ANALYSIS

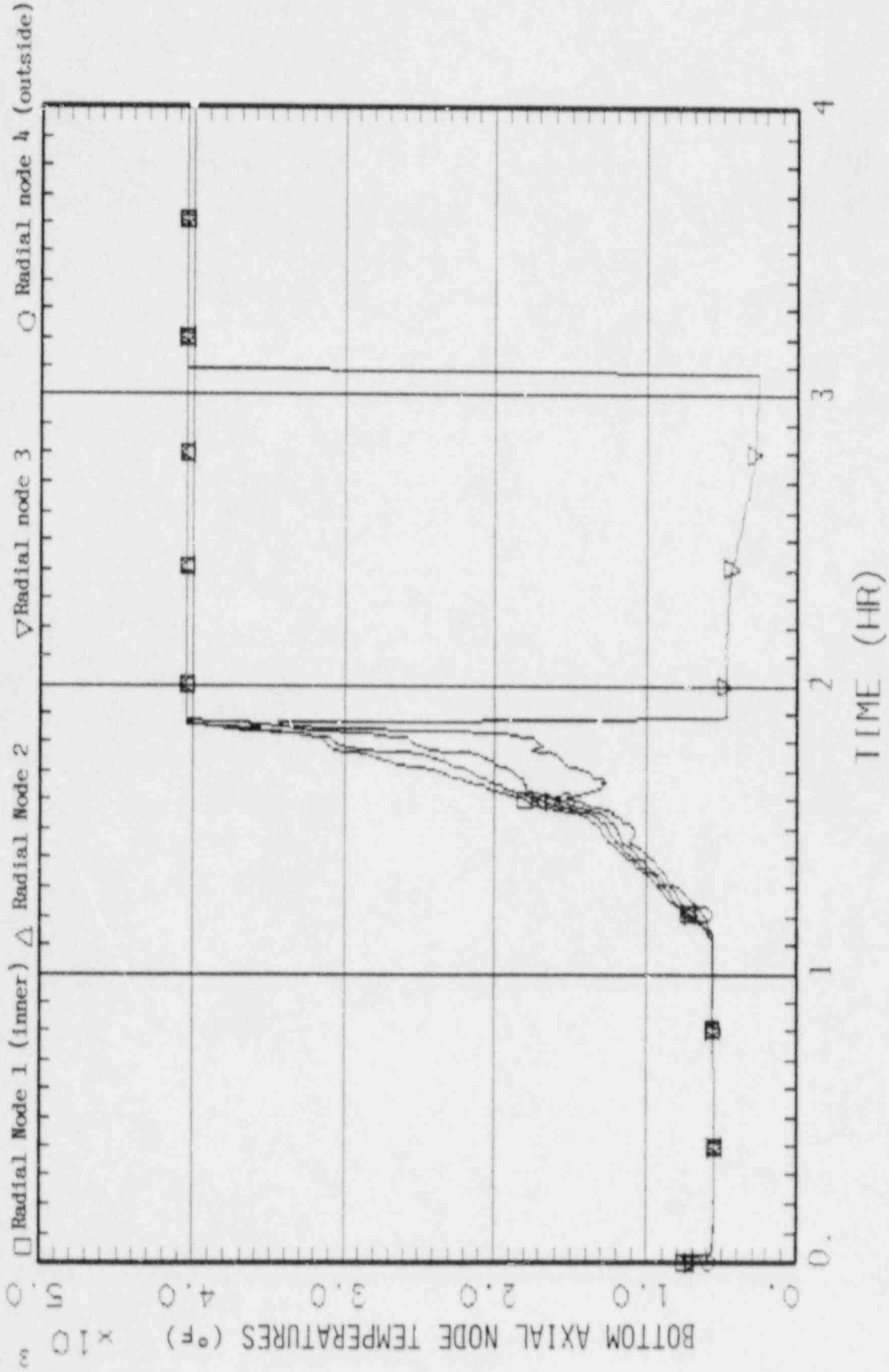


Figure 4.15 Bottom of Active Fuel Axial Node X 4 Bottom Radial Nodes

APPENDIX 5

The following documentation describes the models HEATUP and ACCUM which are currently incorporated within the MAAP 3.0B computer code. Complete documentation for the remaining MAAP models can be found in JDCOR Technical Report 16.2-3, MAAP (3.0) Modular Accident Analysis Program User's Manual - Vol. II, February 1987.

CORE-COOLANT INTERACTIONS

1.0 INTRODUCTION

The HEATUP subroutine predicts the behavior of the reactor core during and after uncover, as it is heated by fission product decay and by Zircaloy oxidation. The HEATUP subroutine includes models for calculating the steaming rate from the core, hydrogen formation rates, fuel melting, natural circulation flows, and upper head injection cooling from external accumulators.

The HEATUP subroutine was originally intended to substitute for the detailed PWR heatup code (EPRI PWRCHC) while that program and the MAAP code were under development. Another reason for developing this HEATUP subroutine was to provide a core heatup model with an execution time commensurate with the main PWR MAAP code. This has been achieved through several simplifications and assumptions described in detail in the model descriptions. The main simplifications are:

1. The core is divided into a maximum total of 70 nodes.
2. Only the heatup of the fuel rods is considered. Other structural materials such as grids and control rods are ignored.
3. The boiled-up water level is assumed to be uniform across the core.
4. Radial temperature gradients in the fuel rods are usually neglected.
5. Axial radiation heat transfer is neglected.
6. The melting model for the fuel rods is simplified in its representation of material interactions and internal heat transfer processes.

These simplifications reduce the computational complexity while still providing a realistic overall description of the core behavior.

In accordance with the computational procedure of the main MAAP program, the HEATUP subroutine calculates rates of change of the core state variables. These rates are determined from mass and energy balances and are integrated externally to provide updated values of the state variables at the next time step. The main core state variables include the nodal masses of UO_2 , Zr, and ZrO_2 , the internal energies of the core nodes, the cladding strains (ballooning model), and the fraction of the decay energy in each node which is not associated with fission products tracked by the fission product routines. The rates of steam and hydrogen production and the rate at which molten corium leaves the core boundaries, which drive many of the processes modeled in the rest of the MAAP code, are the most significant outputs of the subroutine.

2.0 MODEL DESCRIPTION

2.1 General Core Model

The reactor core is assumed to consist only of fuel rods and coolant flow channels as shown in Fig. 1. The fuel rods contain UO_2 pellets, which generate decay heat, clad in Zircaloy. The coolant channels may be partially covered by a water pool. Steam generated in the pool boils up the pool and flows in the uncovered part axially along the coolant channels and radially between them. Since there are no barriers for radial flow in the core, and the steam flow velocities are small, a uniform boiled-up water level is assumed across the core.

When the cold leg nozzles are empty, the core and the downcomer are hydraulically disconnected from the rest of the primary system. In this case, water may flow from the downcomer to the core, or vice versa, to equalize the static liquid heads in both regions. Thus, during core uncovering the water level in the downcomer essentially equals the collapsed water level of the core.

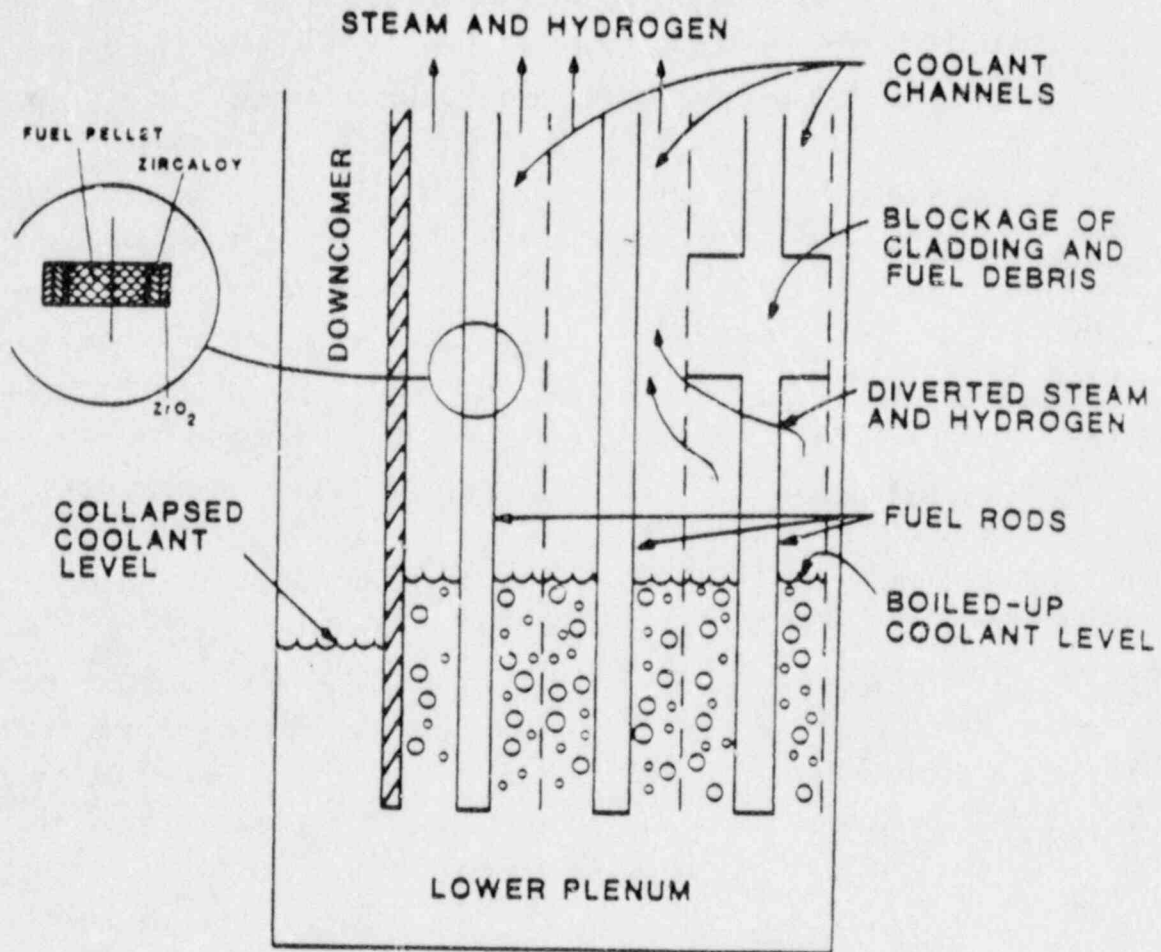


Fig. 1 Schematic description of a PWR core during uncovering.

During "normal" boildown of the core, the heat generated in the covered part of the core is transferred into sensible and latent heat of the water pool. Hence, the temperature of this part is limited to the pool saturation temperature. In the uncovered part of the core, on the other hand, heat can be removed by convection to the gas stream, and by pin-to-pin radiation across the core. This heat removal rate is generally less than the decay heat generation and thus the temperature in the uncovered region increases.

As the uncovered core heats up, differences in gas density across the core can cause natural circulation flows to be set up between the core and the upper plenum. Eventually, the Zircaloy reacts with steam in the flow channel to form ZrO_2 and hydrogen. This reaction is exothermic and results in further heating of the uncovered part. Ballooning and clad rupture may further contribute to the oxidation rate as the surface area increases and as the inner clad surface becomes exposed to steam. When the temperature at any location in the core reaches the Zircaloy melting point (2100 K) or a higher temperature if the Zircaloy reacts with oxygen or UO_2 , Zircaloy may melt and refreeze as it slumps or drains on the outer cladding surface. The flow channels thus may become blocked, and the steam and hydrogen mixture flowing below the blockage are then diverted to all the remaining unblocked channels. When the temperature in the uncovered core reaches the melting temperature (e.g. 2500K for typical U-Zr-O eutectics), the molten core components, namely UO_2 , Zr, and ZrO_2 (corium) leave the original node boundary.

When water from an external accumulator is injected into the upper part of the reactor pressure vessel it may quench the core by entering from the top or it may bypass the fuel rods to mix directly with the water pool. Both processes will cool the core.

Some accident sequences may involve very rapid injection of water into the core through the downcomer after the core has been uncovered for an extensive period (such as in TMI-2). In this case inverted annular flow can result where a film of steam would cover the hot fuel rods while water would be present in the central part of the flow channels. In this case, the covered part of the core can be at substantially higher temperatures than the water pool and may therefore oxidize.

A detailed description of the models used to calculate these processes are described in the following subsections.

2.2 Calculational Structure

The HEATUP subroutine primarily calculates the rate of change of the mass and energy of the major components of the core. These components are UO_2 , Zr, ZrO_2 , water (and steam), and hydrogen. The first three components are the major constituents of the "core material" while the other components are present in the flow channels.

The mass and energy rate of change of the core material components are calculated for each node in the core. Nodal temperatures are determined by subroutine TNODE from the core material masses and energy in the node. The masses of all the solid components are summed up to a total core mass. The water pool is treated as a lumped mass and energy control volume. The overall pool rates of change are determined by all the inlet and outlet flows and by the overall pool energy source terms. Similarly, water energy and mass balances are computed for the downcomer.

Steam and hydrogen are assumed to flow along the uncovered (and unblocked) flow channels, and the mass flow rates and enthalpies in each channel are calculated by tracking the generation and consumption of each component at each axial level. The channel exit values are summed to form a total steam and hydrogen flow from the core and an overall gas enthalpy.

When subroutine HEATUP is called for the first time in PWR-MAAP the following major user-specified definitions are made:

1. Number of radial rings and axial rows. All nodal variables are dimensioned to a total maximum of 70 nodes. The maximum number of rings is 7 and the maximum number of rows is 20. Any combination of the number of rings and rows which (a) does not exceed the corresponding maximum limits of 7 and 20, and (b) yield an overall number of nodes not exceeding 70, is acceptable. For example, 7 rings x 10 rows or 3 rings x 20 rows are

acceptable; 5 rings x 16 rows (more than 70 nodes) or 8 rings x 8 rows (more than 7 rings) are unacceptable. The top node in each ring represents the unfueled upper fission gas plena.

2. Fuel rod and channel geometry.
3. Power and flow area fractions are normalized, if not already done so by the user.

2.3 Physical Processes Modeled

The major models used by the HEATUP subroutine are:

1. Heatup and steam generation in the water pool,
2. Zircaloy oxidation and hydrogen formation,
3. Core-upper plenum natural circulation,
4. Radial radiation model,
5. Heatup of an uncovered node,
6. Corium melt model,
7. Upper head injection,
8. Clad ballooning.

The models are formulated with the primary concern of providing a realistic overall description of the dominant physical processes while minimizing the computational complexity. A lumped control volume approach is used for all mass and energy balances. The model is quasi-steady in the sense that the exit flows are determined by the inlet flows and steaming, i.e. changes in internal core flow rates due to pressure changes are neglected.

2.3.1 Heatup of the Water Pool and Covered Nodes

The covered part of the core extends from the bottom of the core to the location of the boiled-up level. Since the boiled-up water level is assumed to be uniform across the core, its location is determined by relating the boiled-up water volume to the free volume in the reactor vessel. This boiled-up volume is obtained from the water mass, density and the average void

fraction in the pool. The boiled-up water level is calculated externally to HEATUP (in PRYSIS) by subroutine VLEVEL by specifying the water mass in the core, the water and steam specific volumes, the height at which the inlet flows became saturated in the last time step, and the steam flow rates below and in the core. These flow rates determine the average void fractions in the lower plenum and in the core.

In the lower plenum, steam is generated by interaction of water with the molten corium. This steam flow, $W_{st;cm}$, is calculated by subroutine PLSTM, and the resulting void fraction is applied to the entire lower plenum.

In the covered part of the core, steam can be formed by boiling and also by flashing if the pressure in the RPV changes with time. Steam generation by boiling is assumed to take place only when the pool is saturated. The boiling steam flow rate, $W_{st;b}$, is determined from the heat transferred to the water pool, $Q_{w;pool}$, by:

$$W_{st;b} = (Q_{w;pool} - Q_{sub})/h_{fg} \quad (1)$$

where h_{fg} is the latent heat and Q_{sub} is subcooling of the inlet flow.

The time scale for the heat transfer from the fuel rods to the pool during "normal" core boildown, is much smaller than the core heatup time scale. Thus, $Q_{w;pool}$ is evaluated in this case by:

$$Q_{w;pool} = \frac{U_{cover} - U_{cover}^{pool}}{\tau_{pool}} + f_c Q_{DCN} \quad (2)$$

where U_{cover} is the internal energy of all the covered nodes, U_{cover}^{pool} is the internal energy of all covered nodes if they were at the pool temperature, τ_{pool} is the relaxation time set to the maximum time step allowed, f_c is the fraction of the node which is covered, and Q_{DCN} is the decay heat in the node. For partially uncovered nodes, if the water level is decreasing, $Q_{w;pool}$ is limited to the last term since including the other term would artificially couple the covered and uncovered parts of the node; this algorithm improves

the accuracy of the code when relatively few axial nodes are used by not delaying the onset of node heatup until the node is fully uncovered. When the pool is subcooled, $Q_{w;pool}$ is applied to increase the sensible energy of the pool.

However, immediately following a scram, the fuel is still hot and covered with water. In this case, the heat transferred into the pool is determined by the overall fuel-to-coolant heat transfer resistance rather than the internal heat generation. This resistance is the sum of an effective conduction heat resistance in the fuel and a convective heat resistance in the coolant:

$$h = \frac{1}{\frac{x}{k_f} + \frac{1}{h_c}} \quad (3)$$

In Eq. (3) k_f is the fuel thermal conductivity, h_c is calculated using Dittus-Boelter correlation and x is an effective conduction thickness. Some side calculations of the fuel-to-coolant heat transfer rates using an effective thickness and a detailed heat conduction model through the fuel pin, showed good agreement for $x = 0.3 r_{\text{pellet}}$, where r_{pellet} is the radius of the fuel pellets. The heat transfer to the water pool is calculated as the sum of all the individual covered node heat transfer rates:

$$Q_{CN} = h A_{CN} (T_{CN} - T_{\text{pool}}) \quad (4)$$

where A is the heat transfer area and subscript CN denotes covered nodes.

The actual heat transfer to the water pool is taken as the minimum of $Q_{w;pool}$ (Eq. 2) and $\sum Q_{CN}$ (Eq. 4).

In the case where the core is recovered from below after an extensive period of being uncovered, the heat transfer rate from the hot fuel pin into the pool is limited by two-phase hydrodynamic stability considerations. A maximum gas superficial velocity exists beyond which liquid droplets would

be entrained in the gas stream and be carried out of the pool. This maximum velocity is [1]

$$j_E = K \sqrt[4]{\frac{\sigma g (\rho_l - \rho_g)}{\rho_g^2}} \quad (5)$$

where σ is the surface tension, g is the acceleration due to gravity, ρ_l and ρ_g are the liquid and gas densities respectively, and K is the Kutateladze number. This number is taken as 3.0 when the original geometry is intact, and a user-specified number (default: 0.3) when the core has collapsed. The resulting maximum steam flow rate is

$$W_{st;max} = j_E A_f \rho_g \quad (6)$$

where A_f is the total area inside the core barrel. The maximum heat that can be transferred to the pool is

$$Q_{w;max} = W_{st;max} h_{fg} \left[1 + 0.1 \left(\frac{\rho_g}{\rho_l} \right)^{0.25} \frac{h_w - h_p}{h_{fg}} \right] \quad (7)$$

where h_w is the enthalpy of saturated water and h_p is the enthalpy of the water pool. The second term in the parenthesis of Eq. (7) is a correction for the case where the pool is subcooled ($h_p < h_w$). When the pool is saturated $h_w = h_p$ and this term is zero. If $Q_{w;pool}$ is larger than $Q_{w;max}$ or if the total steam flow from the covered core exceeds $W_{st;max}$, the heat transferred from each covered node to the pool is reduced by $Q_{w;pool}/Q_{w;max}$ so that $Q_{w;pool}$ is always less than or just equal to $Q_{w;max}$.

Steam generation by flashing, $W_{st,f}$, is calculated in subroutine POOL and RATES, (called from PRISYS) as:

$$W_{st,f} = \frac{U_w - M_w h_{w;sat}}{h_{fg} \cdot \tau_f} \quad (8)$$

where U_w is the energy of the water, $h_{w;sat}$ and h_{fg} is the water saturation enthalpy and latent heat corresponding to the current system pressure, respectively and τ_f is the flashing time scale.

The void fraction in the covered pool is determined from the total steam flow out of the pool by functions VFSPAR and VFVOL (in subroutine VLEVEL). However, in the case of core recovery from the bottom, large amounts of steam could be generated from the top of the pool due to the quenching process. This would lead to high average void fractions and numerical oscillations in the boiled-up level. To avoid this unrealistic average void fractions, the steam generation from the just-recovered nodes is not accounted for in the void fraction calculation during recovery.

The steam flow rates described above contribute to the pool mass and energy balances and determine the void fractions in the pool.

The pool mass rate of change, \dot{M}_w is:

$$\dot{M}_w = - (W_{st;cm} + W_{st;b} + W_{st,f}) + W_{w;dc} + W_{w;ps} + W_{w;up} \quad (9)$$

where $W_{w;ps}$ is the sum of water flow rates from the rest of the primary system, $W_{w;dc}$ is the water flow rate from the downcomer, and $W_{w;up}$ is the flow rate from the core upper plate due to UHI flows.

The pool energy rate of change includes all the heat content of the various streams described by Eq. (9), and the heat transferred from the fuel.

The energy rate of change of core material in a covered node is

$$\dot{U}_N = Q_{decay} - Q_{w;pool} + Q_{reaction} - Q_{melt} \quad (10)$$

where Q_{decay} is the decay heat generated in a node, $Q_{reaction}$ is the heat generated in a node due to clad oxidation and Q_{melt} is the energy rate carried with the melting fuel. Oxidation and melting can occur in the covered part

only during recovery from core degradation and is discussed in the next sections.

2.3.2 Zircaloy Oxidation and Hydrogen Formation

Zircaloy may react with steam according to the following chemical reaction:



where ΔH_R is the heat of reaction per mole of Zr. This oxidation takes place at the Zr/ZrO₂ interface leading to an increase in the oxide layer thickness. The reaction rate equation proposed by Cathcart, [2] is used for Zircaloy temperature, T, up to 1850 K and the Baker-Just equation [3] is used for higher temperatures. The rate of change of the oxide layer thickness, \dot{x}_o is thus:

$$\dot{x}_o = \frac{294 \exp(-1.654 \cdot 10^8/RT)}{2 \rho_{\text{Zr}}^2 x_o} \quad 400 < T \leq 1850 \text{ K} \quad (12)$$

$$\dot{x}_o = \frac{3.33 \cdot 10^3 \exp(-1.884 \cdot 10^8/RT)}{2 \rho_{\text{Zr}}^2 x_o} \quad T > 1850 \text{ K} \quad (13)$$

where R is the gas constant, and ρ_{Zr} is the Zircaloy density.

Zircaloy oxidation is assumed to be terminated if either:

- a. The node has less than a user-specified non-fuel fraction due to accumulation of once-molten material from higher nodes.
- b. The node is melting.

This logic is intended to represent the diversion of steam away from nodes with little flow area and small hydraulic diameters, and the decrease in oxidation rates due to reductions in surface to volume ratios.

For uncovered nodes the radial temperature gradient is small and therefore T in Eqs. (12) and (13) is taken as the node temperature. In the covered part of the core, during recovery of hot nodes, a significant radial temperature gradient may exist. Hence, the cladding temperature, rather than the node temperature, should be used. The cladding temperature is calculated iteratively by

$$T_{\text{clad}} = T_{\text{CN}} + \frac{Q_{\text{reaction}} - Q_{\text{CN}}}{A_{\text{CN}} k_f/x} \quad (14)$$

where Q_{CN} is the heat transfer to the water,

$$Q_{\text{reaction}} = \Delta H_R \frac{W_{\text{ZrO}_2}}{\text{MW}_{\text{ZrO}_2}} \quad (15)$$

MW_{ZrO_2} is the ZrO_2 molecular weight and W_{ZrO_2} is the rate of ZrO_2 generation. This rate is calculated from Eq. (13) as

$$W_{\text{ZrO}_2} = \rho_{\text{ZrO}_2} A_{\text{ox}} \dot{x}_o \quad (16)$$

where A_{ox} is the oxidation area of a node computed in subroutine GNODE. Normally this area should equal the outside surface area of the cladding. However, if a flow channel (possibly ballooned) is ruptured, the area may be increased by a user-specified factor.

For a covered node, oxidation may continue after the onset of melting if the user defeats the submerged blocking model with $\text{IEVNT}(202) = 1$.

The actual oxidation rate is limited by either the rate at which Zr may oxidize, Eq. (16), or by the availability of steam. The latter limit is

Based on the channel steam flow and the stoichiometry of Eq. (11). The rates of hydrogen and ZrO_2 formation, steam and Zircaloy consumption, as well as the heat generated by the reaction are all calculated from the actual oxidation rate and the stoichiometry of Eq. (12).

2.3.3 Core-Upper Plenum Natural Circulation

Work by various investigators have shown that natural circulation flows can be set up between the upper plenum and the core. Such flows could alter the progression of a severe core accident by delaying the onset of core oxidation, supplying steam to prolong the oxidation process, heating the upper plenum and re-volatilizing fission products, and perhaps causing the primary system to fail due to high temperatures prior to core slump into the lower plenum and failure of the reactor vessel lower head. These considerations lead to the conclusion that a model for the phenomenon should be integrated into subroutine HEATUP.

To make the problem tractable, the geometry of the flow pattern was set a priori based on the results of available detailed hydrodynamic calculations and experiments.

Two different flow patterns are considered. In Fig. 2, the flow pattern for Westinghouse-type reactor vessel geometries is schematically illustrated. As shown, it is assumed that the flow consists of one large "loop" coupling the core to the upper plenum. The return leg from the upper plenum is assumed to flow down the outer, cooler flow channels and to occupy half the total core flow area. In Babcock and Wilcox reactors, on the other hand, a significant flow area exists through the core baffle as shown in Fig. 3. There is therefore a potential for the return flow to pass down the core barrel-baffle annulus and through the baffle into the core. Rather than determining by detailed calculations which of the two flow patterns would be established in such reactors, the approach taken was to allow the user to select either pattern and perform sensitivity calculations.

The flow rate is derived by assuming the flow patterns outlined above. The flow rate W_j in some channel j in a nodalized core is given by

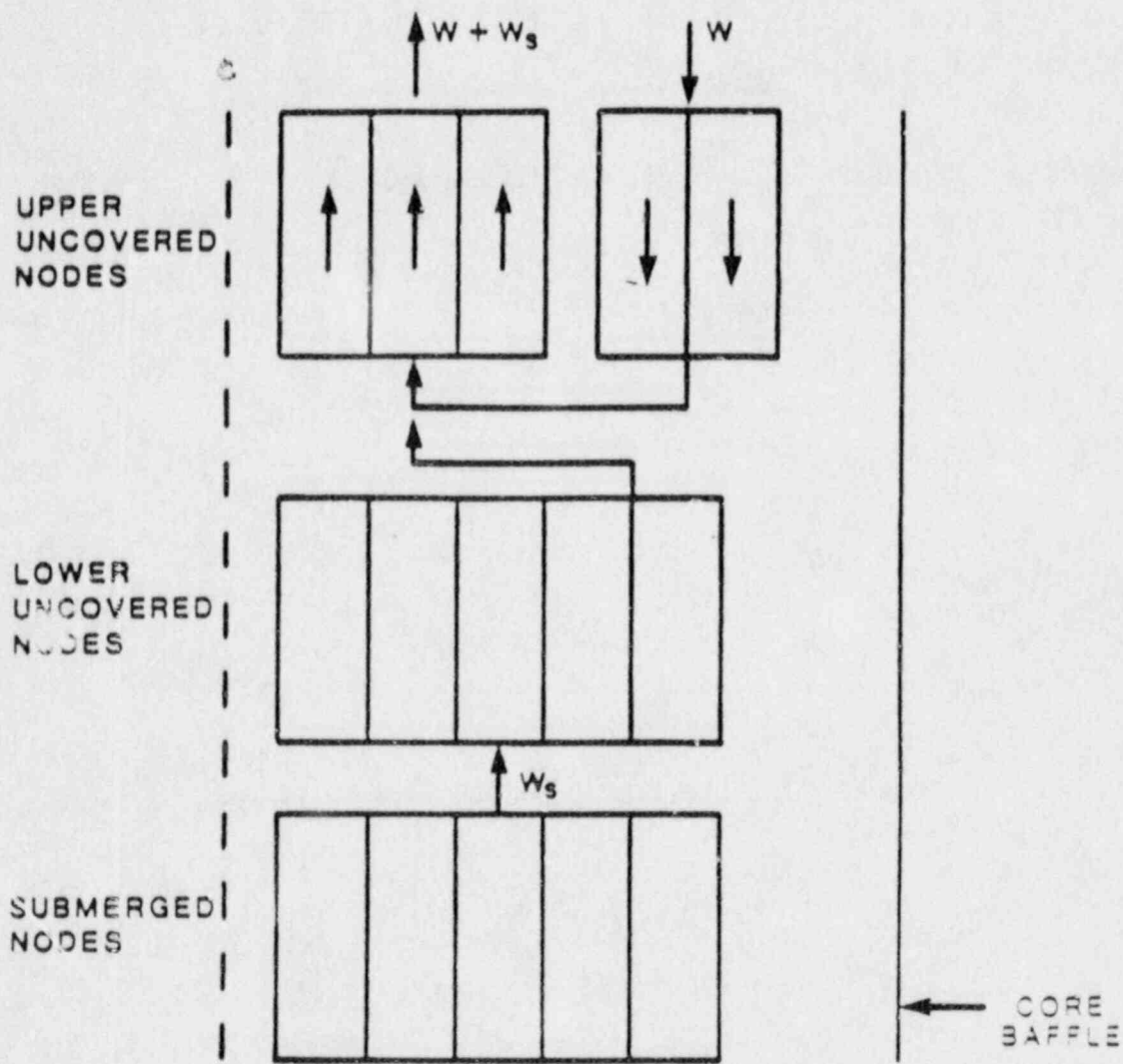


Fig. 2 Flow pattern when through-core-baffle resistance is high.

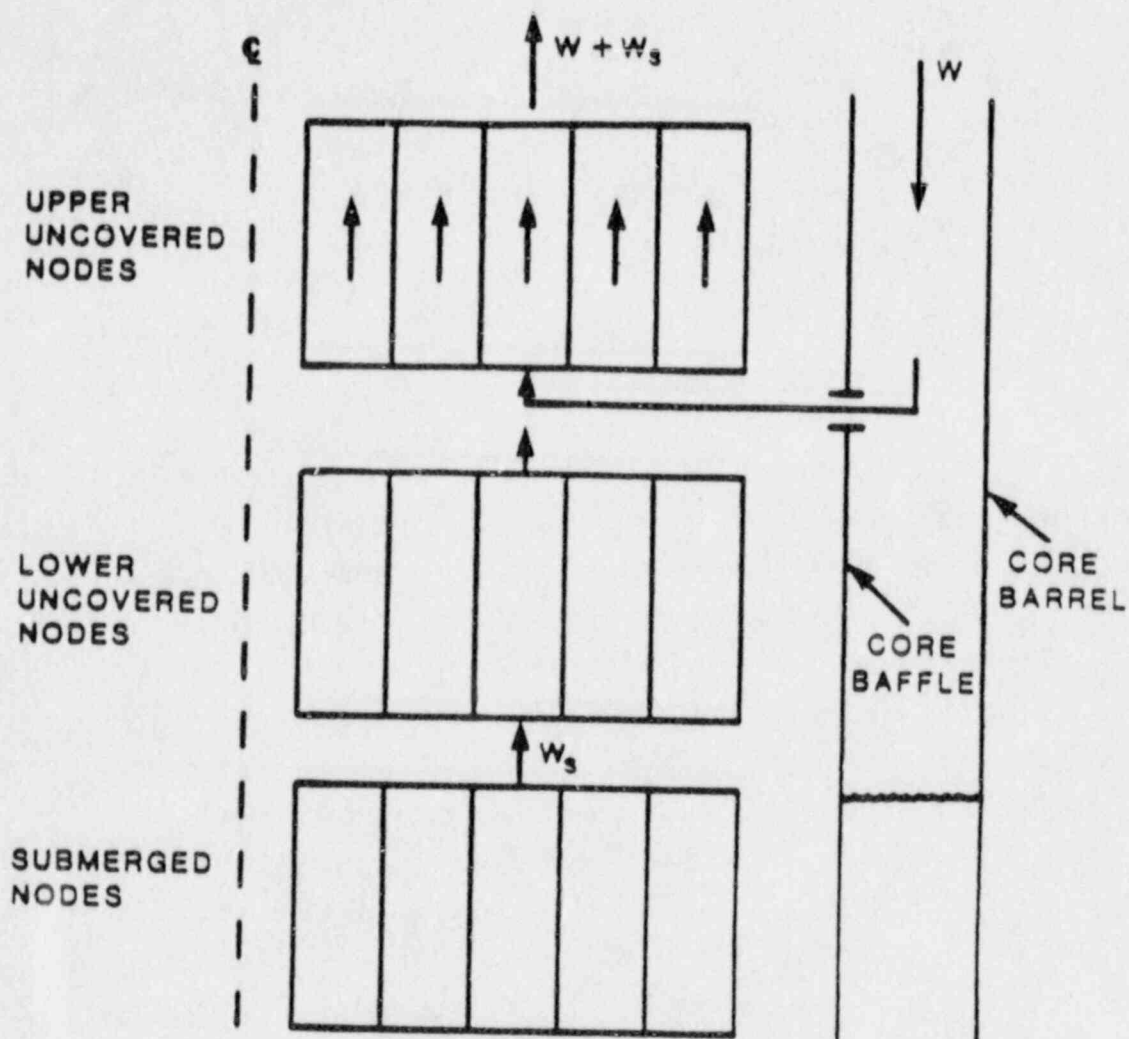


Fig. 3 Flow pattern when the through-core-baffle resistance is moderate.

$$W_j |W_j| = \frac{-d P_{ij}}{dz} \frac{2 D_{ij} \rho_{ij} A_{ij}^2}{f} \quad (17)$$

where

$\frac{dP_{ij}}{dz}$ = axial friction pressure gradient in channel j at row i, denoted (i,j)

D_{ij} = hydraulic diameter at (i,j)

ρ_{ij} = gas density at (i,j)

A_{ij} = flow area at (i,j) in the x-y plane

f = friction factor for axial flow

At this point, the assumption is made that the friction pressure gradient in all up-flowing channels and all-down flowing channels are equal in a row. As discussed in the appendix on subroutine REMIX, this is not strictly true. Small differences in hydrostatic head between channels cause flow redistributions which lead to differences in the friction. The assumption of equality will be made here nonetheless on the basis that it should provide a reasonable estimate for the total flow; the distribution of the total flow among the different channels is treated by subroutine REMIX.

Under this assumption, the total up or down-flow is obtained by summing over the appropriate channels. If the down flow is denoted W , the up-flow will be $W + W_s$ where W_s is the total flow which arises from the covered nodes. Performing the summations we obtain

$$W = \sqrt{\frac{dP_{\text{down}}}{dz_i}} \sum_{\text{down channels at elevation } i} \sqrt{\frac{2 D_{ij} \rho_{ij} A_{ij}^2}{f}} \quad (18)$$

$$W + W_s = \sqrt{\left| \frac{dP_{up}}{dz_i} \right|} \sum_{\substack{\text{up channels} \\ \text{at elevation} \\ i}} \sqrt{\frac{2 D_{ij} \rho_{ij} A_{ij}^2}{f}} \quad (19)$$

If we now solve for the pressure gradients and sum over rows we obtain

$$\Delta P_{down} = \sum_{\text{rows}} \frac{\Delta Z W^2}{\left(\sum_{\substack{\text{down} \\ \text{channels}}} \sqrt{\frac{2 D_{ij} \rho_{ij} A_{ij}^2}{f}} \right)^2} \quad (20)$$

$$\Delta P_{up} = - \sum_{\text{rows}} \frac{\Delta Z (W + W_s)^2}{\left(\sum_{\substack{\text{up} \\ \text{channels}}} \sqrt{\frac{2 D_{ij} \rho_{ij} A_{ij}^2}{f}} \right)^2} \quad (21)$$

where ΔP_{down} is the total pressure drop across the down channels and similarly for ΔP_{up} ; ΔZ is the axial height of each node. Define the flow resistance in row i for down flow as

$$S_{2D_i} = \frac{f \Delta Z}{\left(\sum_{\substack{\text{down} \\ \text{channels}}} \sqrt{D_{ij} \rho_{ij} A_{ij}^2} \right)^2} \quad (22)$$

and similarly for the up flow resistance. Denote the sum over rows of these terms as SD and SU respectively, e.g.

$$SD = \sum_{\text{rows}} S_{2D_i} \quad (23)$$

Substituting Eqs. (22) and (23) into Eqs. (20) and (21), and subtracting the resulting two equations yields

$$\Delta P = \frac{W^2}{2} SD + (W + W_s)^2 \frac{SU}{2} \quad (24)$$

In the limiting case of only one up-channel and one down-channel, the terms on the right hand side of Eq. (24) are easily interpreted as the pressure drops across the two channels induced by the flows.

Note that we have so far neglected the pressure drop induced by the downward moving flow as it turns and moves across the fuel bundles. This pressure drop can be calculated by an expression of the form [4]

$$\Delta P_{\text{cross flow}} = \frac{n f_x W^2}{2 A_x^2 \rho}$$

where

f_x = friction factor for cross flow ($\sim .25 - .45$),

n = number of tube rows crossed by the fluid,

A_x = minimum flow area as the fluid crosses a row of tubes,

ρ = density of the sideways-moving gas.

For the case represented by Fig. 2, the assumption of equal up- and down-flow areas delineates the radial boundary between the up and down portions of the flow loop. This is used to estimate the average number of rows crossed by the fluid. By consulting published hydrodynamic calculations of the flow, the axial extent of the horizontal portion of the loop is estimated to be approximately 0.5 m; this along with the tube pitch defines the area A_x . Users wishing to investigate the sensitivities to these reasonable, but admittedly rather rough assumptions, can vary f_x . Thus, to account for the radial

pressure drop, the following expression for the cross flow resistance is added to the term SD in Eq. (24)

$$\frac{n f_x}{A_x^2 \rho}$$

The total pressure difference ΔP across the core caused by the fluid motion is balanced by the difference in hydrostatic head between the up and down channels:

$$\Delta P = \sum_{\text{ROWS}} (\bar{\rho}_{i,\text{down}} - \bar{\rho}_{i,\text{up}}) g \Delta Z \quad (25)$$

where g is the acceleration of gravity. Equation (25) is solved by area-averaging the densities in the up and down channels at every row.

Equation (24) is solved in the code by substituting Eq. (25). It is instructive to derive from Eq. (24) the conditions necessary for positive natural circulation flow. Rewriting Eq. (24)

$$W^2 \left(\frac{SD}{2} + \frac{SU}{2} \right) + W (SU)(W_s) + \left(W_s^2 \frac{SU}{2} - \Delta P \right) = 0 \quad (26)$$

For positive W , we require the last term be negative, i.e.

$$W_s^2 \frac{SU}{2} < \Delta P \quad (27)$$

The first term in Eq. (27) is just the pressure difference across the up channels due to the steaming flow W_s . Thus, Eq. (27) confirms that the requirement for natural circulation is that the pressure gradients due to buoyancy exceed those due to the forced flow.

The only other unknown which must be determined to solve Eq. (24) is the row number in Figs. 2 or 3 where the flow from the down channels turns horizontal and enters the up channels. At present, this is established by

finding the row where the temperature in the downward moving fluid reaches the temperature of the upward moving fluid in the lower nodes. This algorithm is consistent with observations made in EPRI-sponsored natural circulation experiments on a 1/7 scale model of a PWR at Westinghouse. For further information on these experiments as well as a comparison of the MAAP natural circulation model to the experimental results, the reader should consult Ref. [4].

After reactor vessel failure, natural circulation between the upper plenum and the core is assumed to be replaced by the overall unidirectional natural circulation patterns which are set up in the primary system around the coolant loops. Thereafter, the inlet flows to the core consist in part of the downcomer to core flow rate computed in subroutine FLOW. Such flows persist until the core has completely melted.

2.3.4 Radial Radiation Heat Transfer Model

Typical radial power profiles in LWRs exhibit a significant reduction in the power generation in the outer core region fuel assemblies. Therefore, in an accident involving core uncover, high temperatures may be obtained at the central core assemblies while the temperatures of the outer core assemblies may be much lower. This represents a large potential driving force for radial radiation heat transfer in the core. However, the fuel pins in the outer assemblies will act as radiation shields between the hot inner assemblies and the colder core shroud and the reactor vessel. For example, hand calculations show that in order to allow for radial heat losses from the core of 1 MW with an 8 x 8 fuel assembly, the temperatures of the fuel pins in the outer subassembly would decrease from 1200K at the inner row to 600 K at the outside of the core. For the inner regions of the core, on the other hand, the power generation distribution is more uniform. Therefore as the fuel pins in the inner assemblies become hot (say more than 1200 K), the radiation heat transfer would tend to further flatten the radial temperature profile.

This concept is incorporated in MAAP by an approximate radial radiation model which compares favorably with a more detailed calculations.

The detailed model is discussed in Ref. [4] along with a comparison of the two models.

Consider the radial heat transfer between two nodes containing only fuel pins as shown in Fig. 4. Node i contains $N_R(i)$ fuel pins in the axial slice while node $i + 1$ contains $N_R(i + 1)$ pins. Let j indicate the fuel pin index between the nodes as shown in Fig. 4. With this notation $T_{j=1} = T_i$ and $T_{j=m} = T_{i+1}$.

The model assumes that a given row of fuel pins acts as a radiation shield. Specifically, a fuel pin sees neighboring fuel pins with a view factor of 1 and does not see beyond the adjacent row of pins. If we further assume an emissivity of one, the radial heat fluxes between the fuel pins are:

$$\begin{aligned} q_{1-2} &= \sigma(T_1^4 - T_2^4) \\ &\vdots \\ &\vdots \\ q_{j-j+1} &= \sigma(T_j^4 - T_{j+1}^4) \\ &\vdots \\ &\vdots \\ q_{m-1-m} &= \sigma(T_{m-1}^4 - T_{i+1}^4) \end{aligned} \tag{28}$$

Therefore, in view of the assumption that the heat fluxes between the pins are equal, the heat transfer rate is

$$Q_{\text{rad}}(i) = \frac{\sigma A(i)(T_i^4 - T_{i+1}^4)}{m} \tag{29}$$

where $A(i)$ is the outer surface area of node i . The number of reflective surfaces between the centers of the two nodes, m , is

$$m = \frac{N_R(i)}{2} + \frac{N_R(i+1)}{2} - 1 \tag{30}$$

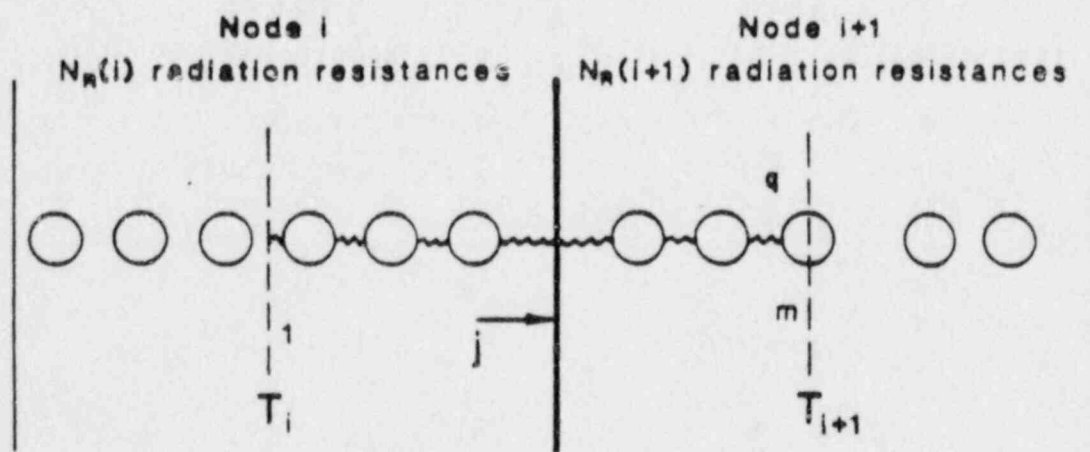


Fig. 4 Schematic illustration of the simplified radial radiation model.

The same procedure is used for radiation between the outermost radial ring and the core barrel. In this case the surface temperature of the core barrel nodes (computed in subroutine PSEQPT) is used and only the radiation resistance of the outermost slice enters into m .

2.3.5 Heatup of an Uncovered Node

The heatup of an uncovered node is governed by the following energy balance:

$$\begin{aligned} \dot{Q}_N = & Q_{\text{decay}} + Q_{\text{reaction}} - Q_{\text{convection}} \\ & - Q_{\text{melt}} - Q_{\text{radiation}} - Q_{\text{UHI}} \end{aligned} \quad (31)$$

where Q_{decay} is the decay heat generated in the node, Q_{reaction} is the net heat gained by the oxidation reaction at the node temperature, $Q_{\text{convection}}$ is the convective heat transfer to the gas, $Q_{\text{radiation}}$ is the net amount of heat lost due to radial radiation, Q_{UHI} is the energy lost to upper head injection water sprayed into the top of the core, and Q_{melt} is the rate at which molten corium energy is leaving (positive) or entering (negative) the node.

Q_{decay} is composed of two parts. The fraction of the decay heat supplied by materials tracked by the MAAP fission product model is calculated by subroutine HEATFP. The remaining fraction is tracked as "nonvolatile" heat which moves with the core materials as they melt. $Q_{\text{radiation}}$ is calculated as described in the preceding section, and Q_{melt} and Q_{UHI} are calculated by models discussed in subsequent sections.

In a given node, $Q_{\text{convection}}$ and Q_{reaction} depend on the gas flow rates in the coolant channels and this depends on the location of the node with respect to the flow patterns shown in Figs. 2 and 3. The calculational scheme used is to calculate gas-node interactions first for the lower, uncovered nodes, next for the group of nodes (if any) in which flow is entering downward from the upper plenum, and finally for the nodes which receive flows from the previous two groups. For convenience, therefore, the terms are computed for a given row of nodes between some ring no. j_{min} and ring no. j_{max}

by calling subroutine ROW. The heat transfer and oxidation models are described in the write-up for subroutine ROW.

2.3.6 Core Melt Progression Model

The detailed phenomena which would occur as core materials began to melt and relocate are quite complicated and not readily amenable to modeling. In earlier versions of the MAAP code, the process was not modeled, and molten material from the core was allowed to heat adiabatically until a user-specified mass had collected. At that point the molten material was assumed to slump.

This earlier procedure gave unphysically large debris temperatures on rare occasions (i.e., in certain sequences with intermittent accumulator action). It was concluded that a simple model should be added to MAAP to track the global downward progression of the core debris.

In rough outline, the model is similar to the so-called meltdown model "A" in the MARCH code [6]. The model treats the melting process itself, the motion of molten material, heat transfer processes within the molten pool, melting of structures underneath the core, and the possibility of core collapse. Each of these processes will be outlined below.

2.3.6.1 U-Zr-ZrO₂ Thermodynamics Model

The constituents of the core (UO₂, Zr, and ZrO₂) are assumed to form a eutectic which melts at a user-specified temperature (e.g., 2500°K) with a user-specified latent heat (e.g., 275 KJ/kg, the latent heat of UO₂). Melting of undissolved Zr is not modeled. It should be noted that this model represents a considerable simplification of experimental results [7] which show that the degree of dissolution of UO₂ by Zr is a strong function of test conditions. In principle, such factors as whether contact between the UO₂ and Zr exists, the heatup rate of the clad, and the Zircaloy oxidation rate should be considered. It was judged that such details were not sufficiently well understood to be included in the model at this time. Instead, the approach

taken was to formulate a simple model and use sensitivity analyses to ensure that the key results were not sensitive to the modeling simplifications.

2.3.6.2 Melt Progression Model

As the materials melt, they run downward until they reach a node which is frozen or until they reach a node which is already completely full. The internal energies of the molten material and still-frozen material are mixed, which usually freezes the molten material. This "candling" process has been widely observed in fuel pin meltdown experiments [8] and is believed to represent a reasonable approximation to the actual behavior.

To further justify this approach, a simple analysis was performed in Ref. [4] to illuminate the drainage processes which would likely occur as melting commenced. The analysis indicated that the simple refreezing algorithm used in the MAAP model is a reasonable approximation, since the ability to refreeze the downward-moving melt is mainly a function only of the fuel pin temperatures encountered by the melt. On the other hand, it should be recognized that the experimental data base is limited, and it would be useful to have additional data focussed on the time-dependent film flow regime itself to confirm this conclusion.

2.3.6.3 Pool Internal Heat Transfer Model

As stated above, melt run-off can potentially be prevented by the existence of lower, completely frozen and filled nodes. This normally occurs for only a short period, and the temperatures of the partially molten nodes above the frozen nodes do not exceed the eutectic temperature. In other words, the energy produced in the partially molten nodes over this delay period is used to melt adjacent still-frozen eutectic. If the period extended long enough, however, temperature gradients would be established between the molten nodes due to differences in fission product heating. A simple model has been written (subroutine QCONHT) to represent convective heat transport within the molten pool and between the molten pool and the frozen material above and below the pool.

The model assumes that convective motion within the pool is sufficient to prevent significant temperature differences. Axial heat transfer between the molten and frozen materials is governed by the film resistance established between the crust and the circulating molten material. This resistance is characterized by a user-specified corium-to-crust heat transfer coefficient which is discussed in the core-concrete model description in the MAAP User's Manual.

In any event, calculations of core melt progression indicate that this process is relatively unimportant due to the rapid increase in molten mass which ensues after the first node begins melting.

Radial heat transfer between two molten nodes is not currently modeled. A simple model has been incorporated, however, for radial heat transfer between a molten node and an unmolten node. In effect, this model replaces the radial radiation heat transfer model when one member of a pair of nodes is molten. To develop the model, consider a node which is at or above the eutectic temperature and separated from an adjacent node, which is below this temperature, by a crust as illustrated in Fig. 5. To estimate the radial heat loss to the colder node, we can assume the crust is fully developed such that it is only conducting away the heat generated in the crust and the inner surface is at the eutectic temperature (T_m). The temperature difference across the crust is given by

$$T_m - T_s = \frac{\dot{q} \delta_F^2}{2 k_F} \quad (32)$$

where T_s is the outer surface temperature, \dot{q} is the volumetric heat generation rate, k_F is the thermal conductivity of the core material and δ_F is the crust thickness. The heat flux at the outer crust boundary is $(\dot{q} \delta_F)$ and this can be equated to the radiation heat flux that can be transferred through the intact node. However, since the principal feature to be represented is the radial heat loss and the radiation transfer occurs at nearly isothermal conditions, the surface temperature can be approximated by the adjacent node temperature (T_j) such that

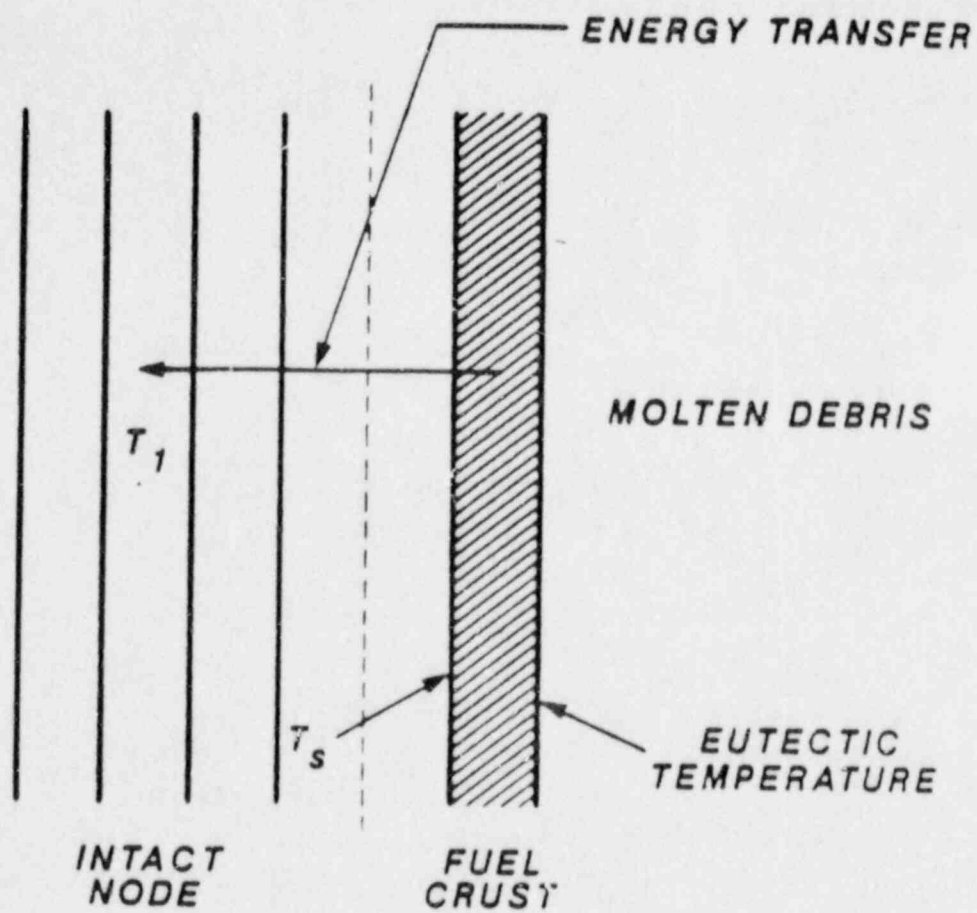


Fig. 5 Energy transfer from fuel crust to intact node.

$$\delta_F = \left[\frac{2 k_F (T_m - T_1)}{\dot{q}} \right]^{1/2} \quad (33)$$

Consequently, the radial heat loss from a node (\dot{Q}) is

$$\dot{Q} = A_R [2 \dot{q} k_F (T_m - T_1)]^{1/2} \quad (34)$$

where A_R is the outer area of the molten node (πDh). This would yield a mass of solid material in the molten node (m_F) of about

$$m_F = \pi dh \delta_F \rho \quad (35)$$

but this should never be greater than the solid mass left in a node (m_{FE}). Hence, the crust thickness is the minimum between Eq. (33) and

$$\delta_{FE} = \frac{m_{FE}}{\rho_F \pi Dh} \quad (36)$$

where m_{FE} is the solid mass in the molten node as determined by an energy balance. This limitation simply means that the lesser of the heat flux given by Eq. (34) and the total decay heat generated in the node should be used.

2.3.6.4 Melting of Below-Core Structures

As the melt leaves the core boundaries, it will begin to attack structures lying below the core, e.g., the lower core support plate and core support forging. It is likely that the support plate would be substantially melted, but recent TMI examinations reveal that the support forging was undamaged. To allow sensitivity studies on the amount of steel melted, a user-specified mass of steel which is denoted the "support plate" mass is melted at the maximum rate allowed by the energy convected by the corium. The melted steel is added to the lower plenum corium pool.

2.3.6.5 Core Collapse

When an attempt to recover the core which underwent extensive oxidation is made, the core may collapse. The collapsing criteria was introduced when the TMI-2 accident was modeled and is based on a user-specified oxidation fraction, which would embrittle the cladding, coupled with high heat transfer from the core. Core collapsing is defined by subroutine EVENTS. In this case, core material moves downward until all nodes have at least as much material as is required by a user-specified bed porosity (or void fraction). The maximum steaming rate from the pool is then limited in this case by a user-specified Kutateladze number as discussed in Section 2.3.1.

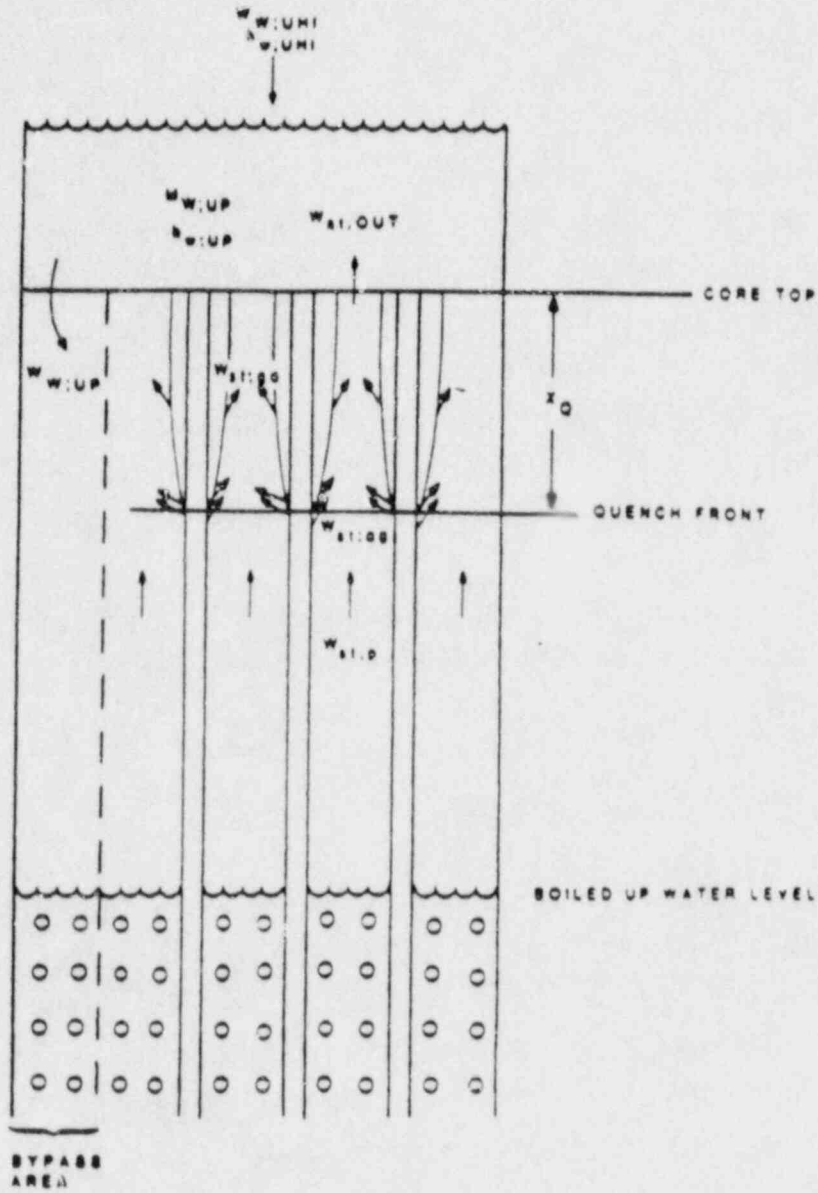
Finally, to save computation time, when the core mass is down to 5% of the original mass, the remainder of the core is dumped to the lower plenum in one time step.

2.3.7 Upper Head Injection (UHI)

Water from external UHI accumulators may enter the top of the core during the heatup process and cool the core. The water flow rate ($\dot{W}_{w;UHI}$) and specific enthalpy ($h_{w;UHI}$) are calculated externally by MAAP in subroutine ACCUM. Water may accumulate on the top of the core and enter the core from the top by quenching the hot uncovered rods. Alternatively it may flow through a bypass area, enter the water pool and reflood the core. The situation is described schematically in Fig. 6.

Currently the HEATUP subroutine treats the UHI as if it either quenches from the top (default) or floods the core from the bottom according to a user-specified event code. These two processes represent a reasonable bound describing the real behavior of the core when the upper head water injection is turned on. The two processes are described below.

Bottom Flooding - In the case of bottom flooding all the UHI flow is diverted directly to the lower water pool, $W_{w;up} = W_{w;UHI}$. The mass inventory of the water pool increases according to Eq. (9) and consequently the pool



W_{UHI} - STEAM FLOW RATE
 h_{UHI} - WATER ENTHALPY

Fig. 6 Schematic description of the UHI model.

water level rises. Steam generated by the flooding process may react with Zircaloy, in the uncovered part of the core, and form hydrogen.

Top Quenching - This model assumes that a uniform quench front descends into the core until it evaporates completely or until it reaches the lower water pool level. The basic assumption is that the rate at which UHI water can enter is governed by a counter-current flooding limitation. That is, the maximum rate at which water which collects above the core can enter is that rate at which the water would just be flooded by the escaping steam. This is evaluated by the Kutateladze criterion [1] as presented in Ref. [5]:

$$j_{g,max} = \frac{3.0 \sqrt[4]{\sigma g (\rho_w - \rho_g)}}{\sqrt{\rho_g}} \quad (37)$$

where $j_{g,max}$ = maximum gas superficial velocity,

ρ_w, ρ_g = density of water and steam,

σ = interfacial surface tension,

g = acceleration of gravity.

Assuming that the mass of water in the quenched film is small, the rate of steam generation is equal to the flow rate of water from the upper plenum. This flow rate is the smaller of the flooding flow rate

$$W_{flood} = j_{g,max} \rho_g A_{core} \quad (38)$$

or the flow rate obtained by summing the UHI to upper plenum flow rate plus that due to any water stored in the upper plenum from previous time steps.

Given the flow rate into the core, HEATUP determines the row number in which the film disappears, either because in that row the film evaporates completely or the row in which the unevaporated part of the film runs into the core pool. HEATUP also calculates the steam production rate in the lowest row of nodes receiving UHI water. This information is passed to subroutine ROW,

which evaluates the effect of the UHI on the core temperatures and channel flows.

2.3.8 Clad Ballooning Model

For fuel pins which have not yet ruptured, the increase in internal gas pressure arising from heating of the pins can cause the clad to balloon. Ballooning is tracked in MAAP by integrating an ordinary differential equation for the rate of clad strain at each node. The rate of strain is computed by subroutine STRETH (see write-up). The value of the strain is used by subroutines GNODE and ROW (see write-ups) to define the heat transfer area, Zircaloy dioxide thickness, gas flow area, etc.

Ballooning can continue until the clad fails. This occurs either due to exceeding an ultimate stress criterion in STRETH, or by exceeding a user-specified failure temperature at some axial location on the pin. Failure of the cladding also initiates fission product release.

3.0 COMPARISON WITH THE DETAILED HEATUP CODE

3.1 Introduction

The PWR-MAAP HEATUP subroutine was tested by using its stand-alone version which includes routines for the time step selection and integration. The initial conditions include the following parameters: (1) the elapsed time from scram at which the water level in the reactor equals the height of the top of the core (t_0), (2) the system pressure (P) which was assumed constant, and (3) the inlet (makeup) flow into the downcomer (W_{in}). All the core material and water inventory is assumed to be at saturation at time t_0 .

Predictions of the rate and the amount of hydrogen generated due to the core heatup is compared with a detailed core, PWRCHC [6], developed by EPRI as part of the IDCOR effort.

The detailed code, the initial conditions (reference cases) and the resulting hydrogen generation are discussed in the following subsection. It

should be noted that these comparisons were performed with early versions of both codes. While these versions did not model many of the phenomena now treated in the codes, they treated consistent sets of phenomena. Thus, the comparison provides a measure of confidence in the simplified MAAP model, even though the comparisons have not been repeated for the latest versions.

3.2 The Detailed Heatup Code

The PWRCHC, Ref. [9] is a detailed heatup code which predicts the heat transfer among fuel, cladding, structure, and steam and hydrogen mixtures for an intact PWR geometry. Its major differences from the PWR-MAAP HEATUP subroutine are:

1. The reactor pressure vessel and core geometry are described with more nodes.
2. The energy balances allow for temperature differences between the fuel, cladding, nonfuel (control rods), and the coolant based on radial nodalization of the fuel pins and channels and a detailed calculation of heat transfer rates.
3. The gas compressibility and axial heat convection are included in the mass and energy balances over the uncovered flow channels.
4. Axial variation in temperature and void fraction are considered in the water pool.

PWRCHC includes, as options, models for inter-fuel assembly radiation heat transfer and the hydrogen blanketing effect on cladding oxidation. These options were not activated in the comparison runs.

3.3 Reference Case Descriptions and Comparisons

For comparison of the PWR-MAAP and detailed heat-up codes, three reference accident conditions were defined. They are representative of the

general conditions that would be observed for a large break loss of coolant accident (LOCA), a small break LOCA and a plant transient, such as loss of all AC power. The initial conditions for the core uncover in these reference cases are given in Table 1. For the large break LOCA, the primary system is assumed to be depressurized with an early core uncover beginning at 300 seconds and no injection. For the small break LOCA, a primary system pressure of 7 MPa is assumed with an uncover time of 7200 seconds, which is an approximate representation of a TMI-2 type event. For the plant transient initiator, the primary system is assumed to remain at a pressure required to lift the pressurizer safety valves with a core uncover time of 7200 seconds. This accident sequence would be representative of a loss of off-site and on-site AC power without a degradation of the reactor coolant pump seals.

The total masses of hydrogen generated in the sample problems are shown in Figs. 7, 8, and 9. Initially, the hydrogen generation rate is slow until a considerable part of the core becomes uncovered and participates in the oxidation reaction. As the core heats up, the oxidation and hydrogen generation rates increase. Later into the transient, the steam generation rate decreases (less decay heat, smaller covered core) and the flow channels become blocked. As a result, the hydrogen generation rate decreases and the total mass of hydrogen levels off.

As shown in Figs. 7 and 8 both the PWR-MAAP HEATUP subroutine and the PWRCHC predict essentially the same hydrogen generation rates. The deviations between the two are less than 10% during the rapid hydrogen generation period resulting in less than a 5% difference in the amount produced at the end of the calculation. For the third sample problem, simulating a transient accident (Fig. 9), the PWR-MAAP HEATUP subroutine predicts a faster rate of H_2 generation by about 25% in the rapid generation period, but the total amount differs by only 10-15% for the two models. This larger deviation stems mainly from the difference in the decay heat curve used by the two computer codes. Since the latent heat is smaller at higher system pressure, larger deviations in steaming rate results. When using the same decay heat curve for both programs, the deviations are also less than 5%.

Table 1
INITIAL CONDITIONS FOR THE REFERENCE ACCIDENT CASES

	Simulated Accident		
	Large Break LOCA	Small Break LOCA	Transient
t_0 (sec)	300	7200	7200
P (MPa)	0.3	7.0	17.0
w_{in} (kg/s)	0	0	0

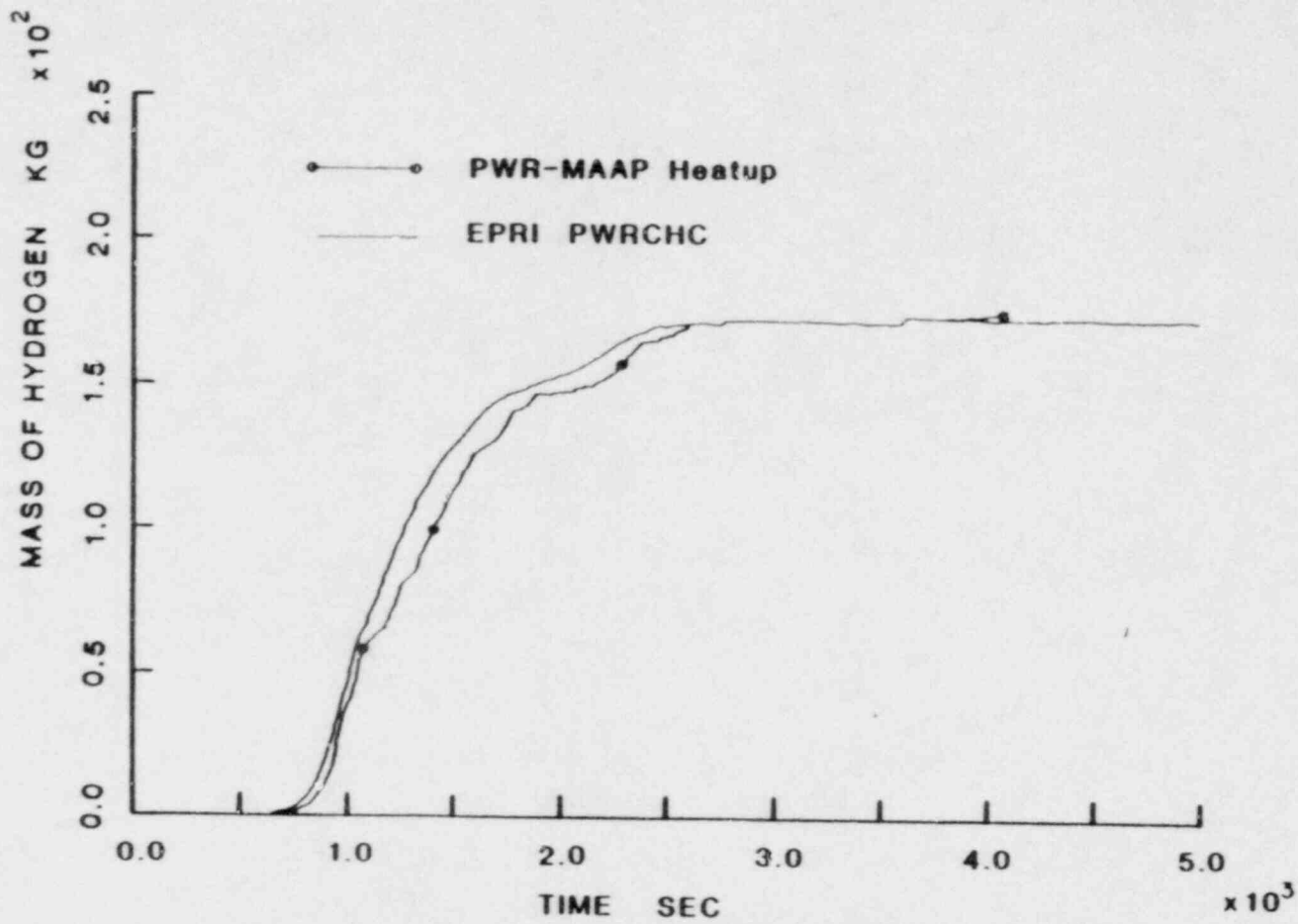


Fig. 7 HEATUP code comparison: hydrogen generation history for a reference accident simulating a large break LOCA.

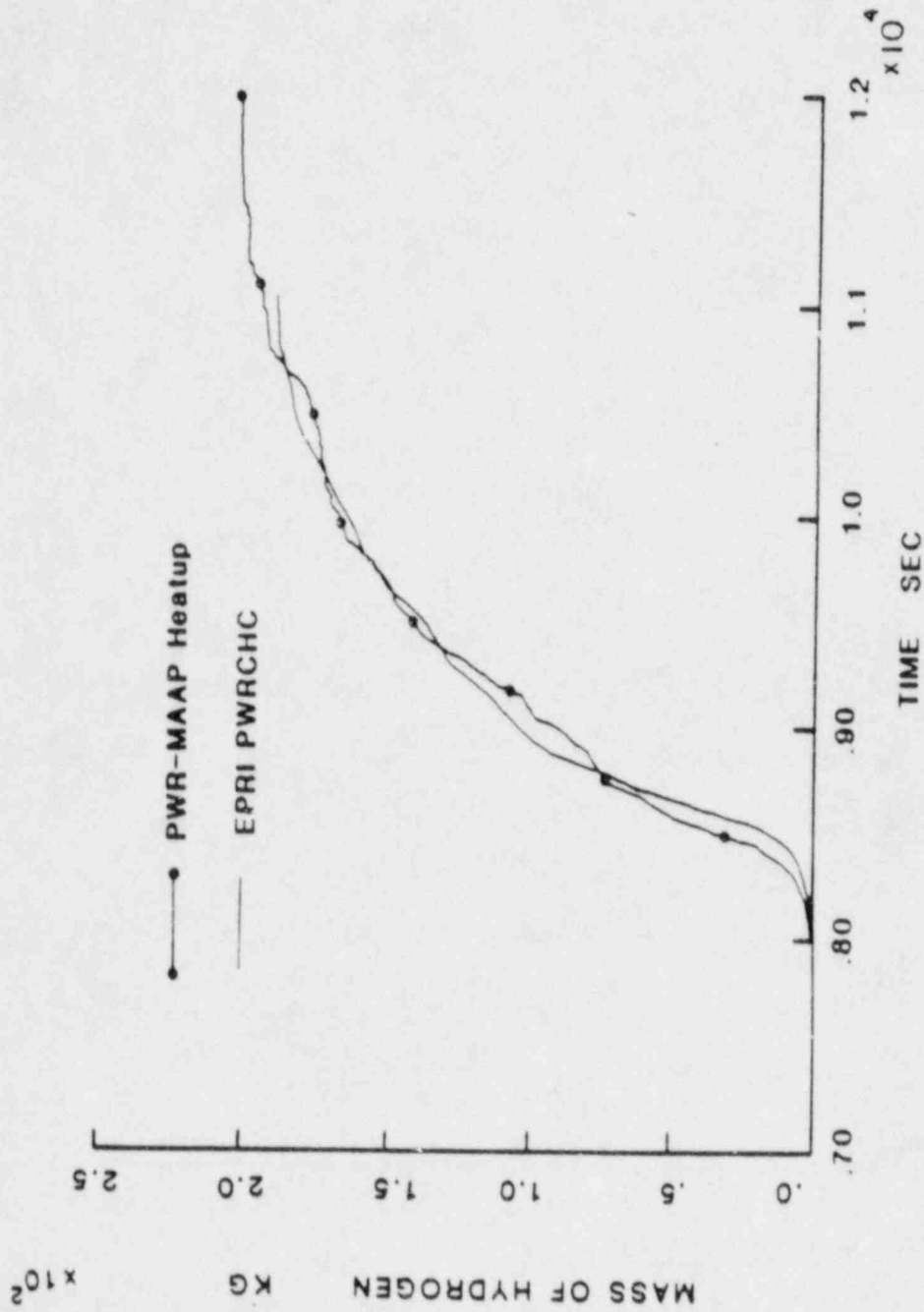


Fig. 8 HEATUP code comparison: hydrogen generation history for a reference accident simulating a small break LOCA.

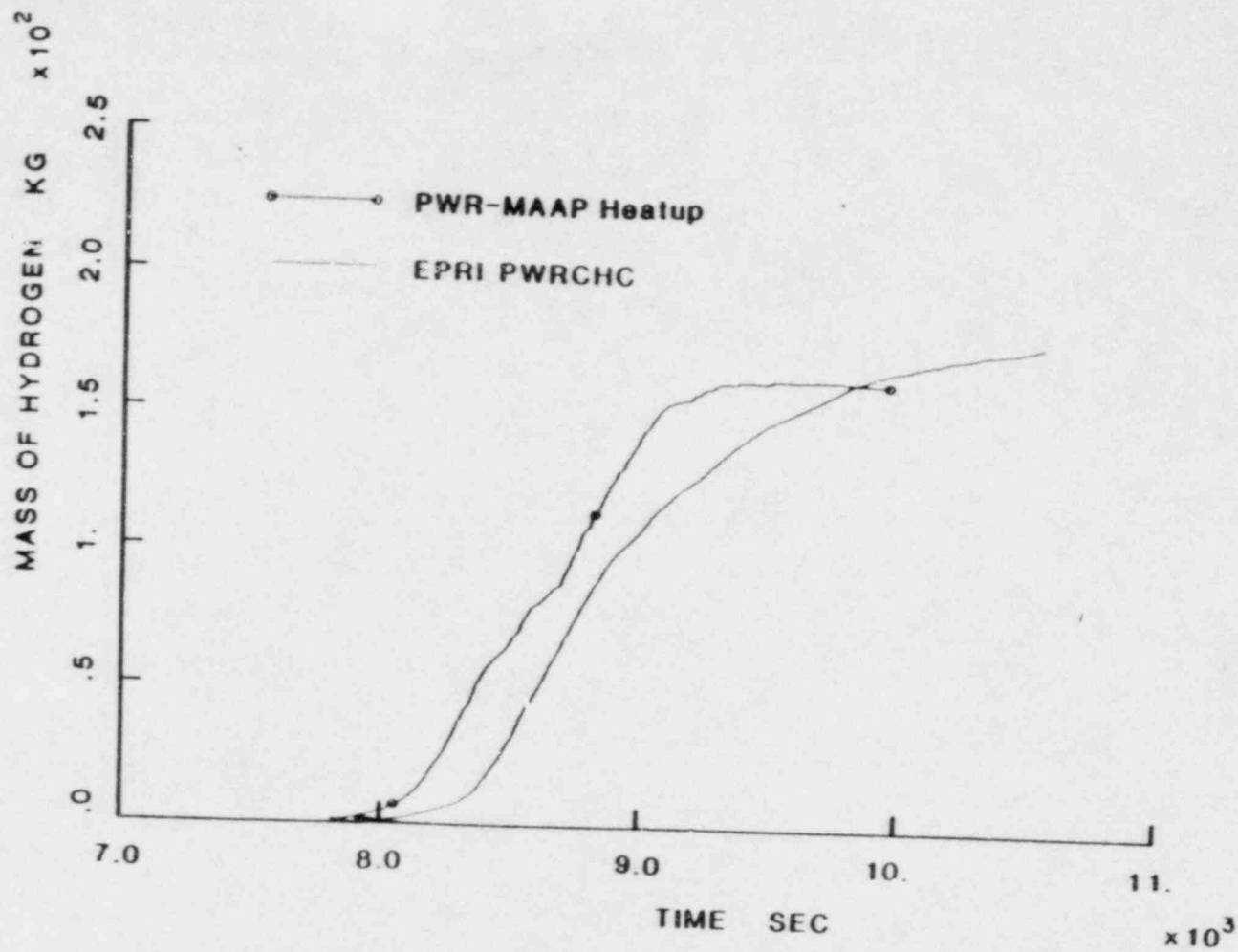


Fig. 9 HEATUP code comparison: hydrogen generation history for a reference accident simulating a PWR transient.

The execution time of the PWR-MAAP stand-alone heatup model is at least an order of magnitude smaller than the PWRCHC. On a VAX 11/750 computer with a floating point accelerator, the execution times are about 1 CPU minute for the PWR-MAAP and about 100 CPU minutes for the PWRCHC.

4.0 REFERENCES

1. S. S. Kutateladze, "Elements of the Hydrodynamics of Gas-Liquid Systems," *Fluid Mechanics - Soviet Res.*, 1, 4, 29, 1972.
2. J. V. Cathcart, et al., "Zirconium Metal-Water Oxidation Kinetics IV. Reaction Rate Studies," ORNL/NUREG-17, August 1977.
3. L. Baker, Jr. and L. C. Just, "Studies of Metal-Water Reactions at High Temperatures III. Experimental and Theoretical Studies of the Zirconium-Water Reaction," ANL-6548, May 1962.
4. Fauske & Associates, "Technical Support for Issue Resolution," IDCOR Report 85-2, July, 1985.
5. H. K. Fauske, "Boiling Flow Regime Maps in LMFBR HCDA Analysis, *Trans. ANS*, Vol. 22, pp. 385-386, 1975.
6. R. O. Wonten, et al., "MARCH2 (Meltdown Accident Response Characteristics) Code Description and User's Manual," NUREG/CR-3988, BMI-2115, September, 1984.
7. P. Hofmann and D. K. Kerwin-Peck, "Chemical Interactions of Solid and Liquid Zircaloy-4 with UO_2 Under Transient Nonoxidizing Conditions," Paper presented at the International Meeting on Light Water Reactor Severe Accident Evaluation, Cambridge, Massachusetts, August, 1983.
8. S. Hagen and S. O. Peck, "Temperature Escalation of Zircaloy-Clad Fuel Rods and Bundles Under Severe Fuel Damage Conditions," Paper presented at the International Meeting on Light Water Reactor Severe Accident Evaluation, Cambridge, Massachusetts, August, 1983.
9. T. Y. Han, P. I. Nakayama, and R. G. Stuart, "Analysis of In-Vessel Core Melt Progression," User's Manual and Modeling Details for the PWR Core Heatup Code (PWRCHC), Final Draft Report, EPRI/NSAC, December 1982.

ACCUMULATOR FLOW RATE

Subroutine ACCUM calculates the pressure in the accumulators and the flow rate from the accumulators to the primary system. This flow is driven by the pressure difference between the accumulator and the primary system, and by the flow area and the hydraulic resistance of the connecting pipes. Flow from the accumulators will therefore result only if the accumulator pressure P_a is larger than that of the primary system P_{PS} , and if the connecting pipes are not blocked by the operator.

Assuming an isothermal expansion of the gas space in the accumulator due to the depletion of water, the pressure in the accumulator is:

$$P_a = \frac{V_a - m_o v}{V_a - m v} P_o \quad (1)$$

where V_a is the volume of the accumulator, m and v are the mass and specific volume of water, and subscript o denotes a nominal operating value as supplied by the user.

The water flow rate through a unit area based on the driving pressure difference W_1 , is determined by calling WFLOW. This call requires that values be passed to WFLOW for accumulator pressure, primary system pressure, void fraction, accumulator temperature, and a loss function f_{CD} based on the overall loss coefficient for flow between the accumulator and primary system. This loss function is calculated in ACCUM as,

$$f_{CD} = (f L/D + K)^{-1/2} \quad (2)$$

where f is the friction factor (taken as 0.02), L/D is the connecting pipe length to diameter ratio, and K is the minor loss coefficient, assumed equal to 1. The total flow rate between the accumulators and the primary system is then given by,

$$W = n A W_1 \tag{3}$$

where n is the number of accumulators and A is the flow area of the connecting pipe, and

$$W_1 = \left[\frac{2(P_a - P_s)}{v} \right]^{1/2} f_{CD} \tag{4}$$

ACCUM also calculates the derivative of the flow rate with respect to the primary system pressure for use in determining primary system pressure when one of the special cases for determining primary system pressure exists (see PRISYS).

The variable sequence used when calling ACCUM is:

CALL ACCUM (I, n, P_o, P_{PS}, m_o, m, v, T_a, V_a, A, L/D, W, P_a, $\frac{dW}{dP_{PS}}$)

where I is a Boolean indicator that is true if the accumulators are blocked by the operator (see subroutine EVENTS).

APPENDIX 6

Decay Heat History for Catawba Reload Cycles of 390
days for 3.8 w/o Westinghouse Optimized Fuel Assemblies.

TOTAL DECAY HEAT RESULTS

TIME(SEC)	MW	FRACTION OF BLOCK 1 PWR	FRACTION OF RATED POWER	ENERGY ADDED (BTU)
0.000E+00	3412.339	1.0003920	1.0003910	0.0000E+00
0.100E+01	202.432	0.0593468	0.0593468	0.9671E+05
0.500E+01	174.708	0.0512191	0.0512191	0.8116E+06
0.100E+02	159.045	0.0466270	0.0466270	0.1602E+07
0.300E+02	133.942	0.0392677	0.0392677	0.4379E+07
0.600E+02	118.487	0.0347367	0.0347367	0.7968E+07
0.120E+03	103.739	0.0304130	0.0304130	0.1429E+08
0.180E+03	95.926	0.0281224	0.0281224	0.1996E+08
0.240E+03	90.792	0.0266173	0.0266173	0.2527E+08
0.300E+03	87.004	0.0255068	0.0255068	0.3033E+08
0.360E+03	83.989	0.0246230	0.0246230	0.3519E+08
0.420E+03	81.463	0.0238826	0.0238826	0.3990E+08
0.480E+03	79.273	0.0232405	0.0232405	0.4447E+08
0.540E+03	77.330	0.0226707	0.0226707	0.4892E+08
0.600E+03	75.577	0.0221569	0.0221569	0.5327E+08
0.900E+03	68.683	0.0201357	0.0201357	0.7378E+08
0.120E+04	63.661	0.0186634	0.0186634	0.9259E+08
0.150E+04	59.725	0.0175096	0.0175096	0.1101E+09
0.180E+04	56.519	0.0165697	0.0165697	0.1267E+09
0.210E+04	53.845	0.0157858	0.0157858	0.1424E+09
0.240E+04	51.577	0.0151209	0.0151209	0.1573E+09
0.270E+04	49.629	0.0145496	0.0145496	0.1717E+09
0.300E+04	47.936	0.0140533	0.0140533	0.1856E+09
0.330E+04	46.451	0.0136180	0.0136180	0.1990E+09
0.360E+04	45.138	0.0132331	0.0132331	0.2120E+09
0.390E+04	43.968	0.0128902	0.0128902	0.2247E+09
0.420E+04	42.919	0.0125826	0.0125826	0.2371E+09
0.450E+04	41.973	0.0123051	0.0123051	0.2491E+09
0.480E+04	41.113	0.0120532	0.0120532	0.2609E+09
0.510E+04	40.329	0.0118234	0.0118234	0.2725E+09
0.540E+04	39.611	0.0116127	0.0116127	0.2839E+09
0.570E+04	38.950	0.0114188	0.0114188	0.2951E+09
0.600E+04	38.338	0.0112395	0.0112395	0.3060E+09
0.630E+04	37.770	0.0110731	0.0110731	0.3169E+09
0.660E+04	37.242	0.0109181	0.0109181	0.3275E+09
0.690E+04	36.748	0.0107732	0.0107732	0.3380E+09
0.720E+04	36.284	0.0106374	0.0106374	0.3484E+09
0.900E+04	34.000	0.0099678	0.0099678	0.4084E+09
0.108E+05	33.795	0.0099075	0.0099075	0.4662E+09
0.126E+05	32.439	0.0095102	0.0095102	0.5227E+09
0.144E+05	31.336	0.0091868	0.0091868	0.5771E+09
0.162E+05	30.398	0.0089117	0.0089117	0.6298E+09
0.180E+05	29.588	0.0086742	0.0086742	0.6810E+09
0.198E+05	28.884	0.0084678	0.0084678	0.7308E+09
0.216E+05	28.243	0.0082799	0.0082799	0.7796E+09
0.234E+05	27.667	0.0081111	0.0081111	0.8273E+09
0.252E+05	27.146	0.0079584	0.0079584	0.8740E+09
0.270E+05	26.670	0.0078189	0.0078189	0.9199E+09
0.288E+05	26.233	0.0076906	0.0076906	0.9650E+09

TOTAL DECAY HEAT RESULTS

TIME(SEC)	MW	FRACTION OF BLOCK 1 PWR	FRACTION OF RATED POWER	ENERGY ADDED (BTU)
0.306E+05	25.828	0.0075719	0.0075718	0.1009E+10
0.324E+05	25.451	0.0074613	0.0074613	0.1053E+10
0.342E+05	25.098	0.0073579	0.0073579	0.1096E+10
0.360E+05	24.767	0.0072609	0.0072609	0.1139E+10
0.432E+05	23.608	0.0069210	0.0069210	0.1304E+10
0.504E+05	22.649	0.0066399	0.0066399	0.1462E+10
0.548E+05	22.143	0.0064916	0.0064916	0.1555E+10
0.576E+05	21.847	0.0064048	0.0064048	0.1614E+10
0.720E+05	20.525	0.0060174	0.0060174	0.1903E+10
0.792E+05	19.981	0.0058577	0.0058577	0.2041E+10
0.864E+05	19.482	0.0057115	0.0057115	0.2176E+10
0.936E+05	19.031	0.0055793	0.0055793	0.2307E+10
0.101E+06	18.620	0.0054588	0.0054588	0.2435E+10
0.108E+06	18.233	0.0053452	0.0053452	0.2561E+10
0.173E+06	15.717	0.0046079	0.0046079	0.3604E+10
0.259E+06	13.641	0.0039992	0.0039992	0.4806E+10
0.346E+06	12.228	0.0035847	0.0035847	0.5865E+10
0.432E+06	11.173	0.0032755	0.0032755	0.6823E+10
0.518E+06	10.348	0.0030336	0.0030336	0.7704E+10
0.605E+06	9.677	0.0028369	0.0028369	0.8524E+10
0.691E+06	9.122	0.0026742	0.0026742	0.9294E+10
0.778E+06	8.653	0.0025367	0.0025367	0.1002E+11
0.864E+06	8.255	0.0024200	0.0024200	0.1071E+11
0.950E+06	7.911	0.0023191	0.0023191	0.1138E+11
0.104E+07	7.608	0.0022303	0.0022303	0.1201E+11
0.112E+07	7.338	0.0021512	0.0021512	0.1262E+11
0.121E+07	7.096	0.0020803	0.0020803	0.1321E+11
0.130E+07	6.877	0.0020162	0.0020162	0.1379E+11
0.138E+07	6.678	0.0019578	0.0019578	0.1434E+11
0.147E+07	6.495	0.0019041	0.0019041	0.1488E+11
0.156E+07	6.327	0.0018548	0.0018548	0.1541E+11
0.164E+07	6.171	0.0018091	0.0018091	0.1592E+11
0.173E+07	6.025	0.0017664	0.0017664	0.1642E+11
0.181E+07	5.889	0.0017264	0.0017264	0.1690E+11
0.190E+07	5.760	0.0016888	0.0016888	0.1738E+11
0.199E+07	5.639	0.0016532	0.0016532	0.1785E+11
0.207E+07	5.524	0.0016196	0.0016196	0.1831E+11
0.216E+07	5.416	0.0015877	0.0015877	0.1875E+11
0.225E+07	5.312	0.0015573	0.0015573	0.1919E+11
0.233E+07	5.213	0.0015284	0.0015284	0.1962E+11
0.242E+07	5.119	0.0015008	0.0015008	0.2005E+11
0.302E+07	4.563	0.0013376	0.0013376	0.2282E+11
0.363E+07	4.138	0.0012130	0.0012130	0.2532E+11
0.422E+07	3.808	0.0011165	0.0011165	0.2756E+11
0.504E+07	3.455	0.0010129	0.0010129	0.3037E+11
0.544E+07	3.309	0.0009702	0.0009702	0.3166E+11
0.605E+07	3.117	0.0009139	0.0009139	0.3350E+11
0.665E+07	2.953	0.0008656	0.0008656	0.3524E+11
0.726E+07	2.807	0.0008228	0.0008228	0.3689E+11